NASA Contractor Report 163093

F-8C ADAPTIVE CONTROL LAW REFINEMENT AND SOFTWARE DEVELOPMENT

(NASA-CR-163093) F-8C ADAPTIVE CONTROL LAW REFINEMENT AND SOFTWARE DEVELOPMENT Final Report, Jun. 1976 - Jun. 1977 (Honeywell Systems and Research) 184 p HC A09/MF A01 CSCL 01C G3/08 N81-22059 Unclas 42154

Gary L. Hartmann and Gunter Stein

Contract NAS4-2344
April 1981

NASA

NASA Contractor Report 163093

F-8C ADAPTIVE CONTROL LAW REFINEMENT AND SOFTWARE DEVELOPMENT

Gary L. Hartmann and Gunter Stein
Honeywell Systems & Research Center
Minneapolis, Minnesota

Prepared for
Dryden Flight Research Center
under Contract NAS4-2344

NASA
National Aeronautics and
Space Administration
1981

CONTENTS

CONTENTS (continued)

CONTENTS (concluded)

LIST OF ILLUSTRATIONS

LIST OF ILLUSTRATIONS (continued)

LIST OF ILLUSTRATIONS (concluded)

LIST OF TABLES

LIST OF TABLES (concluded)

F-8C ADAPTIVE CONTROL LAW REFINEMENT AND SOFTWARE DEVELOPMENT

Gary L. Hartmann
Gunter Stein
HONEYWELL, INC.

SECTION 1
INTRODUCTION

The NASA Dryden Flight Research Center is currently flight testing a digital fly-by-wire (DFBW) flight control system installed in an F-8C aircraft. This serves as a test vehicle for demonstrations of advanced control laws and redundancy concepts to improve the performance and/or overall effectiveness of future flight control. In support of advanced control law efforts, Honeywell conducted a design program to define a digital adaptive control law suitable for flight test. The initial study (Reference 1) recommended an adaptive concept which combines gain-scheduled control laws with explicit maximum likelihood identification to provide the scheduling variables. This approach was selected from a comparison of three candidate concepts:

- Implicit gain adjustment based on self-excited limit cycles,
- Gain adjustment based on explicit identification using a Liapunov model tracker, and

- Gain adjustment on explicit identification with Maximum Likelihood Estimation.

Later design extensions (Reference 2) added a two-level estimate of gust intensity and provided a new parameter update method based on Kalman estimation of time-varying parameters.

This study provided further development of the Parallel Channel Maximum Likelihood Estimation (PCMLE) design. A number of features have been added to facilitate flight testing of the algorithm. The software was originally designed for on-board implementation. For convenience and flexibility in testing, the algorithm has been implemented on the NASA/DFRC Remotely Augmented Vehicle (RAV) facility (Reference 3). As shown in Figure 1, the PCMLE software resides in a ground computer. The measurements required by the PCMLE algorithm--pitch rate, normal acceleration, and horizontal stabilator position--are received by the ground-based computer via the telemetry downlink. The PCMLE estimates the aircraft characterization parameters and computes a dynamic pressure estimate as a linear function of M_{δ_e}. This quantity is transmitted to the triplex on-board digital computer and used for gain scheduling. As part of the groundrules, measurements were restricted to rate gyros, accelerometers, and servo position. Air data were excluded because aircraft like the F-8C, whose performance requirements can be met with air-data-scheduled control laws, benefit most from adaptive control through the elimination of air-data schedules.

The next section contains the list of symbols used throughout this report. Section 3 describes the PCMLE algorithm. The implementation of the algorithm and its acceptance test are summarized in Section 4. In

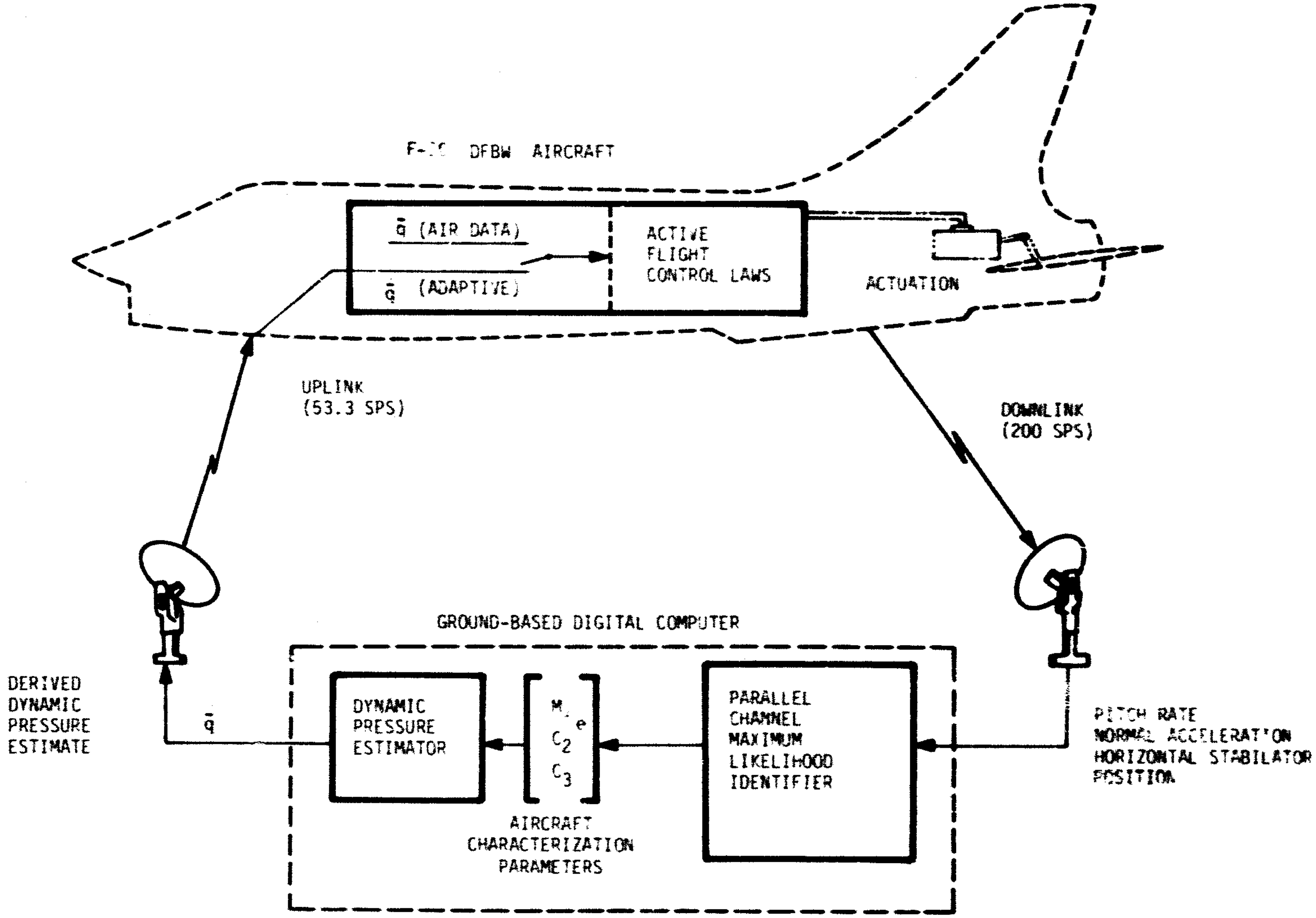

Figure 1. Adaptive Control Flight Test Approach

Section 5, sensor noise statistics are developed from ground test and flight test data. Section 6 contains the parameter estimates from the PCMLE algorithm computed from recorded F-8C flight data. Cross-checks are provided by parameter estimates from a batch maximum likelihood algorithm. Section 7 presents recommendations for flight evaluation of the PCMLE algorithm. Conclusions from this study are given in Section 8. Three appendices to this report contain time histories of the flight maneuvers and PCMLE outputs.

SECTION 2

SYMBOLS

Operators

s	Laplace operator
$(\dot{\ }) = \frac{d}{dt}$	Time derivative
Δ	Increment
∇	Gradient vector with respect to parameter vector ζ
∇^2	Second partial derivative matrix with respect to parameters ζ
∇_p	p-th component of $\nabla(.)$
Σ	Summation
$\|x\|$	Absolute value

Superscripts

$(\hat{\ })$	Estimated value
$(\bar{\ })$	One-step predicted value
$(\ )^{(i)}$	Value for parallel channel i
$(\ )^{o}$	Nominal value

Subscripts

$(\ )_m$	Measured value
$(\ )_k$	Value at time t_k

Upper Case Symbols

A	Discrete system dynamics matrix
B	Discrete system input matrix
C*	Response variable $N_z + V_{co}q$
D	Measurement matrix, y due to u
H	Measurement matrix
I	Identity matrix
J	Partial likelihood function $L - 1/2\Sigma \ln \det B$
K	Kalman filter gains
L	Likelihood function
L_w	Vertical gust field scale length
M	Number of parallel channels
$M_q, M_\alpha, M_\delta (M_{\delta_e}), M_\alpha$	Pitching moment coefficients to indicated variables
M	Trim pitching moment
$M_{\delta o}$	M_δ value for rigid airframe (without quasi-static flexibility)
$M_{\delta t}$	True value of $M_{\delta o}$
N	Number of data samples
N_z, N_y	Normal and lateral acceleration
P	Kalman filter covariance matrix
P_o	A priori parameter covariance matrix
R	Residual covariance matrix

U_N	Sequence of N control inputs
V	True air speed (m/s)
V_{co}	Crossover velocity in C* response
Y_N	Sequence of N measurements
Z_α, Z_δ	Normal force coefficients due to indicated variables
$Z_\alpha V$	Normal force coefficient in normal acceleration equation

<u>Lower Case Symbols</u>

$\underline{c}, c_i$	Parameter vector with components c_i
$\underline{c}_o$	A priori estimate of c
$\underline{c}_t$	True value of c
d	Sensor displacement from c.g. (4.62m)
g	Gravity
h	Altitude
i^*	Index of the minimum-L channel
n	System order
p	Roll rate
$\bar{q}$	Dynamic pressure
r	(1) Yaw rate (2) Number of measurements
t	Time
u	Control input vector

x	State vector
y	Measurement vector

Greek Symbols

Upper Case

Γ	Discrete system noise input matrix

Lower Case

α	Angle-of-attack
α_g	Gust angle-of-attack
β	Angle of sideslip
$\delta_e(\delta)$, δ_a, δ_r	Aerodynamic surface positions
ζ	Dummy argument for values of parameter vector $\underline{c}$
η	White noise process
ν	Kalman filter residuals
ξ	White noise process
σ, σ_x	Standard deviation of variable x
τ	Time constant
ϕ	Roll attitude
ω	Natural frequency

SECTION 3

PCMLE SOFTWARE DEVELOPMENT

This section summarizes the development of the Parallel Channel Maximum Likelihood Estimation (PCMLE) software. This software implements an adaptive gain schedule for the F-8C aircraft based on explicit parameter estimation. The software is designed for flight research using the Remotely Augmented Vehicle (RAV) facility at NASA/DFRC. It represents a further development and refinement of an adaptive design recommended in References 1 and 2. The theoretical background relevant to this study is contained in these reports.

A complete documentation of the PCMLE software including program listings and flowcharts is available as a separate volume (Reference 4).

THE BASIC ALGORITHM

The PCMLE algorithm is based on standard Maximum Likelihood Estimation theory as applied to longitudinal short-period F-8C dynamics. Instead of using the usual iterative calculations to maximize likelihood functions, however, it uses the parallel channel implementation shown in Figure 2. Several Kalman filter channels operate at fixed locations in parameter space. Likelihood functions are computed for each. Sensitivity equations are then solved only for the maximum likelihood channel and used to interpolate from there to the final parameter estimate with a single

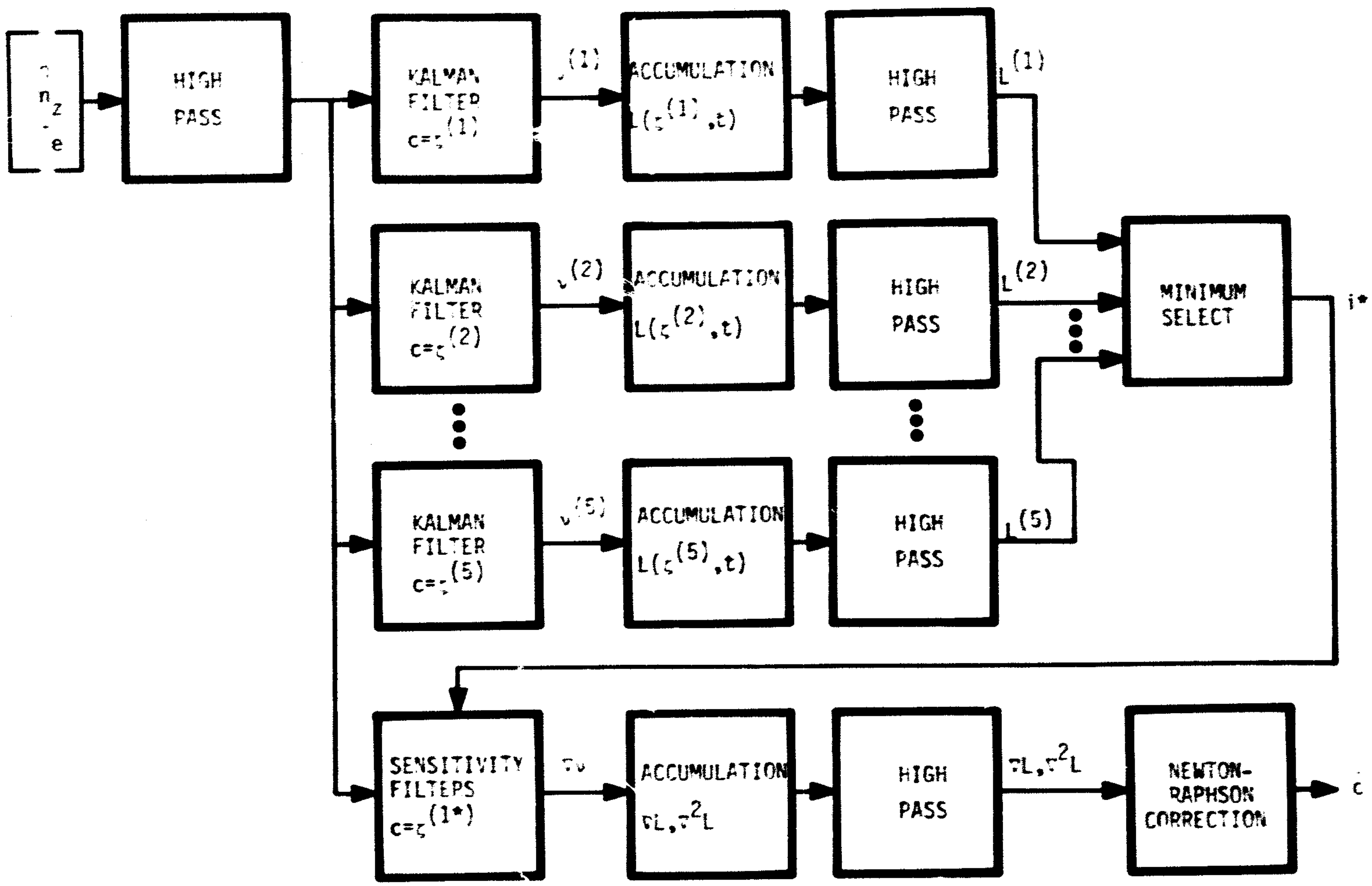

Figure 2. Basic PCMLE Algorithm

Newton/Raphson parameter correction. This fixed structure avoids real-time iterations and eliminates convergence problems.

Theoretical identifiability results were used to determine the number of parameters that could be identified with small test inputs. This accuracy analysis also provides insight into the number and location of the filter channels.

Nominally, five parallel channels are used to handle the F-8C aircraft over its entire operational flight envelope. The locations of these channels in M_{δ_O}-M_α parameter space are shown in Figure 3. Up to four parameters--surface effectiveness (M_{δ_O}), pitching moment due to angle-of-attack (M_α), airspeed (V), and normal force due to angle-of-attack ($Z_\alpha V$)--can be estimated. Estimation accuracy depends strongly on the signal levels in the control loop. For the small test signals producing less than 0.05 g RMS of normal acceleration, errors are 10 to 20 percent in M_{δ_O} and 20 to 30 percent in M_α and V which are typical in six-degree-of-freedom simulation runs. Theoretical accuracy analyses confirm these error levels.

The gain adjustment in the pitch and lateral control laws is done on the basis of estimated M_{δ_O} only using scheduling functions defined in Reference 1. However, the MLE design was selected in large part for its potential to identify additional parameters which may be needed for scheduling in other applications.

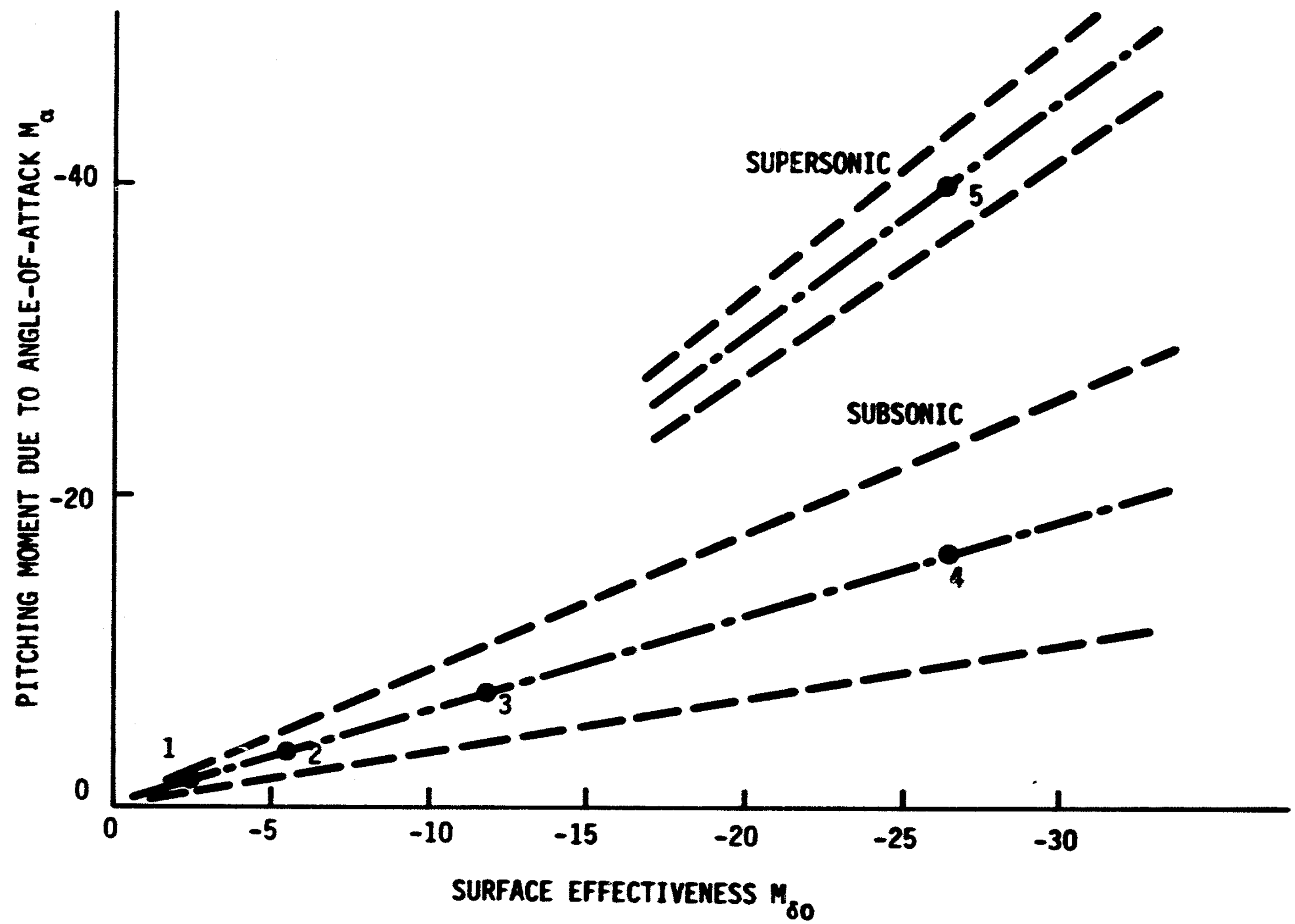

Figure 3. F-8C Identifier Channel Locations

PCMLE SOFTWARE FEATURES

The PCMLE software implements the above identification algorithm in a flexible manner suitable for flight test experimentation. Specific options and features of the implementation include the following:

- Variable number and locations of Kalman filter channels,
- Variable Kalman filter update rates (sample skipping options),
- Variable number of identified parameters (up to four),
- Output variables to monitor identification validity,
- Provisions for four uplink parameters with fail-safe integrity tests,
- Gust and rigid-body angle-of-attack estimation,
- An optional Kalman parameter correction (instead of Newton-Raphson steps) for improved tracking,
- Optional automatic adjustment of channel gains with gust intensity, and
- An optional second Newton-Raphson parameter correction step.

These features and options are achieved through a combination of software structure, channel model structure, and algorithm modifications. The software structure is discussed in detail in Section 4. Model structure and algorithm modifications are described below.

Nominal Channel Models

Four-state filter models are used for each channel with the following discrete-time form:

$$\hat{x}_{n+1} = A\hat{x}_n + B u_n + K(y_n - H\hat{x}_n) \tag{1}$$

Elements of matrices A, B, K, and H are computed in a non-real time initialization mode from the continuous F-8C model for a specified sample time.

The continuous model is

$$\begin{aligned} \dot{x} &= Fx + Gu + \Gamma_c \xi \\ y_k &= Hx_k + W\eta_k \end{aligned} \tag{2}$$

Individual terms appear as

$$\frac{d}{dt}\begin{bmatrix} q \\ \alpha_T \\ \alpha_g \\ \delta_e \end{bmatrix} = \begin{bmatrix} M_q & M_\alpha & 0 & M_\delta \\ 1 & Z_\alpha & -V/L_w & Z_\delta \\ 0 & 0 & -V/L_w & 0 \\ 0 & 0 & 0 & -K \end{bmatrix}\begin{bmatrix} q \\ \alpha_T \\ \alpha_g \\ \delta_e \end{bmatrix} + \begin{bmatrix} 0 \\ 0 \\ 0 \\ K \end{bmatrix}\delta_{es} + \begin{bmatrix} 0 & 0 \\ 0 & \sigma_\alpha\sqrt{\frac{2V}{L_w}} \\ 0 & \sigma_\alpha\sqrt{\frac{2V}{L_w}} \\ \sigma_\delta\sqrt{2K} & 0 \end{bmatrix}\xi(t)$$

$$y_k = \begin{bmatrix} q \\ N_z \end{bmatrix}_k = \begin{bmatrix} 1 & 0 & 0 & 0 \\ dM_q & dM_\alpha - Z_\alpha V & 0 & dM_\delta - Z_\delta V \end{bmatrix} \begin{bmatrix} q \\ \alpha_T \\ \alpha_g \\ \delta_e \end{bmatrix} + \begin{bmatrix} \sigma_q^2 & 0 \\ 0 & \sigma_{N_z}^2 \end{bmatrix} \eta_k \quad (3)$$

where

M_q, M_α, M_δ	=	pitching moment derivatives	functions of parameters to be identified ($M_{\delta o}$, C_2, C_3, C_4)
$(Z_\alpha V)$, $(Z_\delta V)$	=	normal force derivatives	
V	=	true airspeed	
K	=	actuator bandwidth (12.5 rad/sec)	
d	=	distance of accelerometer aft of c.g.	
L_w	=	gust field scale length (580 m)	
σ_i	=	standard deviations of noise processes	

Subroutine MODEL computes the discrete matrices A and B from standard formulas:

$$A(t) = \mathcal{L}^{-1}[sI - F]^{-1} \quad \text{evaluated at } t = \Delta t$$

$$B = \int_0^{\Delta t} A(t - \tau) G \, d\tau$$

The resulting matrices have the following form:

$$A = \begin{bmatrix} V & V & V & V \\ V & V & V & V \\ 0 & 0 & C & 0 \\ 0 & 0 & 0 & C \end{bmatrix} \qquad B = \begin{bmatrix} V \\ V \\ 0 \\ C \end{bmatrix}$$

where V denotes elements which vary with flight condition and C denotes constant elements. Strictly speaking, $A(3,3) = e^{-V/L_w}$ varies with flight condition also because it depends on the bandwidth of a first-order gust model. However, since the incoming measurements are high-passed (Figure 2), the high-pass frequency, ω_{HP}, dominates and is therefore used to replace V/L_w.

The Kalman filter gains K and the residual covariance matrix R are defined by the discrete Riccati equation:

$$R = (HPH^T + WW^T)$$

$$K = (APH^T + \Gamma_D W^T)R^{-1}$$

$$P = (A - KH)P(A - KH)^T + (\Gamma_D - KW)(\Gamma_D - KW)^T \tag{5}$$

These equations are solved via a doubly iterative algorithm carried out in subroutine's DIAK and CAL. The discrete noise input matrix, Γ_D, is computed from Γ_c and F according to the second-order approximation

$$\Gamma_D = \Delta t\, \Gamma_c (I + \Delta t\, F/2) \tag{6}$$

In order to compute state and residual sensitivities in real time, each nominal model also includes sensitivities (first partials with respect to parameters M_{δ_o}, C_2, C_3, C_4) of the matrices A, B, H, and K. These are computed by numerical finite differencing techniques.

All model parameters are initialized in non-real time and are stored in labelled arrays for later real-time use.

Algorithm Modifications

Modification of the basic PCMLE algorithm of Figure 2 were required to implement the following three options provided by the PCMLE software:

- Kalman parameter corrections,
- Automatic gain adjustment with gust intensity, and
- Two-step Newton-Raphson parameters corrections.

The first two of these options were studied under the Design Extension Study (Reference 2) of the original PCMLE design program. They led to the algorithm modifications summarized in Figures 4 and 5. Further details can be found in Reference 2. The third option implements a two-step parameter correction by introducing a "roving" channel located at point $\hat{c}$ which is the estimate obtained from the first Newton-Raphson step. Likelihood functions and sensitivities are computed for the roving channel and are used to provide the second update step:

$$\hat{\hat{c}} = \hat{c} - [\nabla^2 L] \quad \nabla L \Big|_{c = \hat{c}}$$

These algorithm modifications are summarized in Figure 6.

Models for the Second Newton-Raphson Step

Because the second Newton-Raphson step involves a channel which is not fixed in parameter space, the filters and sensitivity models for this channel must be

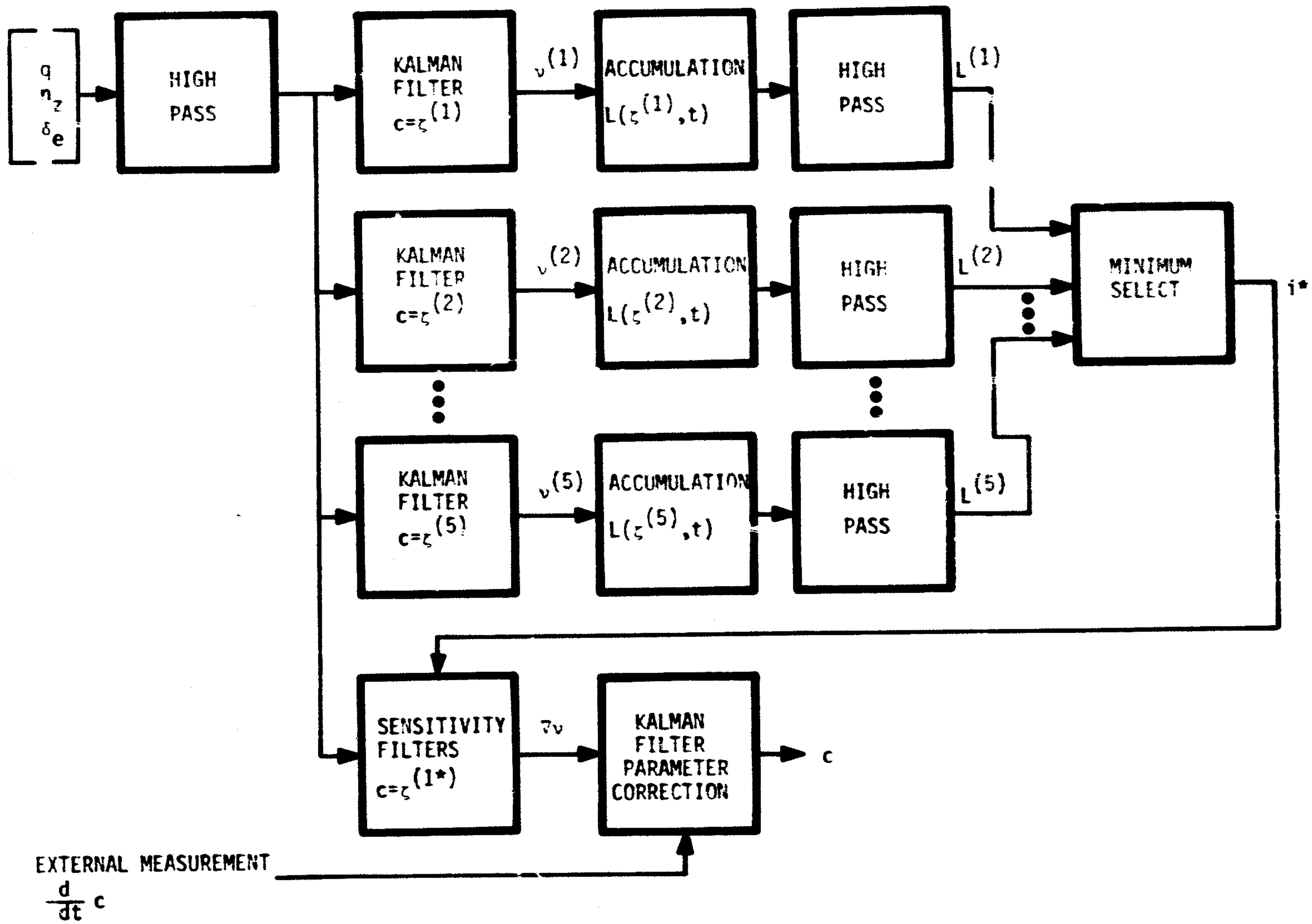

Figure 4. Identifier with Kalman Filter Parameter Corrections

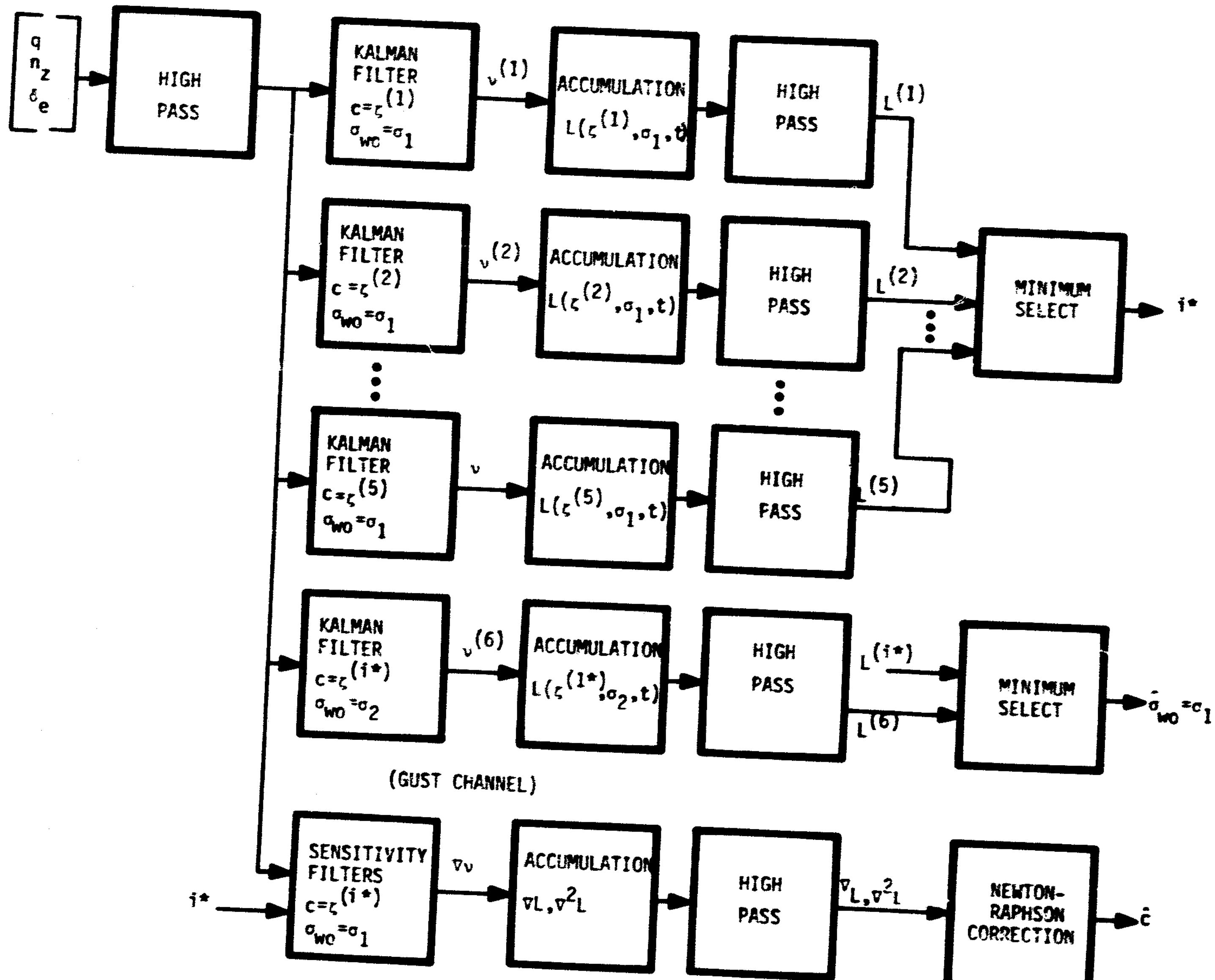

Figure 5. Identifier with Two-Level Gust Estimation and Automatic Gain Adjustment

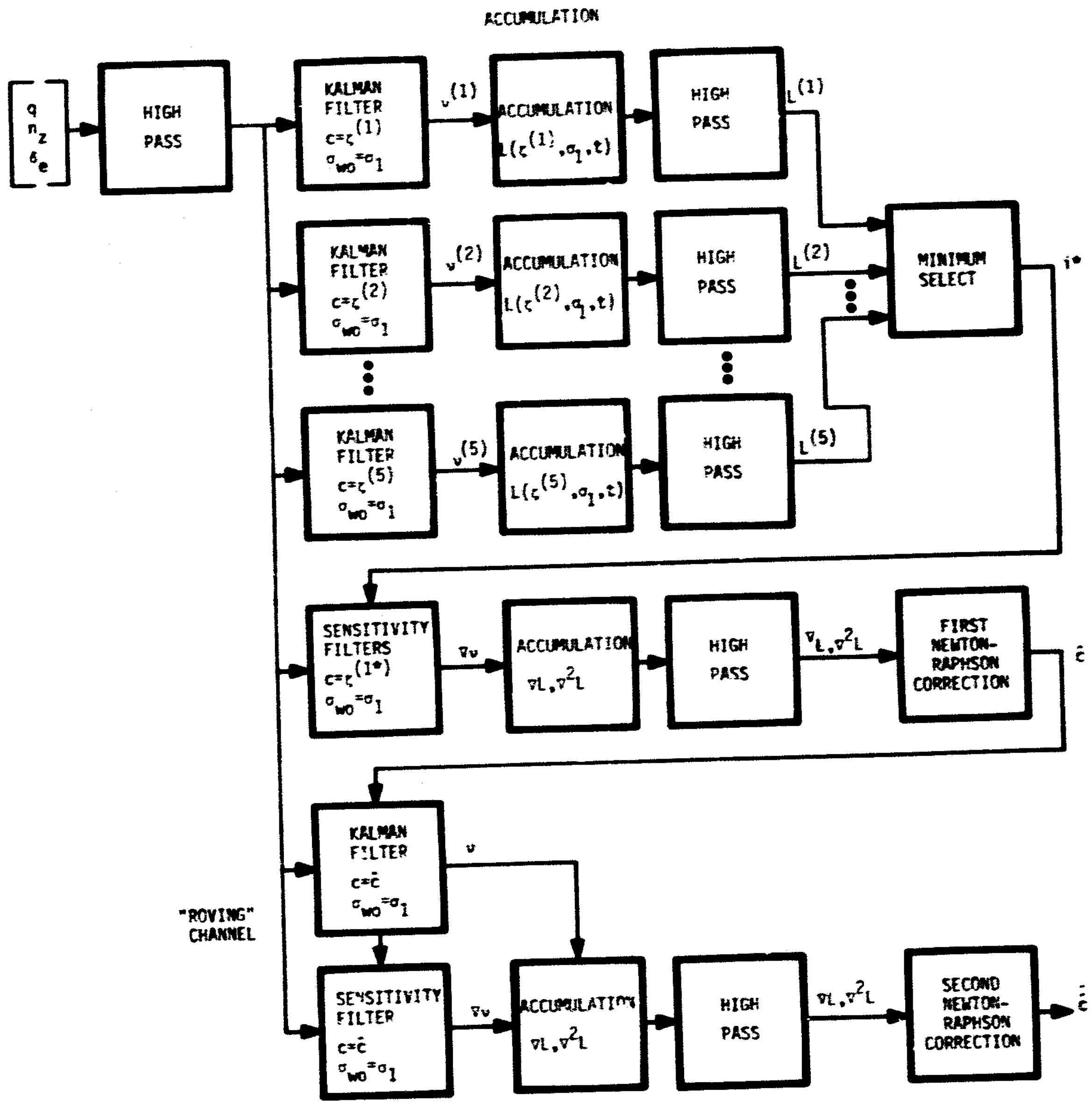

Figure 6. Identifier with Two-Step Parameter Correction

updated in real time. To make this process computationally efficient, the following approximations of the fixed channel modeling procedure are used in the software:

- Matrices A and B are approximated as described below.
- Gain matrices K are approximated from current min-L channel data:

$$K = K(i^*) + \nabla K\big|_{i^*} (\hat{c} - c^{i^*})$$

- Sensitivities for the approximated A, B and for H are explicit.
- Sensitivities for K are taken from the current min-L channel:

$$\nabla K = \nabla K\big|_{i^*}$$

These approximations are reasonable for small $\Lambda = \hat{c} - c^{i^*}$ and should not adversely affect the ability of the second Newton-Raphson step to estimate parameters. If Λ becomes very large, of course, the approximations deteriorate. It is even possible to get unstable A and K combinations. To protect against this possibility, the second Newton-Raphson step is automatically bypassed if its likelihood function diverges.

The A and B matrices used for the second Newton-Raphson step have the following approximated form:

$$A = \begin{bmatrix} 1 + M_q \Delta t & \Delta t M_\alpha & V & \Delta * M_\delta \\ V & 1 + \Delta t Z_\alpha & V & \Delta * Z_\delta \\ 0 & 0 & C & 0 \\ 0 & 0 & 0 & C \end{bmatrix}$$

$$B = \begin{bmatrix} B * A * M_\delta \\ B * A * Z_\delta \\ 0 \\ C \end{bmatrix}$$

where

$$A = \frac{\Delta t}{2} \left(1 + \exp(-12.5\,\Delta t)\right)$$

$$B = \frac{\Delta t}{2A} \left(1 - \exp(-12.5\,\Delta t)\right)$$

M_δ and Z_δ are corrected for flexibility

The seven terms circled in the A and B matrices are updated in real time. Elements A (1,1), (1,2), and A (2,2) use a first-order approximation in Δt. Elements A (1,4), A (2,4), B (1,1), and B (2,1) have essentially a second-order approximation. The variation of three terms in the A matrix, A (1,3), A (2,1), A (2,3), is neglected. These are small terms with small percentage variations and are fixed at the model values for which the second Newton-Raphson step was initialized.

In order to provide flexibility for tuning the above model approximations, the coefficients M_q, M_α, M_δ, Z_α, $Z_\delta V$ can be adjusted independently from the nominal channel values. Their values are set through the common block F8 MODL which is read via NAMELIST VARL at initialization. This feature was specifically used to modify the M_q function at supersonic conditions to better match damping of the exact and approximated models.

SECTION 4

PCMLE SOFTWARE IMPLEMENTATION

This section describes the software structure, software management and control procedures, and acceptance test procedures which were used to implement the PCMLE algorithm on DFRC's RAV facility.

The PCMLE software was developed for and successfully verified on the Control Data CYBER 73-28 computer at NASA/DFRC. All the software is written in standard FORTRAN IV and is intended to be transferrable to the RAV computer (Varian V-73) for eventual flight test experiments.

SOFTWARE STRUCTURE

An overview of the PCMLE software organization is shown in Figure 7. The computations are divided into a background (non-real-time) segment to define and initialize Kalman filter channels and a real-time segment to process sensor data for parameter identification. Calculations performed in each of these segments are divided among a number of subroutines, as listed in Table 1. The functions of each segment and their input/output structures are briefly described below. The core required for PCMLE is 5655 locations for subroutines plus 2730 locations for storage arrays.

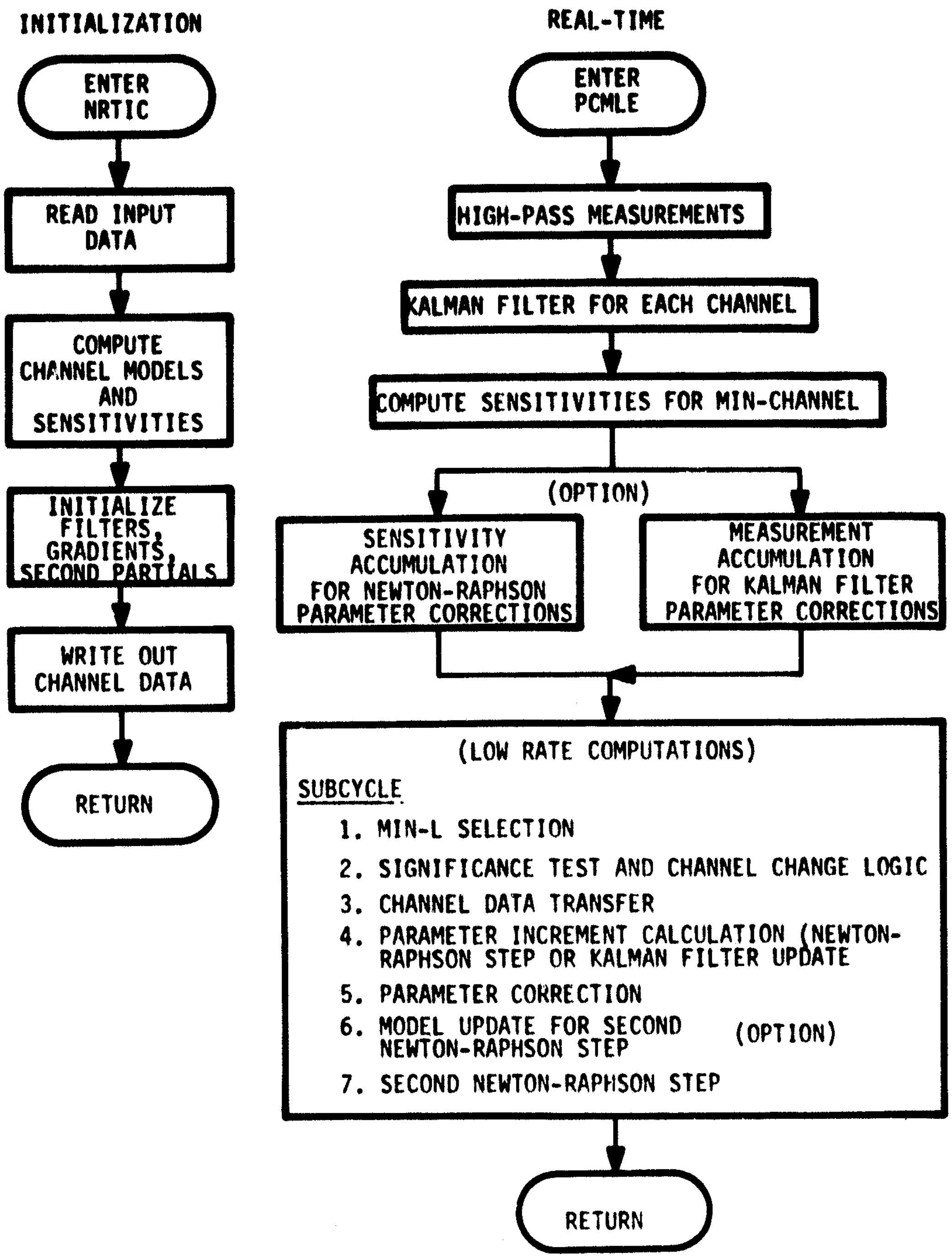

Figure 7. PCMLE Software Structure

TABLE 1. PCMLE SUBROUTINES

Non-Real-Time Subroutines	Functions	Core Required (decimal)
NRTIC	Main executive routine for non-real-time operation. Reads data to define number and location of channels, number of parameters estimated, sample rate, etc. Performs all initialization with calls to other subroutines.	930
MODEL	Defines the system matrices and sensitivities for the discrete four-state model described in Section 2.	638
FHIC	Computes high-pass filter coefficients and initializes filter states for each measurement to be high-passed.	13
DIAK CAL	Solves Ricatti equations for the Kalman filter gains of a discrete system, using double iteration procedures.	401
POLES, QRCALL QR, HESSEN	Computes eigenvalues for channel models and their Kalman filter dynamics.	730
Real-Time Subroutines		
PCMLE	Main executive routine for parallel channel MLE real-time computations.	1767
FH	High-pass filter applied to measurements.	14
TSIG	Produces test signal and two random numbers for simulated sensor noise.	41
FILT	Performs fourth order Kalman filter update computation.	95

TABLE 1. - Concluded.

Real-Time Subroutines	Functions	Core Required (decimal)
SENS	Performs a sensitivity filter update for a given parameter.	176
ACCNR	Accumulates likelihood gradients and approximate second partials for a Newton-Raphson parameter correction.	177
SENS2	Performs sensitivity filter updates for "roving" channel of second Newton-Raphson step.	176
ACCNR2	Accumulates likelihood gradients and approximate second partials for second Newton-Raphson step.	177
ACCK	Accumulates measurements for a Kalman filter parameter correction.	32
KBF	Performs a Kalman filter parameter correction.	288

Initialization

The initialization of PCMLE is performed in non-real time with a call to subroutine NRTIC. This subroutine reads the input data deck and user options (UX and LX arrays) and checks the input data for reasonableness. It then defines the specified numbers of channels, each at its specified parameter values. Each channel is a four-state Kalman filter. The states are pitch rate, total angle-of-attack, gust angle-of-attack, and elevator surface position. The two measurements are pitch rate and normal acceleration. The input to the filter is elevator servo position. Two sets of gains are computed and stored for each channel, corresponding to low and high turbulence levels. Sensitivities are computed for each channel and gust level by individually perturbing each of four parameters to be estimated. Eigenvalues are computed for each channel model and each Kalman filter. All computations are performed for the sample rate specified.

Real-Time Operation

All real-time computations are executed with CALL PCMLE (IT, IOUT), where IOUT is a four-component vector for uplink. IOUT(1) is the uplink parameter used for gain scheduling. The scalar IT is not currently used but would be available to further partition the real-time calculations should this be required by the RAV executive. PCMLE is called once per sample time. On the CYBER 73-28 computer, each call required 5 to 6 msec of computer time.

During each call, the sampled values of pitch rate, normal acceleration, and elevator servo position are high-passed. Residuals and likelihood functions are computed for each channel (fixed in parameter space). Gradients and second partials are accumulated if Newton-Raphson parameter corrections are selected. Otherwise, measurements are defined for a Kalman filter parameter correction. The remaining real-time operations are spread over seven subcycles executed in sequence, as shown in Figure 7. During real-time operation, the detailed performance of the algorithm can be monitored by the UX array. This is defined later in the subsection on outputs from PCMLE.

If the sample skipping option is selected, the sample time is modified automatically by NRTIC. However, PCMLE must then be called at the appropriate new sample rate. Either one or two samples may be skipped in this manner.

Real-Time Inputs to PCMLE--Real-time inputs to PCMLE from the RAV program are assigned to user array elements UX(11) through UX(18) and UX(20). UX(11) through UX(13) hold the usual measurements needed by the identifier; UX(14) and UX(15) are used to compute an average elevator servo position when the sample skipping option is used. UX(16), UX(17) and UX(18) are used to communicate "true" values of $M_{\delta o}$, M_{α}, and $\bar{q}$ when these quantities are supplied by a simulation, and, finally, UX(20) provides real-time adjustment of test signal magnitude. These inputs and their units are summarized in Table 2.

Real-Time Outputs from PCMLE--Provision has been made for four outputs to be supplied via the calling argument IOUT. At present only IOUT(1) is used. It is a $1/\bar{q}$ estimated from $M_{\delta e}$ and scaled to be between 0 and 512. (Scale factor is 50000.)

Other outputs from PCMLE are contained in the real-time UX array. The scaled test signal is in UX(19). The remaining outputs are in UX(1) through UX(10) and UX(21) through UX(50). These are primarily used for monitoring PCMLE performance. All PCMLE outputs are defined in Table 3.

TABLE 2. REAL-TIME INPUT VARIABLE ASSIGNMENT

User Variables	Description	Mnemonic Expression	Units
UX(11)	Pitch rate	Y (1)	rad sec^{-1}
12	Normal acceleration	Y (2)	ft sec^{-2}
13	Servo position at current time t_k	DELTA (1)	rad
14	Servo position at t_{k-1}	DELTA (2)	rad
15	Servo position at t_{k-2}	DELTA (3)	rad
16	RAV $\bar{q}$ estimate	QBART	lbs ft^{-2}
17	RAV $M_{\delta o}$ estimate	MDOT	sec^{-2}
18	RAV M_{α} estimate	MAT	sec^{-2}
20	Test signal magnitude	SIGUT = SIGUTO + UX (20) $0 \leq$ SIGUT $\leq$ 40**	ft sec^{-2}

TABLE 3. REAL-TIME PCMLE OUTPUTS

User Variables	Description	Mnemonic Expression	Units
UX(1)	Channel indicator	10 * (IG-1) + JS	--
2	First $M_{\delta o}$ estimate	ZP1	sec^{-2}
3	First M_{α} estimate	MA	sec^{-2}
4	First V estimate	V	$ft\ sec^{-1}$
5	First $Z_{\alpha}V$ estimate	ZAV	sec^{-1}
6	Residual level estimate	SIGSQ	--
7	First $M_{\delta o}$ error	100 *(ZP1-MDOT)/Min(ZP1, MDOT)	Percent
8	First M_{α} error	100 *(MA-MAT)/Min(MA, MAT)	Percent
9	First $\bar{q}$ error	100 * (QRAR-QBART)/Max(QBAR, QBART)	Percent
10	Minimum probable $M_{\delta o}$	Z1MIN	sec^{-2}
19	C* test signal	UT/100	$ft\ sec^{-2}$
21	PCMLE output index	INDEX = 17 + UX(21) $1 \leq INDEX \leq 17$	--
22	Second $M_{\delta o}$ estimate	ZP12	sec^{-2}

TABLE 3. - Concluded

User Variables	Description	Mnemonic Expression	Units
23	Second M_α estimate	(0.61 + 0.92 *ZP22)*ZP12	sec^{-2}
24	Second V estimate	(200. + ZP32) * SQRT (-ZP12)	sec^{-1}
25	Second $Z_\alpha V$ estimate	(53. + ZP42) * ZP12	sec^{-1}
26	PCMLE output scale	SCALE = 1000. + UX(26) E-10 ≤SCALE ≤ E + 10	Variable
27	Second $M_{\delta o}$ error	100 (ZP12 - MDOT)/ZP12	Percent
28	Second $\dot{M}_\alpha$ error	100 (MA2 - MAT)/MA2	Percent
29	Total angle-of-attack	ALPHT	rad
30	Gust angle-of-attack	ALPHG	rad
31-40	User selected outputs	(X(I, INDEX) SCALE, I = 1,2..., 10)	Variable
41-50	Pseudo channel probabilities	100 *SS(I), I = 1,2..., 10	--

Several halt conditions have been defined for PCMLE. These are listed in Table 4. The first two stops occur in the initialization mode if the data does not define a stable filter. The last three stops occur in real time if the parameter update option is not defined. In all the test cases run, these stops have never been encountered. However, in the final flight test software, they may be switched to a mode change operation rather than a halt.

TABLE 4. PCMLE HALT CONDITIONS

Stop	Condition
41	Ricatti equation not converging in subroutine CAL during initialization (Unstable Model).
31	Inverse does not exist in subroutine DIAK for computer filter gains. Check data deck.
21	No inverse exists in Newton-Raphson parameter update.
22	No inverse exists in second Newton-Raphson parameter update.
11	No inverse exists in Kalman parameter update.

User Inputs and Outputs

Both the background (initialization) and real-time program segments provide user inputs and options. These inputs are selected with a nominal data deck and/or by setting the UX and LX user arrays in the RAV software.

The UX array serves different functions depending on whether the program is in the real-time or in the initialization segment. Both functions are defined below.

<u>Data Deck Inputs</u>--Following loading, the RAV program (containing all the PCMLE subroutines) executes the non-real-time initialization segment. During the first such initialization operation, subroutine NRTIC reads a data deck and stores it on a temporary disk file for quick restarts.

The input parameters which are read-in on data cards are defined in Table 5. The data deck defines nominal (default) values for all program parameters including the five channel locations tabulated in Table 6 (and illustrated in Figure 3).

<u>Console Inputs Prior to Initialization</u>--Certain logical variables (LNs) defined in Table 7 may be assigned from the control console prior to initialization. If this step is bypassed, the PCMLE default option will be the basic PCMLE algorithm (Figure 2) with a single Newton-Raphson parameter correction. These logicals cannot be altered in real time. To change them the user must leave real time and reinitialize.

It is also possible to redefine certain data deck parameters prior to initialization by setting UX elements from the console. These elements are listed in Table 8. The redefinition is performed as follows:

$$\text{Variable} = \left\{ \begin{matrix} \text{Nominal} \\ \text{default} \\ \text{value from} \\ \text{data deck} \end{matrix} \right\} + \left\{ \begin{matrix} \text{UX array} \\ \text{value} \end{matrix} \right\}$$

TABLE 5. NAMELIST PARAMETERS

Parameter	Definition	Nominal Value
NX	Number of states in Kalman filter (q, α, αg, δ)	4.
NR	Number of measurements (q, Nz)	2.
NN	Number of noise sources (αg, q sensor, Nz sensor, δ sensor)	4.
NRM	Maximum number of measurements	3.
EE	Convergence criteria in DIAK for Ricatti solution	10^{-6}
ITER	Maximum number of iterations in DIAK for Ricatti solution	20.
DTO	Nominal sample time (automatically increased if samples are skipped)	0.02
DT PRINT	Print interval when LX(5) is true (available in batch mode only)	0.5
NC	Number of channels	5.
NPO	Number of parameters estimated in first Newton-Raphson step	2.
JSO	Starting channel location	3.
IGO	Starting gust level	1.
WUTO	Natural frequency of shaping filter on random test signal	6.
DUTO	Damping of shaping filter on random test signal	1.25

TABLE 5. - Continued

Parameter	Definition	Nominal Value
SIGUTO	Gain of shaping filter on random test signal	4.
UT10	Initial state of shaping filter on random test signal	0.
UT20	Initial state of shaping filter on random test signal (above state initialization is useful for generating deterministic square waves or sine waves with TSIG subroutine)	0.
UTMAX	Magnitude limit of filtered test signal	10.
TAUP0	Time constant of likelihood accumulation filter	5.
TAUP2	Time constant of low-pass filter on L, ∇L, $\nabla^2 L$	0.6
WHP	Cutoff frequency of second-order high-pass on measurements	2.
DHP	Damping of second-order high-pass on measurements	0.7
NP20	Number of parameters in second NR update	2.
SIGGO	RMS statistic assumed for gyro noise (deg/sec)	0.15
SIGACCO	RMS statistic assumed for accelerometer noise (g)	0.02
SIGWLO	RMS statistic assumed for low w gust level (ft/sec)	1.0
SIGWHO	RMS statistic assumed for high w gust level (ft/sec)	5.0

TABLE 5. - Continued

Parameter	Definition	Nominal Value
HYSTO	RMS statistic assumed for elevator servo hysteresis (rad)	10^{-4}
RTJGO	Threshold parameters controlling gust level switch	0.01
THRTJGO		3.22
RTJCO	Threshold parameters controlling channel switch	0.1
THRTJCO		3.22
RTJZO	Threshold parameters controlling Z1MIN selection	0.1
THRTJZO		13.8
RTJSO	Threshold parameter for significance of likelihood function	0.25
ZP1 MAX	Maximum value limit of parameter 1 estimate	-1.
ZP2 MAX	Maximum value limit of parameter 2 estimate	1.3
ZP3 MAX	Maximum value limit of parameter 3 estimate	120.
ZP4 MAX	Maximum value limit of parameter 4 estimate	10.
ZP1 MIN	Minimum value limit of parameter 1 estimate	-75.
ZP2 MIN	Minimum value limit of parameter 2 estimate	-0.3
ZP3 MIN	Minimum value limit of parameter 3 estimate	-60.
ZP4 MIN	Minimum value limit of parameter 4 estimate	-10.

TABLE 5. - Continued

Parameter	Definition	Nominal Value
GSQLO	Diagonal elements of $\nabla^2 L$ matrix (four numbers)	0.001 0.1 0.0003 0.01
ZP	Matrix defining location of channels (4 parameters per channel x 10 channels max = 40 numbers)	See Table 6
NRKF	Number of measurements in KF parameter correction (q, Nz)	2.
NXKF	Number of states in KF parameter model ($Z_1, Z_2, Z_3, Z_4, \dot{Z}_1$)	5.
NHKF	Number of gradient measurements available in KF parameter correction	4.
T1KFO	Parameters in KF state model	0.001
T2KF	Parameters in KF state model	1.0
NCYC	Number of subcycles	7.
QDO	Initial covariance matrix for KF parameter correction (five numbers)	0. 5×10^{-6} 0.2 0.0045 0.005
ISKPO	Number of measurements skipped (0, 1 or 2)	0.
NSO	Signal-to-noise ratio (increased residual noise statistics at high signal levels)	0.05

TABLE 5. - Concluded

Parameter	Definition	Nominal Value
MQ0	Coefficients which define channel models from M_δ, C_2, C_3, C_4 via:	-0.23
MQ1		0.028
MQ12	$M_q = MQ0 + (MQ1 + MQ12 * C2)\, M_\delta$	0.03
MA1	$M_\alpha = (MA1 + MA12 * C2)\, M_\delta$	0.61
MA12	$V = (V1 + C3) \sqrt{-M_\delta}$	0.92
V1	$Z_\alpha V = (ZAV1 + C4)\, M_\delta$	200.
ZAV1	$Z_\delta V = ZDV1 * M_\delta$	53.
ZDV1		7.7
DIST	Distance Nz is measured aft of c.g. (ft)	15.15
ACTBW	Bandwidth of first-order actuator model for δ_e (rad)	12.5
FX1	Quasi-static flexibility corrections:	0.016
FX2	$M_\delta = (1. + M_{\delta o}\, (FX1 + M_{\delta o} FX2))$	0.0002
ZP1C	if $M_{\delta o} < ZP1C$ $M_\delta = (1. + ZP1C\, (FX1 + (ZP1C)\, FX2)$	-40.
SL	Scale length in gust model (ft)	1750.
QME	Scale factor between $\bar{q}$ (psf) and $M_{\delta o}$ $(\bar{q} = QME * M_{\delta o})$	-22.
ALPHWL	Bias between water line α and zero lift α (rad)	0.0086

TABLE 6. NOMINAL CHANNEL LOCATION

Channel	Parameters			
	M_{δ_e}	C_2	C_3	C_4
1	-2.34	0	0	0
2	-5.27	0	0	0
3	-11.9	0	0	0
4	-26.7	0	0	0
5	-26.7	1.	60.	0

TABLE 7. INITIALIZATION USER LOGICAL ASSIGNMENTS

User Logical	Function	Mnemonic
LX(1)	Not used	
2	Not used	
3	Enables Kalman parameter correction in place of first Newton-Raphson correction	KAL
4	Not used	
5	Not used	
6	Enables second Newton-Raphson step	NR2
7	Not used	
8	Inhibits initial model printout during initialization	None
10	Adds pseudo-random sensor noise to PCMLE's input measurements	NOYS
9-50	Not used	

Default Values = LX(I) = .F.

TABLE 8. INITIALIZATION USER VARIABLE ASSIGNMENTS

User Variable	Description "Variable Adjust..."	Mneumonic Expression VAR = VARO * UN(I)	Units	Program Imposed Limits a < VAR < b
UN(2)	Test signal bandwidth	VAR = WFT	rad sec^{-1}	1., 10.
3	Test signal damping	DFT	--	0., 10.
4	Gyro noise sigma	SIGG	deg sec^{-1}	0.01, 10.
5	Accelerometer noise sigma	SIGACC	g's	0.001, 1.
6	Low gust sigma	SIGWL	ft sec^{-1}	0., 10.
7	High gust sigma	SIGWH	ft sec^{-1}	0., 100.
8	Elevator noise sigma	HYST	rad	0., 0.2
9	Data accumulation time	TAUP	sec	1., 500.
10	Initial channel	JS	--	1., NC
11-20	(See real-time UN table)			
21-25	Parameter model noise intensity	VAR = QDD(I), I=1,5	--	0., E - 10
26	Parameter model time constant	TIKF	sec	100., E - 10
27	Sample time	DT	sec	.01, .1
28	Number of samples skipped	ISKP	--	0, 2
29	Signal-to-noise ratio	NS		0, 10

TABLE 8. - Concluded

User Variable	Description "Variable Adjust..."	Mnemonic Expression VAR = VARO + UNQ	Units	Program imposed Limits VAR ≤
31	Initial gust level	JG	--	1, 2
32	Number of parameters in first Newton-Raphson or Kalman step	NP	--	1, 4
33	Number of parameters in second Newton-Raphson step	NP2	--	1, 4
34	Gust change trip ratio	RTJG	--	0., 10.
35	Gust change trip threshold	THRTJG	--	0., 100.
36	Channel change trip ratio	RTJC	--	0., 10.
37	Channel change trip threshold	THRTJC		0., 100
38	Parameter probability trip ratio	RTJZ	--	0., 10.
39	Parameter probability trip threshold	THRTJZ	--	0., 100.
40	Residual estimated trip ratio	RTJS	--	0., 10.

Default Values: UNQ = 0

If computed VAR value falls outside limits, VAR is set back to VARO.

Should the adjusted variable fall outside of program imposed limits, the variable is returned to the default value. It is also important to note that RAV resets all UX array values to zero whenever the program leaves real time. Hence, desired changes of the nominal data deck must be reentered into the UX array before each reinitialization.

Console Inputs during Real-Time Operation--The logicals defined in Table 9 can be set and reset during real-time operation. If they are set in non-real time, then the corresponding mneumonic will be defined in the PCMLE subroutine as soon as real time is entered.

Only one user variable, UX(20), can be set from the console in real time. Its function is to alter PCMLE's test signal magnitude (see Table 2).

SOFTWARE CONFIGURATION CONTROL PLAN

Effective on the date of acceptance at DFRC, a software configuration control plan was implemented to protect the integrity of the PCMLE program. The control plan includes the following elements:

- Source file management
- Change reporting and execution
- Verification test

Each of these elements is discussed below.

TABLE 9. REAL-TIME USER LOGICAL ASSIGNMENTS

User Logicals	Function	Mnemonic
LX(1)	Disables automatic channel changes	NOCHC
2	Disables first Newton-Raphson or Kalman step	NOEST
3	Not used	
4	Disables automatic gust level changes	NOCHG
5	Enables printout from PCMLE (use in batch mode only)	PRINT
6	Not used	
7	Not used	
8	Not used	
9	Enables PCMLE algorithm	MLE
10-50	Not used	

Default Values: LX(I) = .F.

Source File Management

Files of controlled software documentation were established following verification of program operation on the RAV facility. Duplicate files are being maintained at both DFRC and Honeywell. Each file contains:

- PCMLE source deck
- Flowcharts
- Listings (current plus two previous versions)
- User information
- Change notices

To maintain a record of the software, changes in any item require a properly executed change notice.

Change Reporting

The change notice required for controlled file alteration is a standard form having the following parts:

A) Reason for change--Brief summary of problem.

B) Description of change--Specific program changes, documentation changes, and affected procedures. Mark-up copies of documents affected by change are attached.

C) Functional checkout--Provisions of checkout procedures required to verify correct operation of modification.

D) Program change report--Listing of who performed the changes, data performed, and verification procedures followed.

Each change notice must be signed off by the originator and approved by Honeywell's program manager. A sample change request form is shown in Figure 8.

Verification Test

Verification tests are those procedures that are performed to assure that software changes are accomplished in the intended manner. The following actions are taken:

- Following change in the master source deck, a new listing is run and checked against the change notice requirements.
- For critical changes, portions of the acceptance test routines are run. These requirements are listed in part (C) of the Change Request.

PCMLE ACCEPTANCE TEST

This section summarizes the procedures followed in conducting the PCMLE Acceptance Test on the F-8C simulation at NASA Dryden Flight Research Center. Test conditions, selected time histories, and interpretation are given below.

Program: PCMLE

FORTRAN SOFTWARE PROGRAM CHANGE REQUEST			Number
Originator	Date	Approval	Date
Effectivity		Title of Change	

A) Reason for Change

B) Description ot Change

Change Statement No. Statement

C) Functional Checkout

D) Change Report

Who performed Change/Checkout Date

Figure 8. Software Change Request Form

Definition of Test Cases

Acceptance test cases were jointly defined by DFRC and Honeywell personnel. They are summarized in Table 10.

Detailed Test Procedure and Conditions

The acceptance test was run on the CDC Cyber 73-28 Computer in real time. The F-8C simulation with the control laws function as one program, the RAV executive with PCMLE as another. Data interchange was accomplished via D/A and A/D trunk lines as presently mechanized in the RAV mode.

The acceptance tests used a standard acceleration maneuver. The F-8C simulation was brought to the 6100 m, 250 KIAS flight condition and trimmed to 1 g flight. The aircraft was then accelerated at constant altitude until it stabilized at a new velocity (approximately 300 m/sec). The simulation was run man-in-the-loop using the F-8C Iron Bird. Small pilot inputs were used as required to maintain trim.

Two eight-channel strip-chart recorders were used to obtain time histories of various aircraft response variables and selected PCMLE outputs. These figures are presented later in this section. For the performance evaluation we have the luxury of knowing "true" values of M_{δ_e} and M_α. These parameters were computed in real time by approximately determining the slope of the C_{M_δ} and C_{M_α} simulation functions. These approximated slopes were used with PCMLE estimates to compute the M_{δ_e} and M_α errors shown in the time histories.

TABLE 10. TEST CASES FOR ACCEPTANCE TEST

Test Case	Description
1	Baseline--Identification of M_{δ_e}, c_2, α_{gust}, and $\alpha_{rigid\ body}$ of the simulated F-8C. The maneuver was a full after-burner acceleration from 250 KIAS to 450 KIAS at 6100 m in the presence of 2 m/sec gust disturbance and no sensor noise. Five channels located as defined in Table 6 were used. The nominal sample rate was 50 sps.
2	Repetition of baseline in absence of gusts to show automatic adjustment of Kalman filter gains.
3	Repetition of Case 2 with a smaller number of parallel channels (4).
4	Repetition of Case 2 with a slower Kalman filter update rate (two samples skipped).
5	Repetition of Case 2 with Kalman filter parameter corrections instead of Newton-Raphson corrections.
6	Repetition of Case 2 with two Newton-Raphson iteration steps.
7	Repetition of Case 2 with two additional parameters estimated (C_3 and C_4).

The detailed test procedure is given in Table 11 and the acceptance criteria are shown in Table 12.

Acceptance Test Results

A successful acceptance test was completed at DFRC on 15 October 1976. Table 13 summarizes the time histories for each of the test cases. In some instances several additional time histories are included to illustrate the performance of the algorithm.

The performance of the algorithm is judged by examining the $\tilde{q}$ error traces and the M_α and M_{δ_e} error traces. For most cases the performance is as expected and compares with results in Reference 2. For the sample skipping cases there is an increase in the errors when the high gust channel is used. This effect warrants further investigation.

TABLE 11. ACCEPTANCE TEST PROCEDURE

Test Case	Procedure
1	PCMLE was initialized by reading the nominal input data cards (Reference 4). The program was then put into real-time operation. After 10 seconds, estimation was armed via logical MLE [LX(9), Table 9] and the accelerated maneuver was initiated. Variables appropriate to judging PCMLE were monitored in real time via CRT displays of UX and LX arrays and via strip chart recordings.
2	Same procedure as Baseline Test Case 1 is followed with no turbulence in the F-8C simulation.
3	PCMLE was reinitialized prior to this run. Only four channels were used. Channel 1 was deleted and Channels 2 through 5 were renumbered as 1 through 4. This verifies that fewer numbers of channels can be used and that their location can be moved. These changes were accomplished with a new input data deck. Following initialization, PCMLE was brought into real time and engaged as discussed under the Baseline case.
4	The PCMLE program was reinitialized with the sample skipping optional [UX(28) = 2, Table 8]. Every third measurement of q and Nz measurement was used, and the δ_e servo position measurements were used to compute an average value valid over the three-sample interval (Reference 4). The sample rate of the Kalman filters was one third of the simulation rate. Real-time operation was the same as discussed under the Baseline case.
5	PCMLE was reinitialized with the logical KAL set [LX(3), Table 7] and then brought into real time as discussed under the Baseline case.

TABLE 11. - Concluded

Test Case	Procedure
6	PCMLE was reinitialized with the NR2 logical set [LX(6), Table 7] and the NOEST logical [LX(2), Table 9]. This combination holds the first Newton-Raphson step at the channel location, and, hence, the second Newton-Raphson step should approximate the first step of the Baseline case. PCMLE was then brought into real time as discussed above. Two parameters were estimated by the second step.
7	PCMLE was reinitialized with NP = 4 [UX(32) = 2, Table 8] to estimate two additional parameters. Real-time operation was the same as the baseline.

TABLE 12. ACCEPTANCE CRITERIA

Test Case	Criteria
1	Qualitative--The channel switching shall be smooth and in the proper sequence (channels ordered in more negative M_{δ_e}). The parameter estimates shall be smooth during channel switches. Quantitative--The error in estimated dynamic pressure shall be within ± 50 percent of the "true" value throughout the transition.
2	The channel indicator shall show a switch to low gains when data permits, although it is not required to remain continuously on the low gust channel. Qualitative characteristics of baseline apply.
3	Since the first channel was not selected as a min-L channel in the baseline run, the results will match the baseline run except for renumbering of the channels (i.e., 1 was 2 in baseline, 2 was 3, etc.)
4	Only qualitative factors of baseline apply. Errors will approximately match baseline.
5	This run shall demonstrate improved tracking over the baseline case (less error in estimated dynamic pressure).
6	The estimates will approximately follow the baseline run. (Differences are due to model approximations included in the second Newton-Raphson computations.)
7	This run shall produce estimates of C_3 and C_4 with the qualitative characteristics of the baseline.

TABLE 13. ACCEPTANCE TEST SUMMARY

Test Case	No CH	Conditions			Time Histories		Comments
		Gusts	Sensor Noise	Maneuver	Aircraft (Figure #)	PCMLE (Figure #)	
1	5	Yes	No	Accel	8A	8B	This is the nominal test case. $\bar{q}$ error is within test requirement "smooth" estimates. Note use of gust channel during most of maneuver.
2	5	No	No	Accel	9A	9B	Same conditions as Case 1 except no gusts.
				Decel		9C	Note use of low-gust channels.
3	4	No	No	Accel	10A	10B	Same performance as Case 2 except channels renumbered.
4	5 5	No No	No Yes	Accel Accel	11A 11C	11B 11D	Slow update rate using Newton-Raphson process every third data point.
5	5 5	No No	No No	Accel Decel	12A	12B 12C	Kalman parameter update--note improved tracking over Case 2 at expense of somewhat noisier estimates.
	5	No	No	Accel		13	Slow update rate--process every third data point.
6	5 5	No No	No No	Accel Decel	14A 14C	14B 14D	Repeat of Case 2 using the roving channel for a second Newton-Raphson parameter update.
7	---	---	---	---	---	---	Extra parameters estimated displayed on CRT. Not plotted.

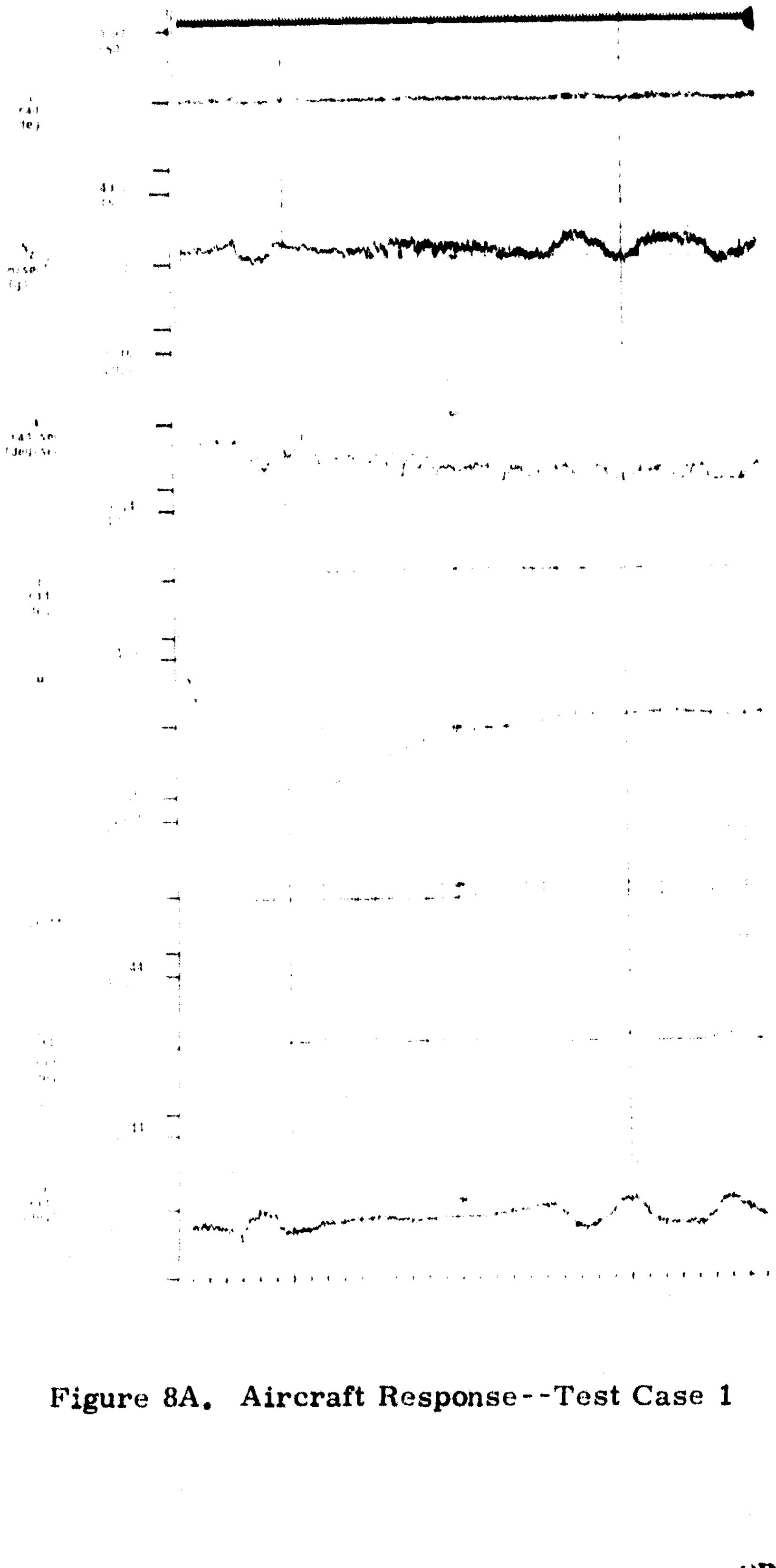

Figure 8A. Aircraft Response--Test Case 1

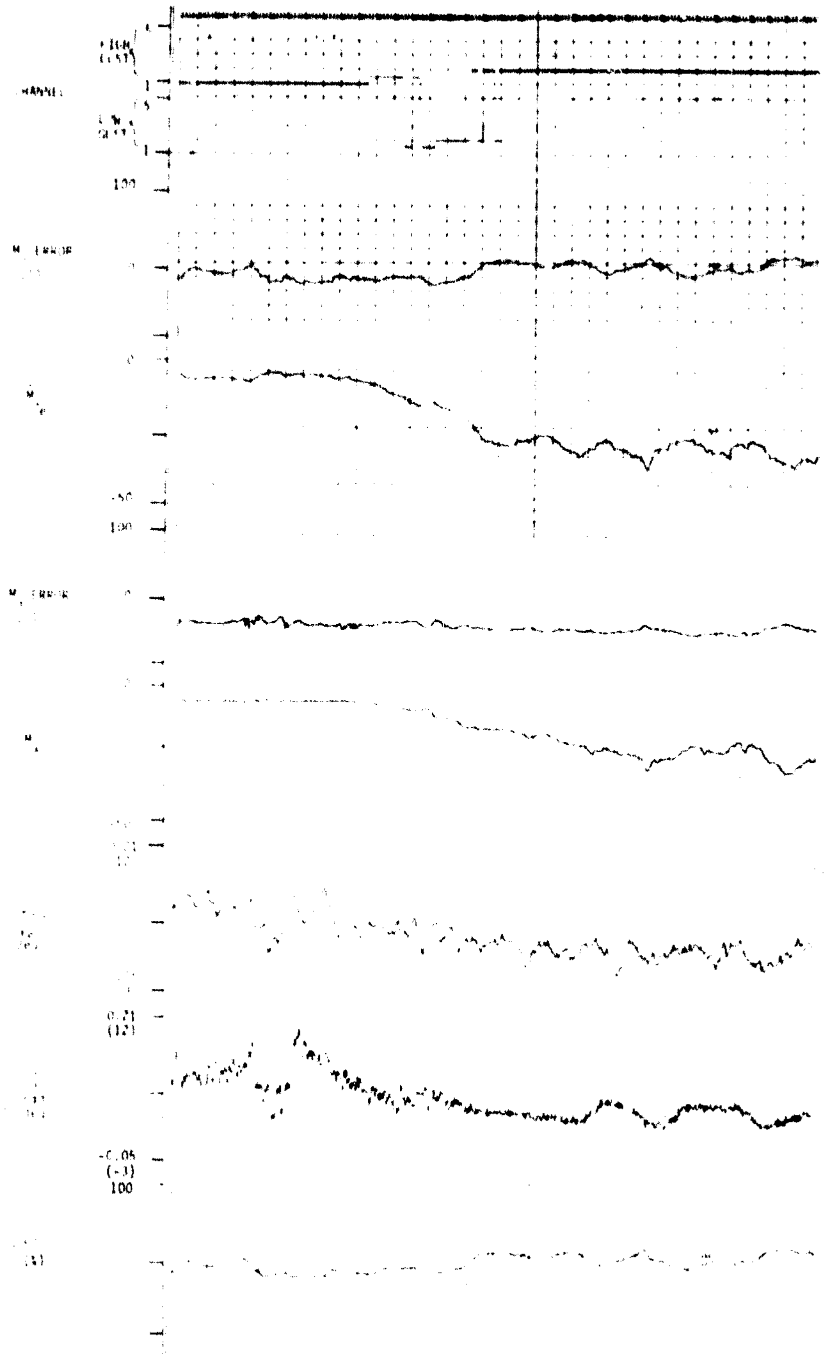

Figure 8B. PCMLE Response--Test Case 1

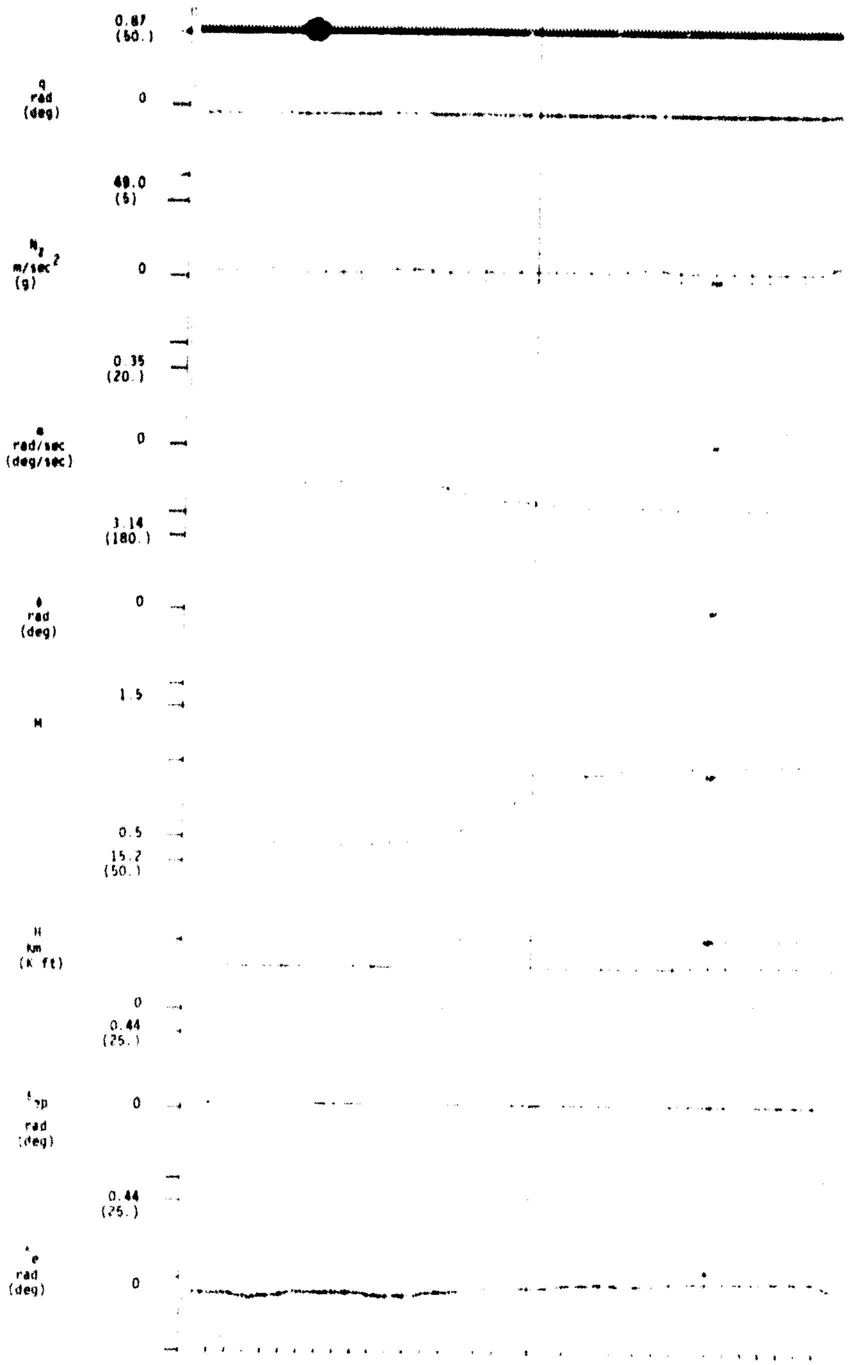

Figure 9A. Aircraft Response--Test Case 2

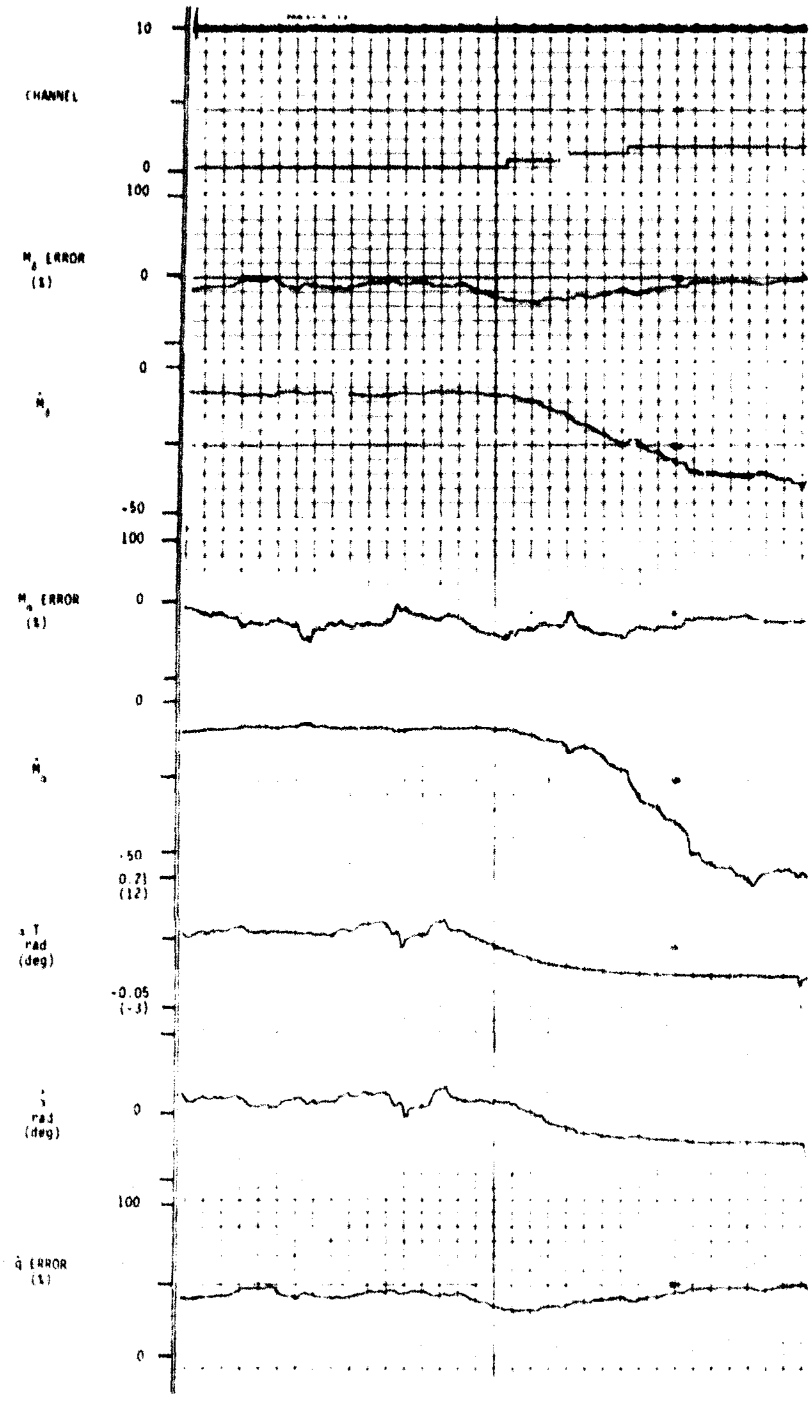

Figure 9B. PCMLE Response--Test Case 2

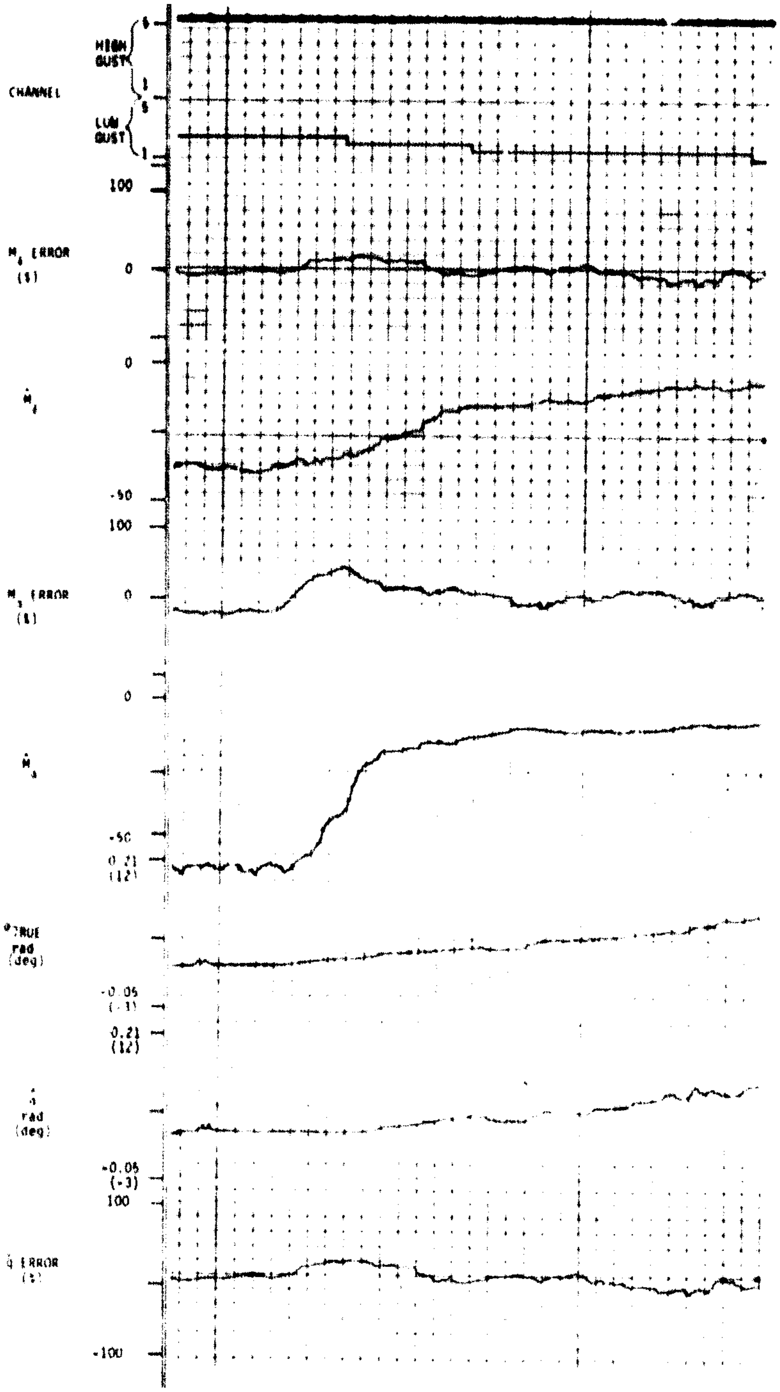

Figure 9C. PCMLE Response--Test Case 2 Deceleration

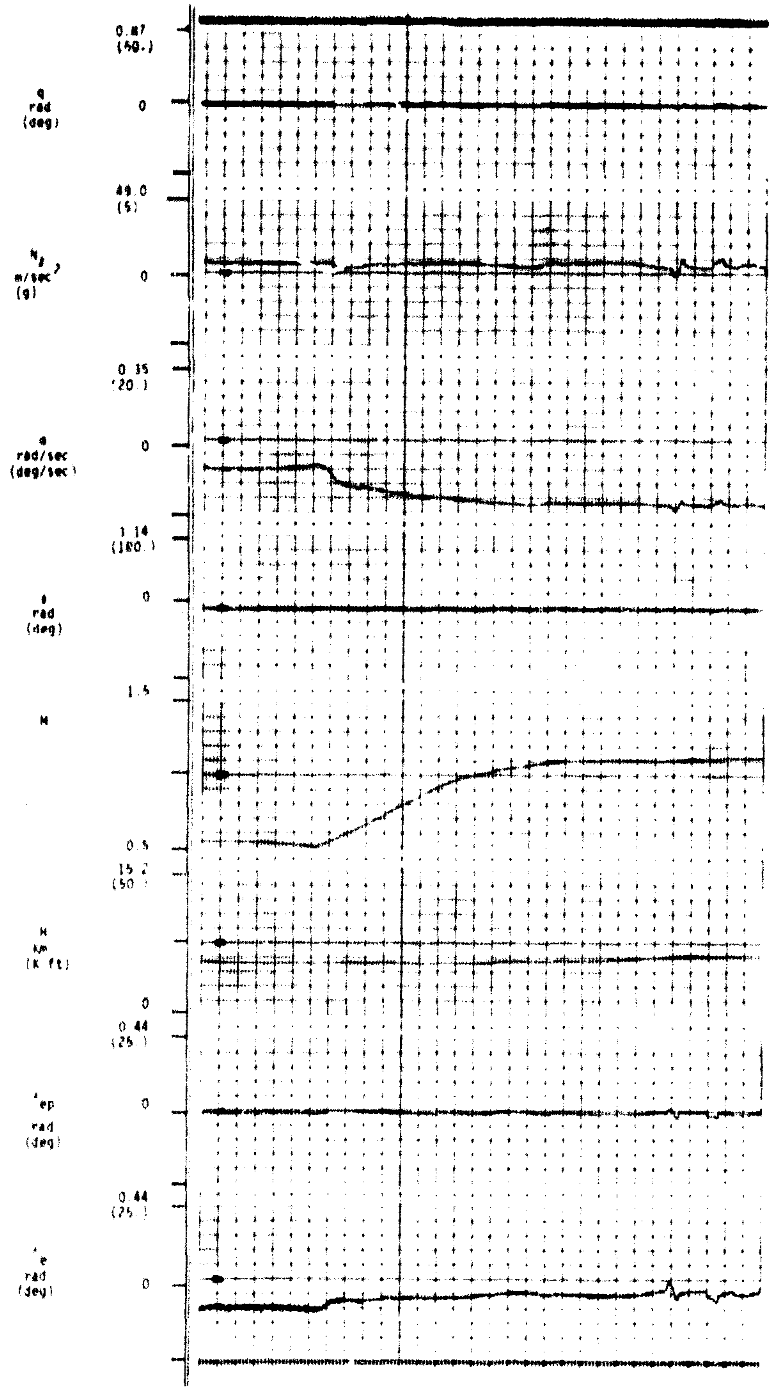

Figure 10A. Aircraft Response--Test Case 3

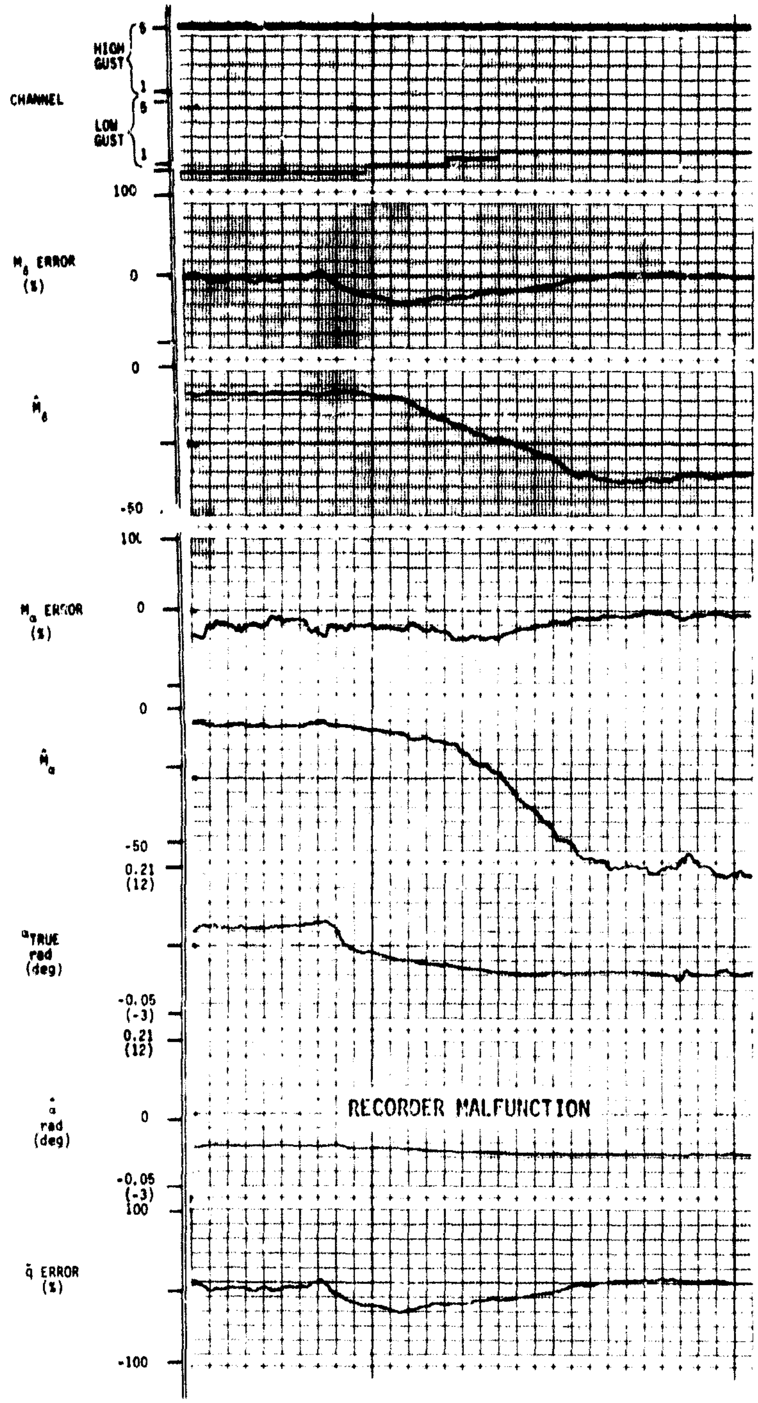

Figure 10B. PCMLE Response--Test Case 3

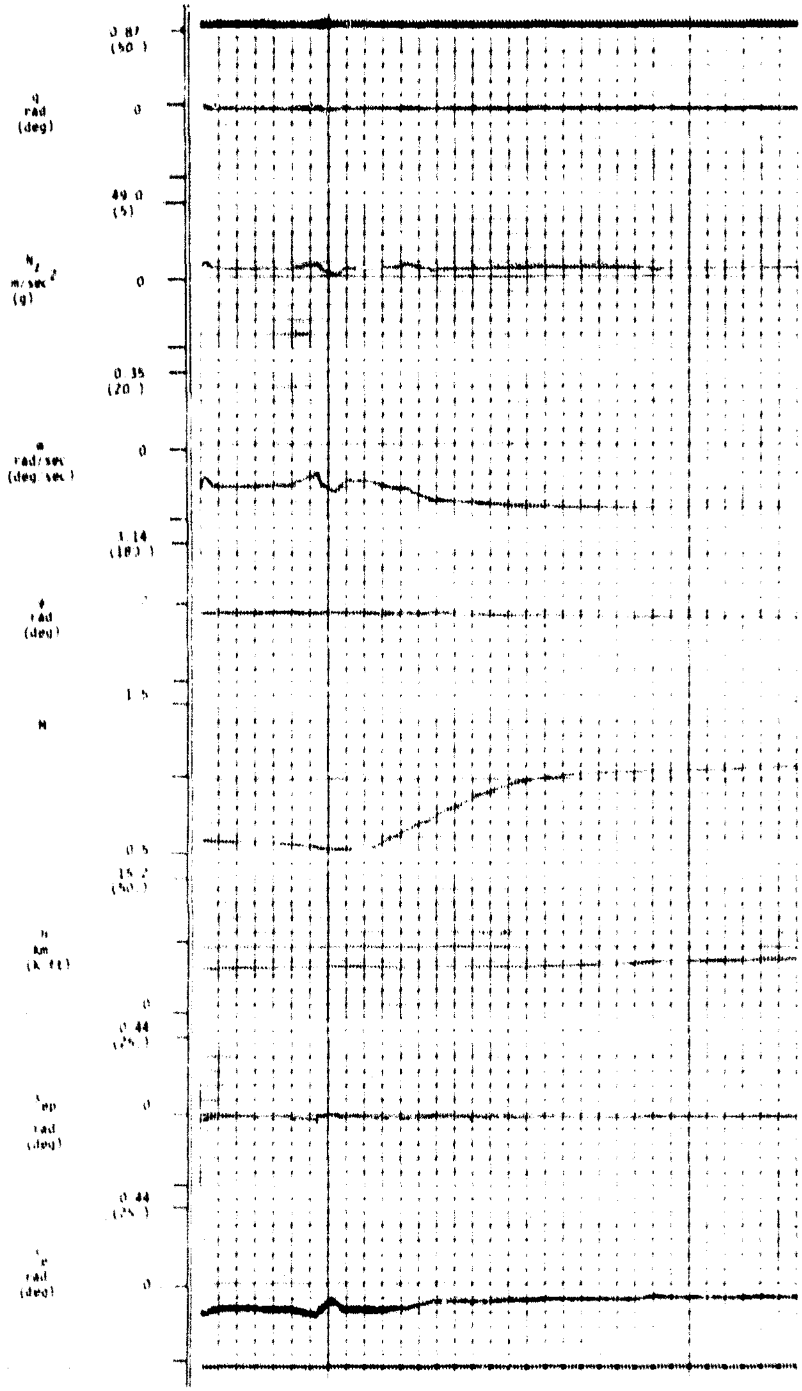

Figure 11A. Aircraft Response--Test Case 4

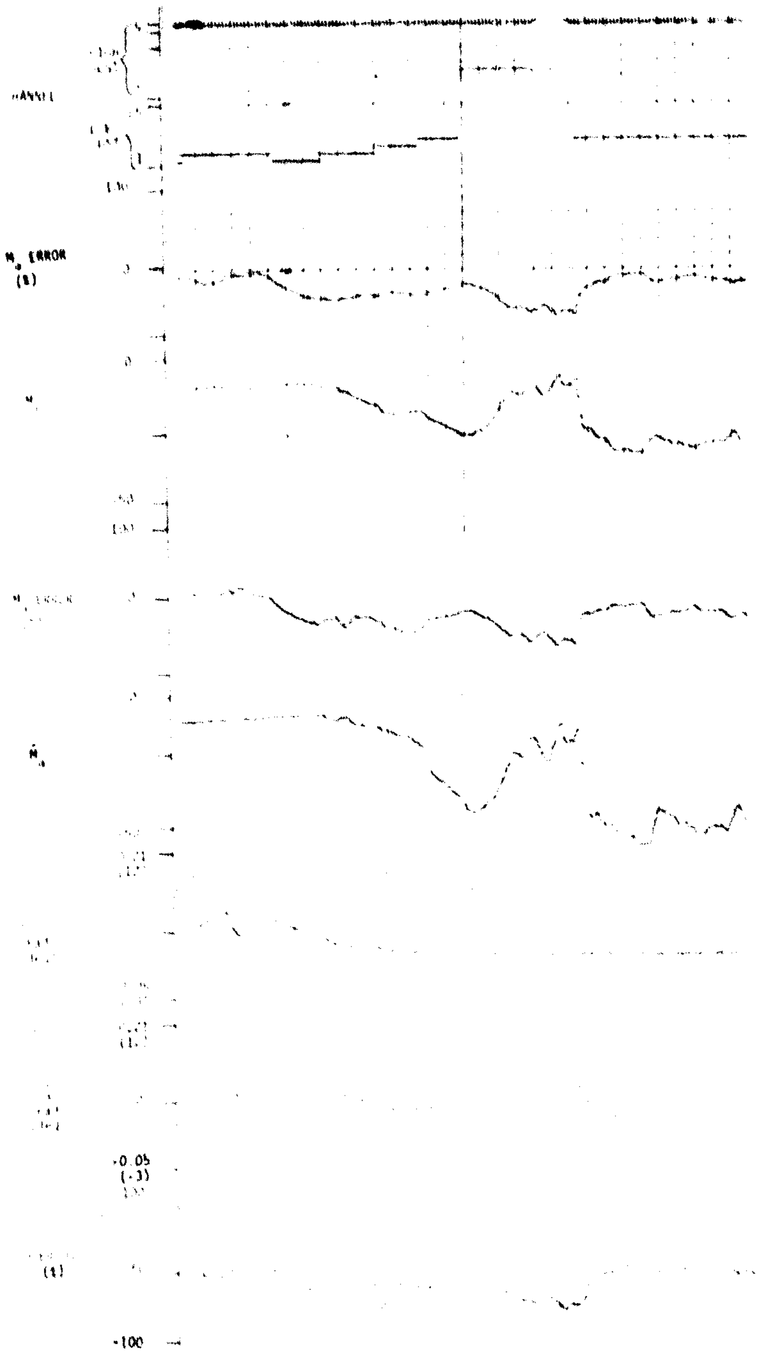

Figure 11B. PCMLE Response--Test Case 4

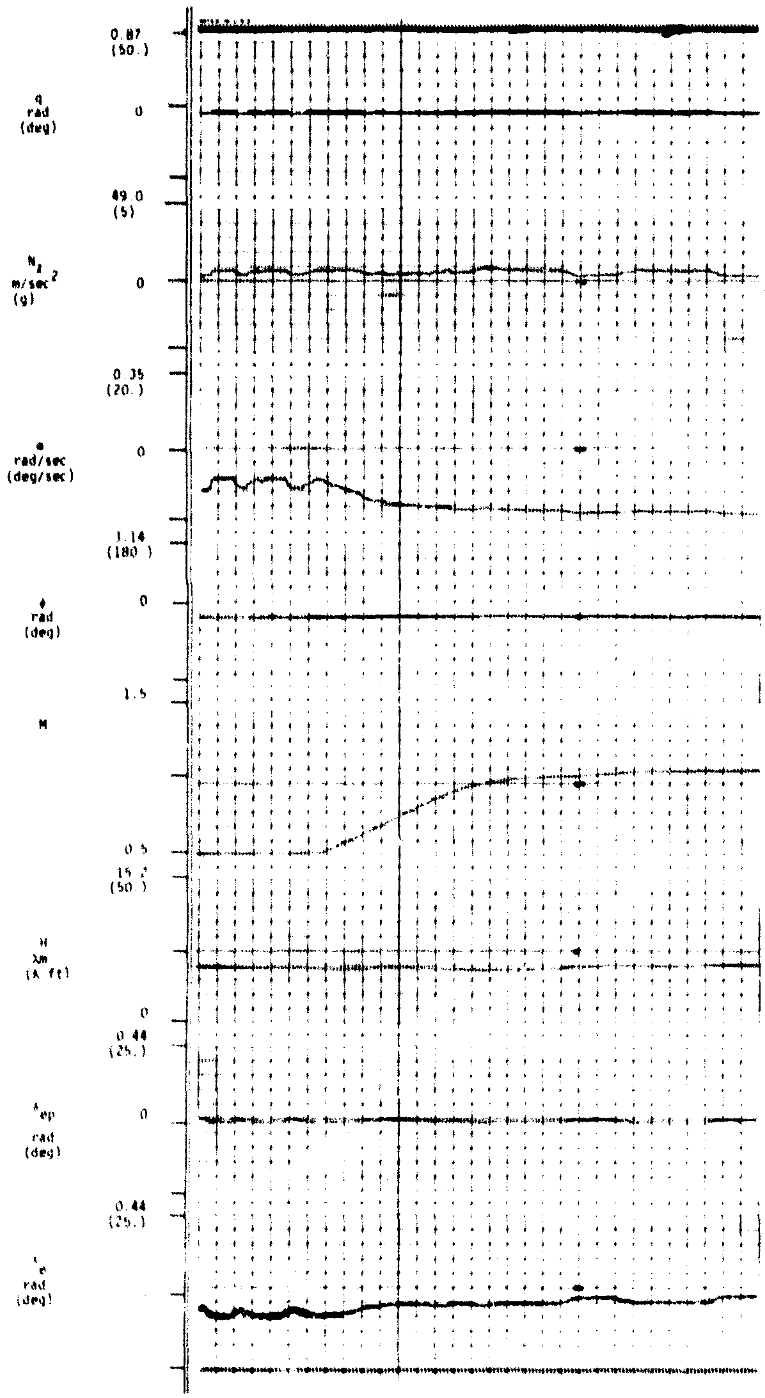

Figure 11C. Aircraft Response--Test Case 4 with Sensor Noise

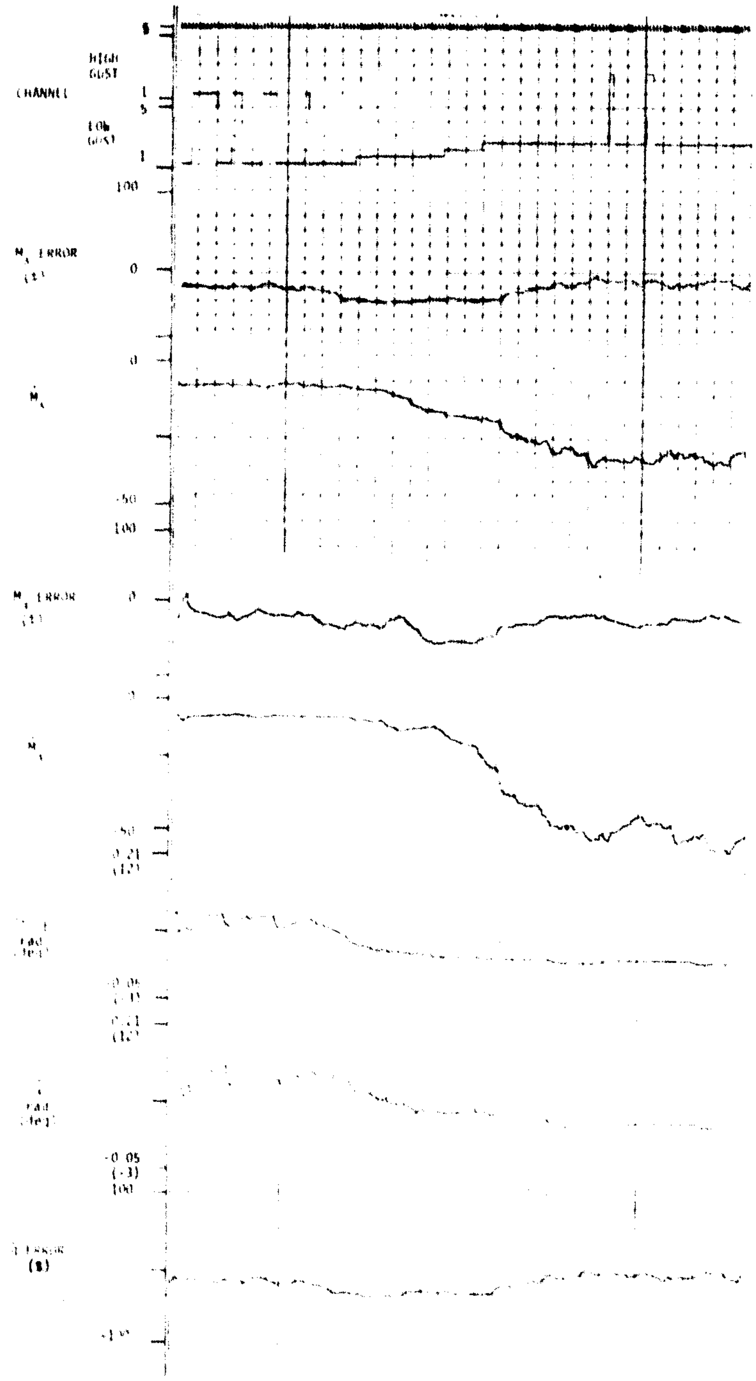

Figure 11D. PCMLE Response--Test Case 4 with Sensor Noise

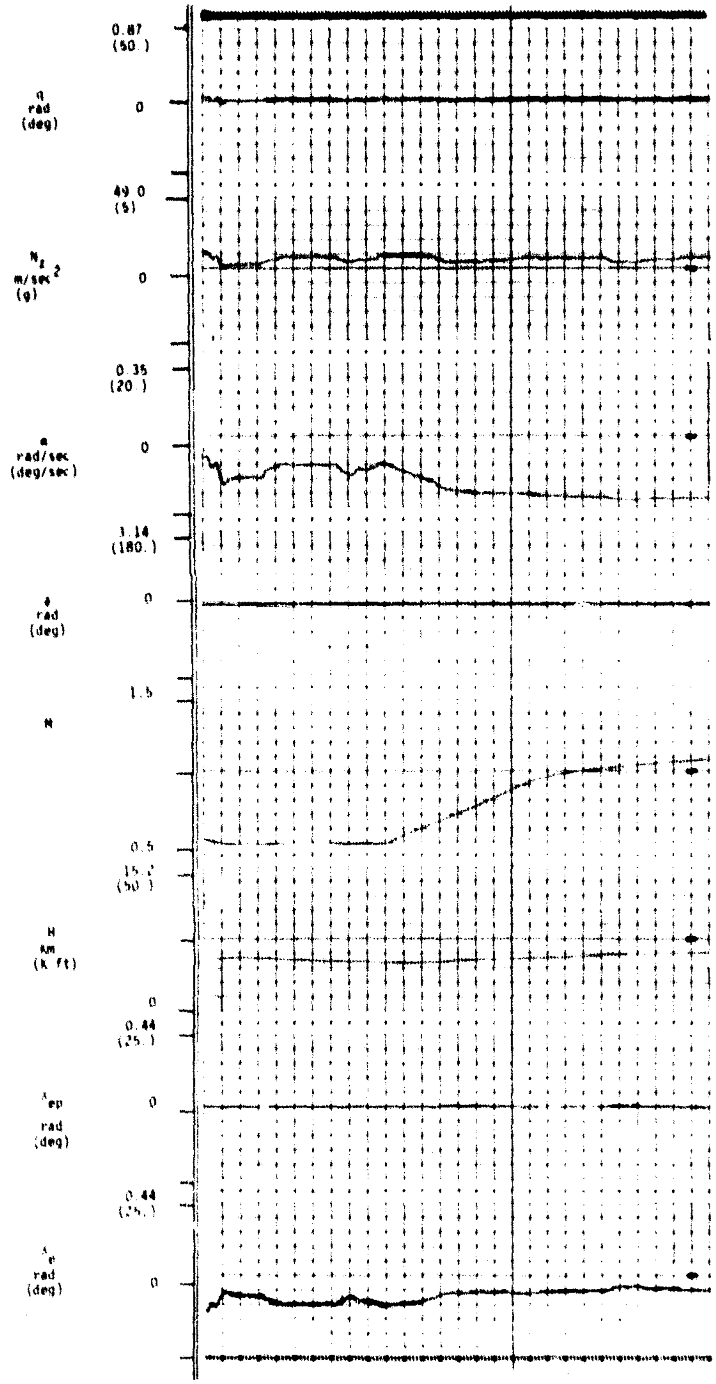

Figure 12A. Aircraft Response--Test Case 5

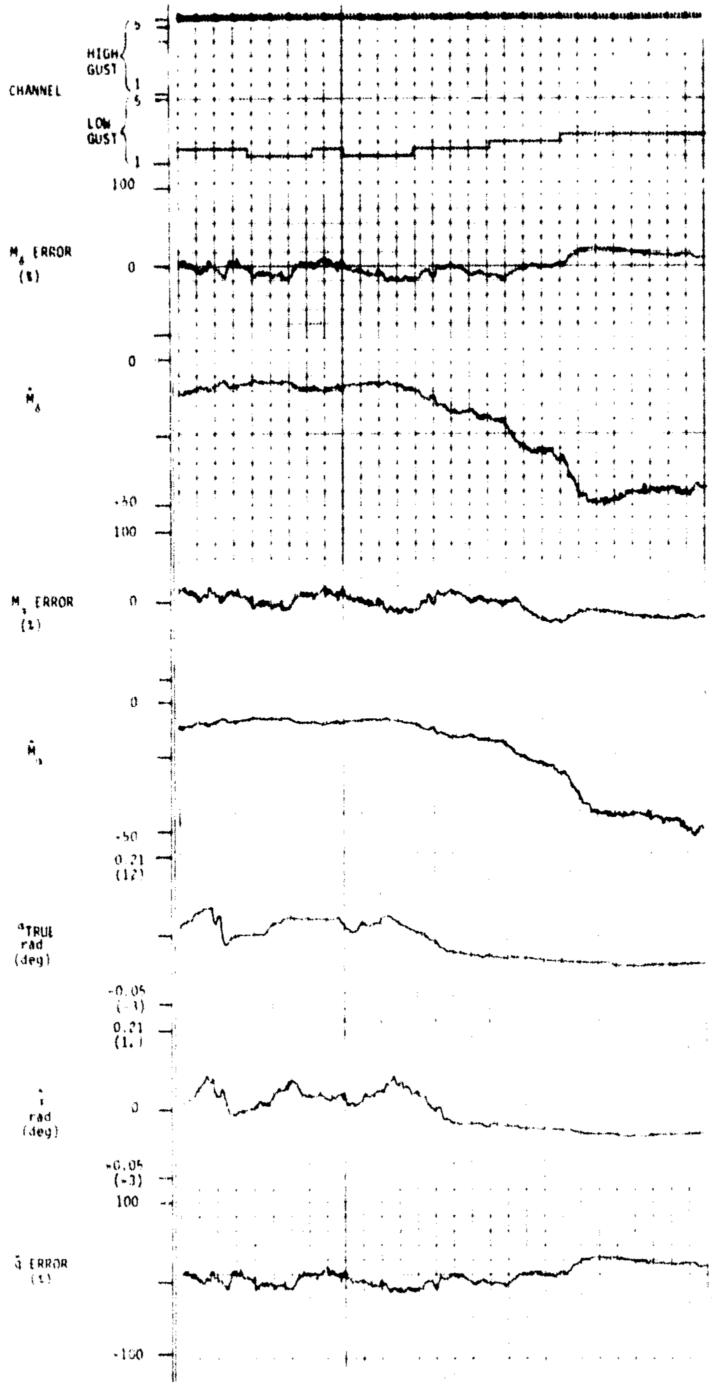

Figure 12B. PCMLE Response--Test Case 5

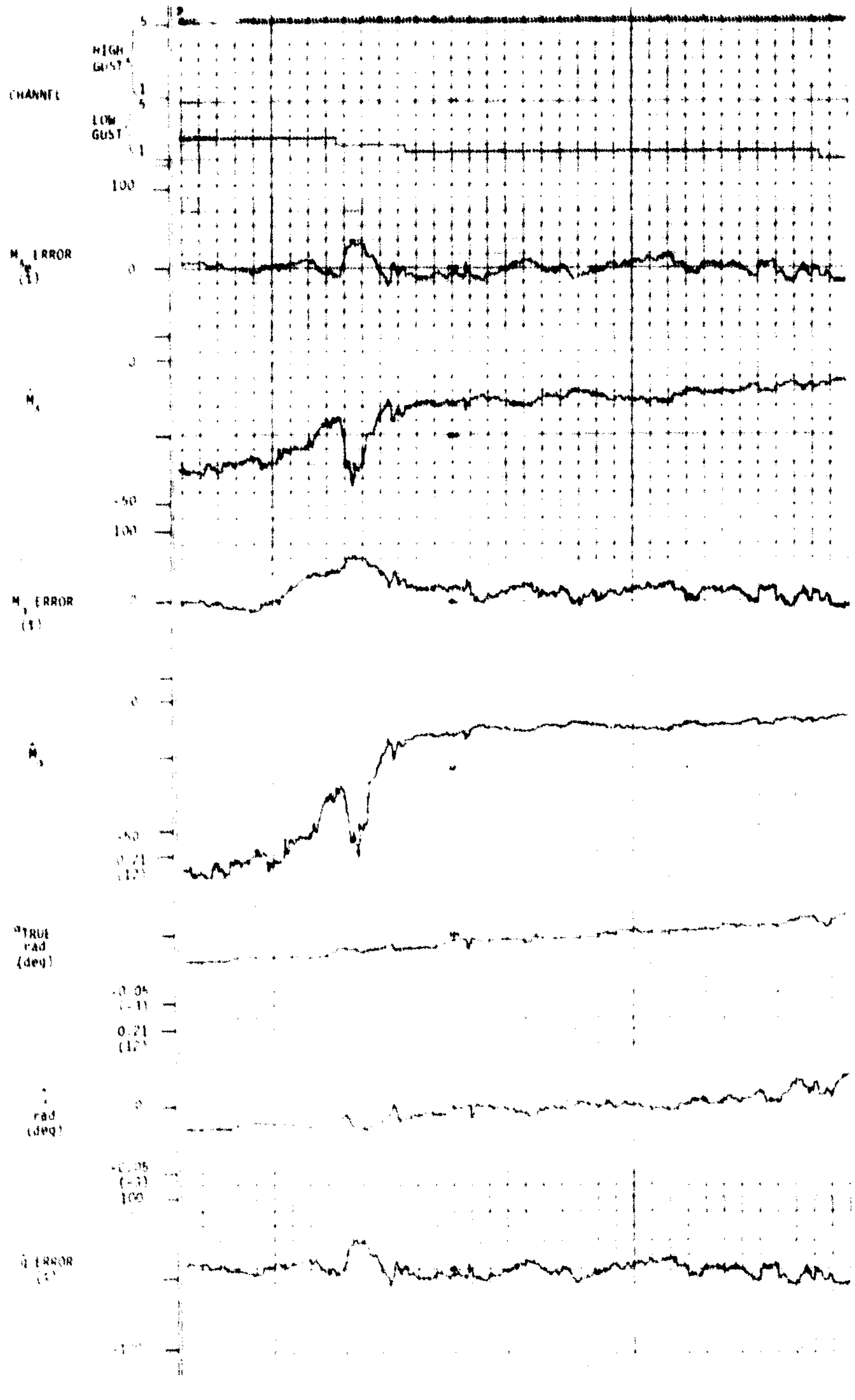

Figure 12C. PCMLE Response--Test Case 5 Deceleration

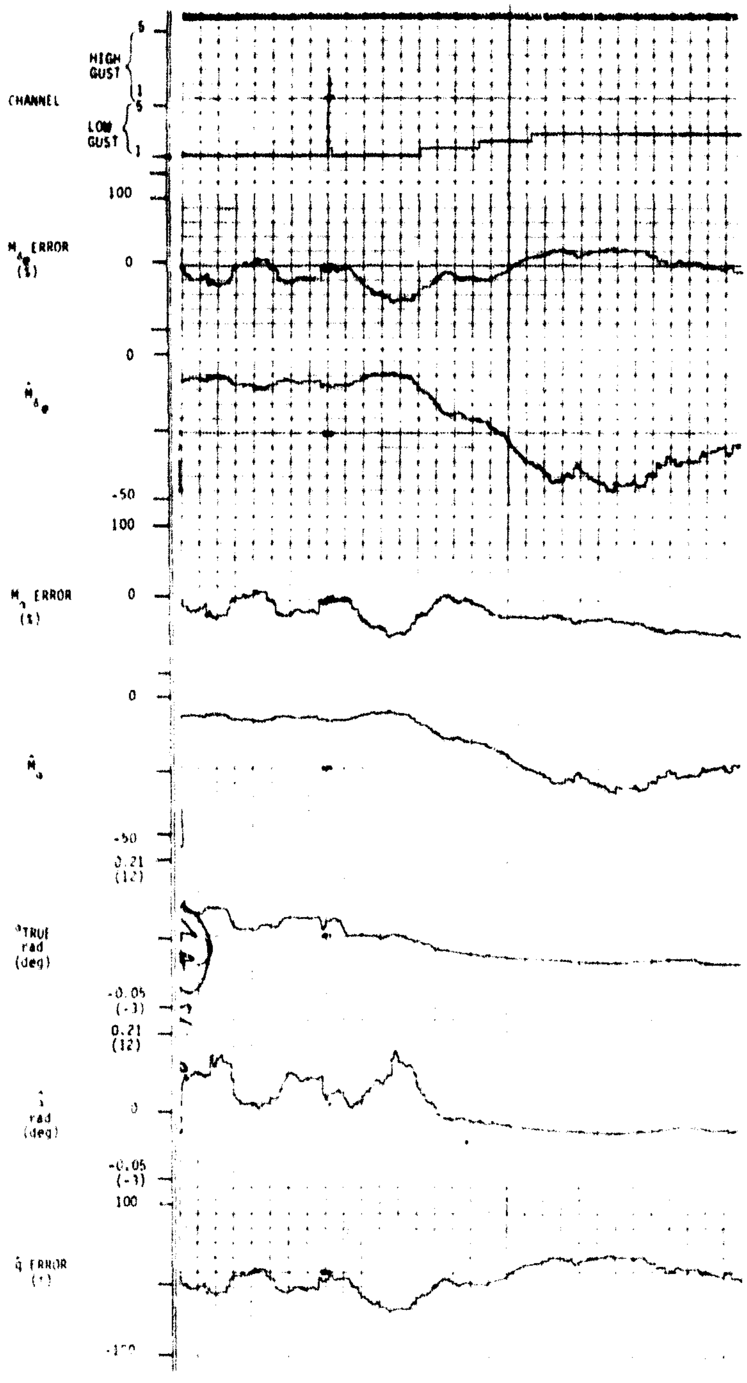

Figure 13. PCMLE Response--Test Case 5 Slow Update Rate

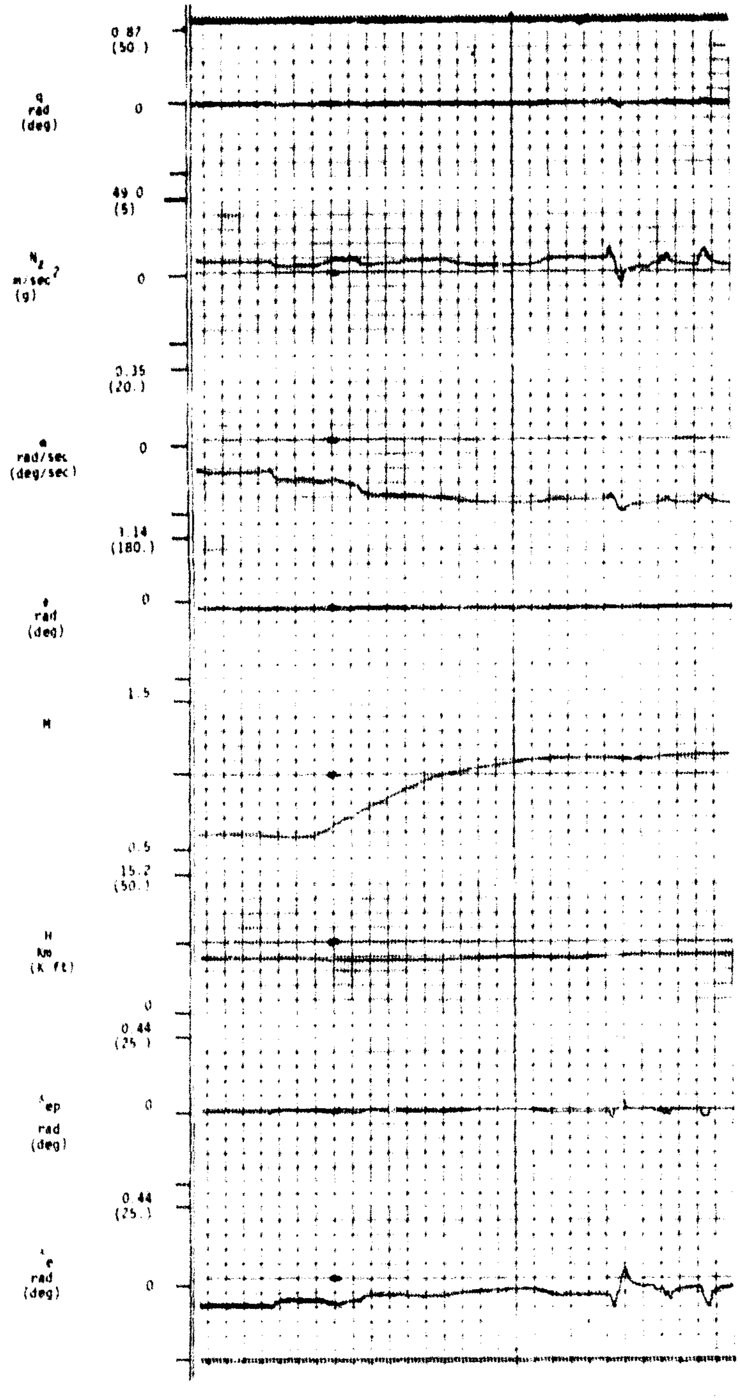

Figure 14A. Aircraft Response--Test Case 6

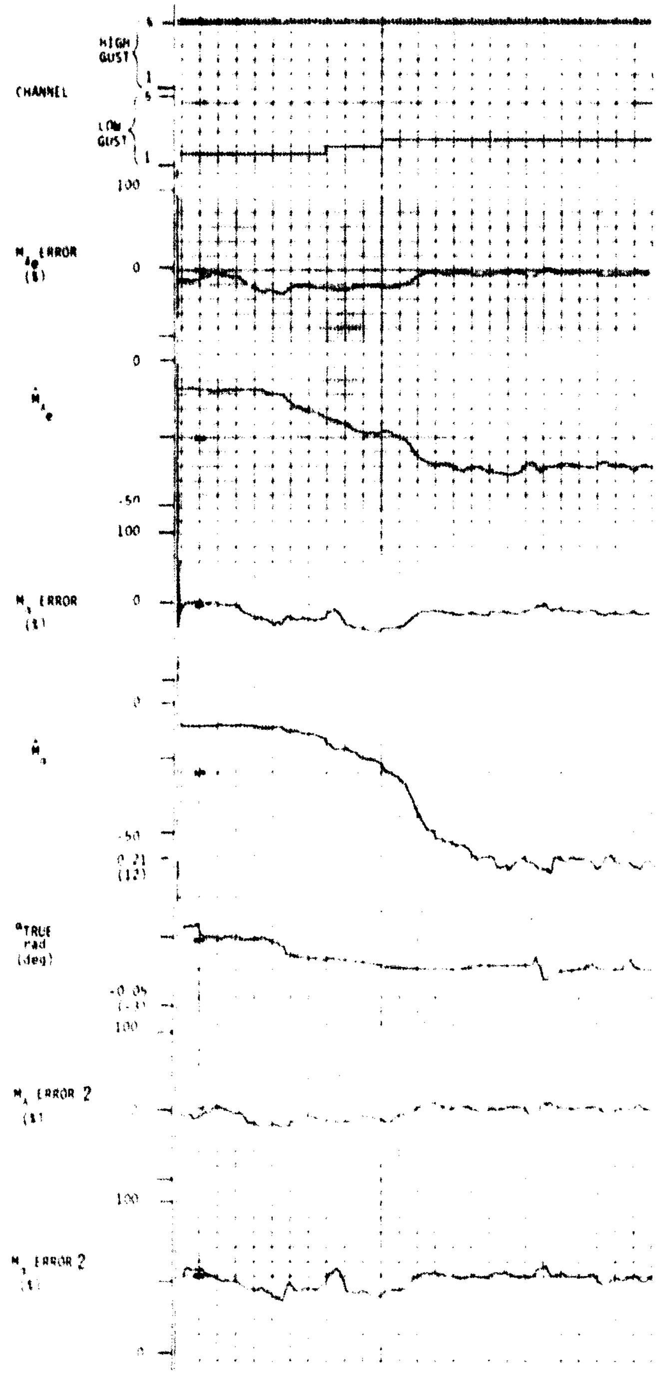

Figure 14B. PCMLE Response--Test Case 6

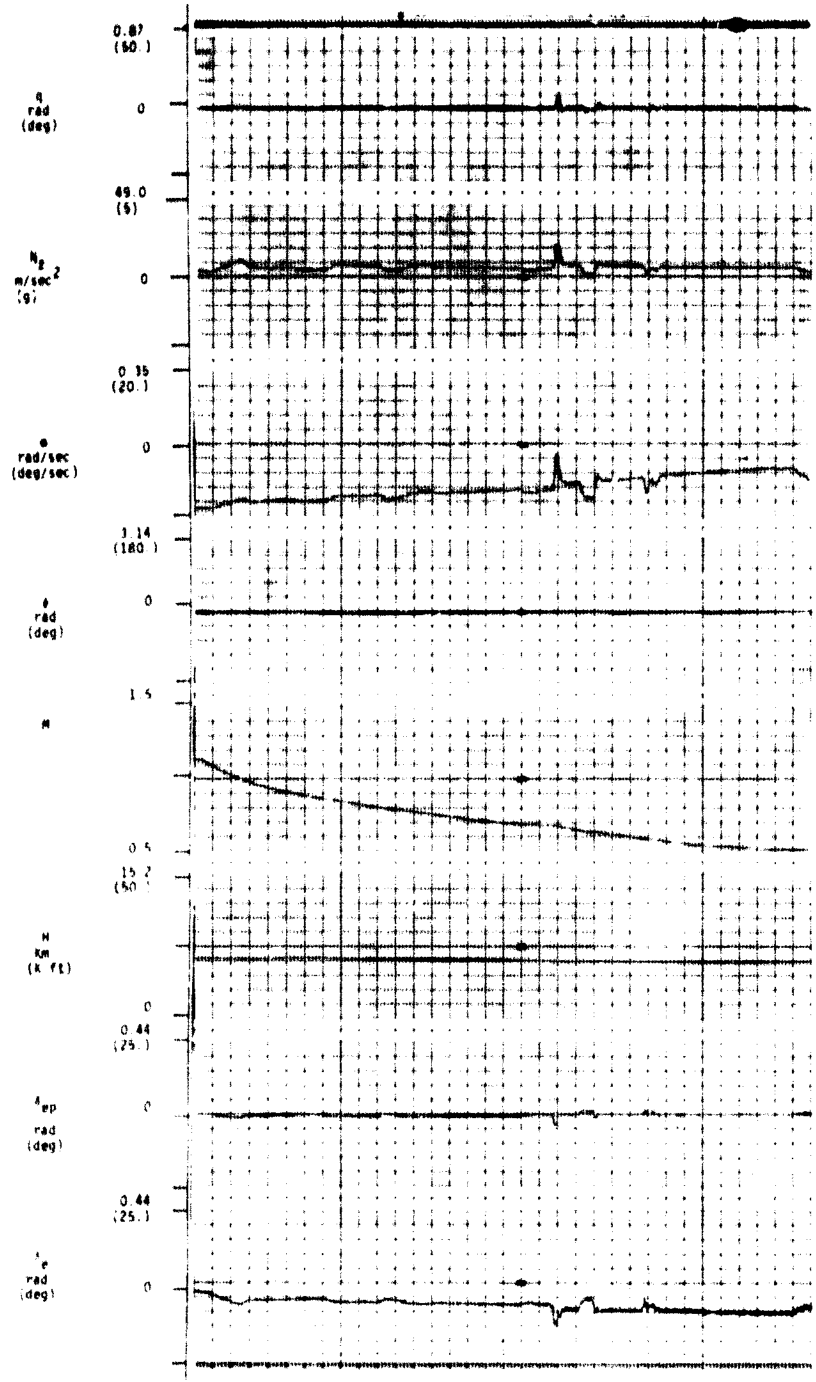

Figure 14C. Aircraft Response--Test Case 6 Deceleration

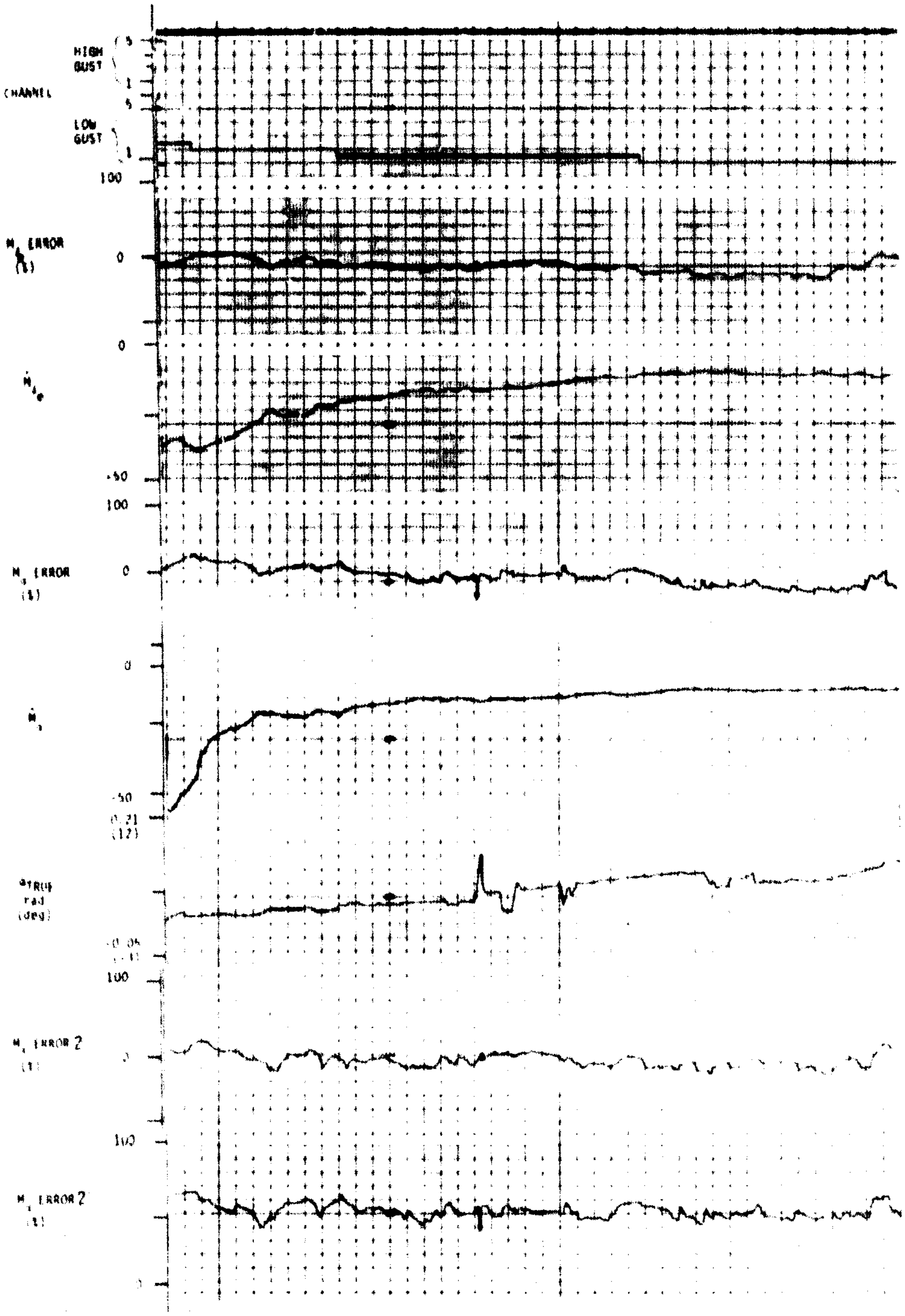

Figure 14D. PCMLE Response--Test Case 6 Deceleration

SECTION 5

SENSOR NOISE MODELING

The PCMLE algorithm was developed under the assumption that sensor noise statistics are constant over the flight envelope and are reasonably well known. Hence, they are not treated as parameters to be identified by the algorithm. The validity of this assumption is investigated in this section. Sensor data from ground tests at engine off, idle, and 80 percent maximum RPM, and from flight tests are analyzed. Results support the assumption that the statistics are constant, but modified nominal values are required to match the test aircraft's effective sensor characteristics.

ENGINE-OFF DATA

An 82-second segment of sampled gyro and accelerometer outputs under quiescent hangar conditions was analyzed. The analyses included mean and variance calculations, histogram plots, and power spectral densities (PSDs) computed via Fast Fourier Transform methods.* The variance calculations are summarized in Table 14. They show RMS levels roughly equal to one-third of each sensor's least-significant quantization bit (LSB). The corresponding histograms are plotted in Figures 15 and 16 and the PSDs are given in Figures 17 and 18. These show that noise in the hangar is dominated by relatively white random motions of

---

*Direct transformation of 4096 data points, with resulting plots smoothed by averaging adjacent frequency samples.

TABLE 14. STANDARD DEVIATION OF SENSOR NOISE

Sensor	Ground Test Data		
	Engine Off	Engine Idle	80% RPM
Normal accelerometer 12-bit resolution LSB = 0.00547 g	0.0018	0.0042	0.016
Pitch rate gyro 12-bit resolution LSB = 0.038 deg/sec	0.011	0.019	0.057

the last one or two quantization bits. Using a Gaussian assumption for the underlying noise processes which move these bits, RMS levels of roughly one-third bit are again obtained for both sensors. Since there is this much similarity between the gyro and accelerometer noise levels, it appears that the bit motions are generated by A/D electronics rather than by internally generated sensor noise.

ENGINE-ON DATA

The RMS sensor outputs increase substantially when the engine is running. This is shown in Table 14 for two engine speeds--idle and 80 percent RPM. PSDs for these conditions are shown in Figures 19 through 22. They indicate that most of the RMS increase can be traced directly to various resonances between 3 and 20 Hz. While these resonances may in fact be legitimate input signals as far as the instruments are concerned (i.e., not internal sensor noise), they must be treated as "effective sensor noise" for purposes of PCMLE because the algorithm includes no models to explain the sensed motion.

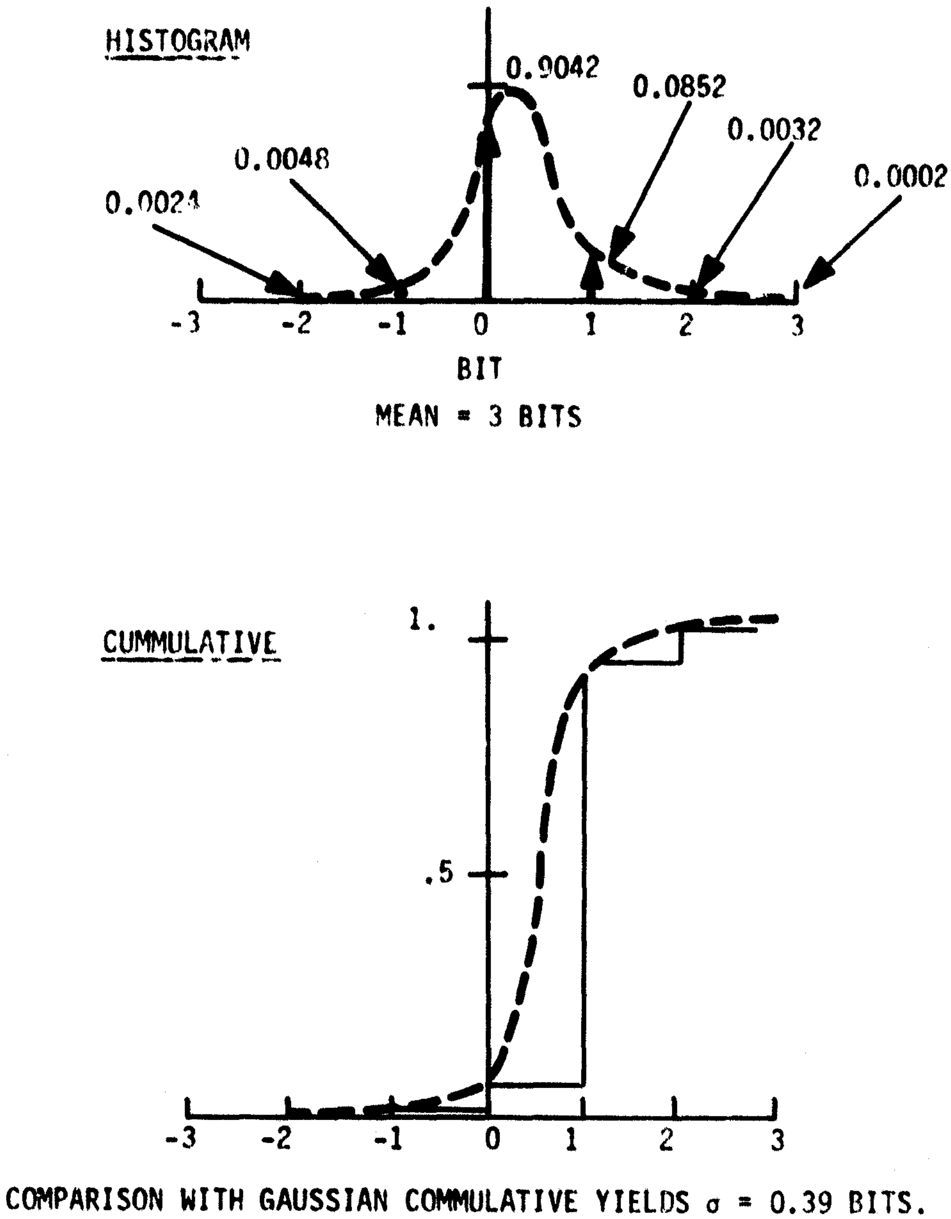

Figure 15. Gyro Noise Distribution (Engine Off)

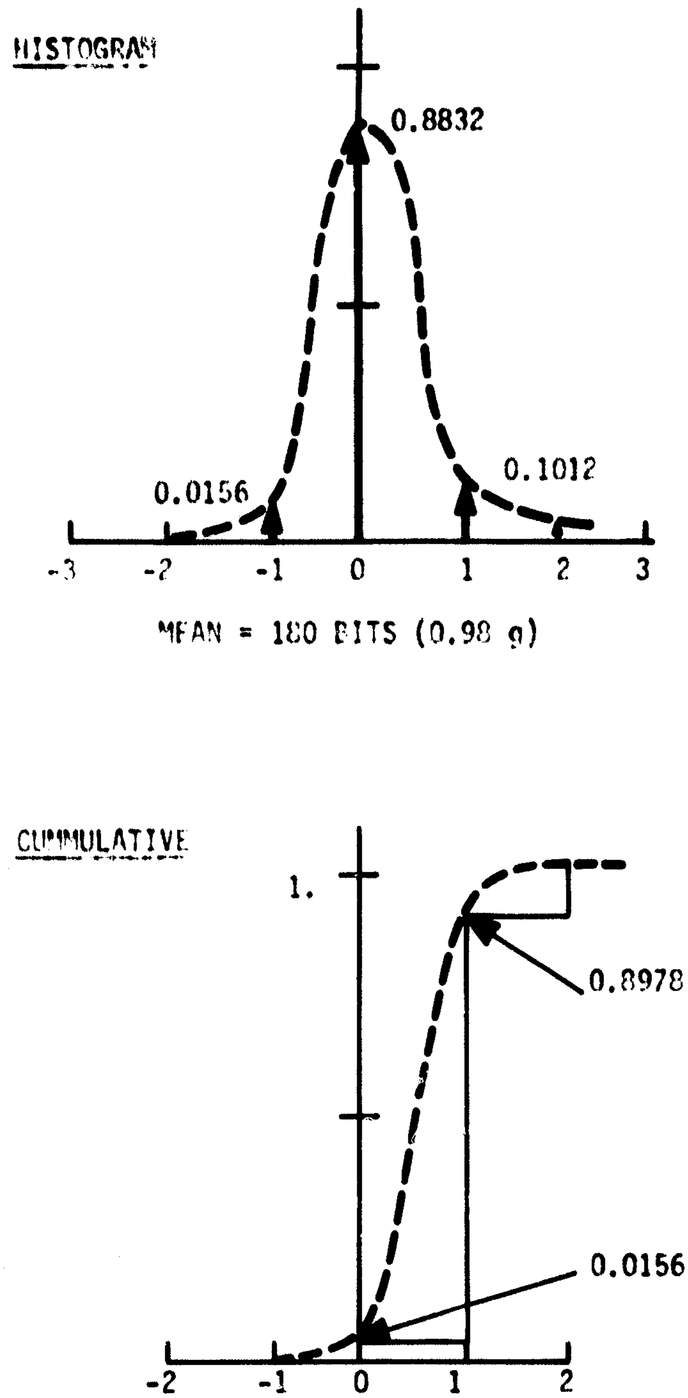

COMPARISON WITH GAUSSIAN APPROXIMATION YIELDS σ = 0.3 BITS.

Figure 16. Accelerometer Noise Distribution (Engine Off)

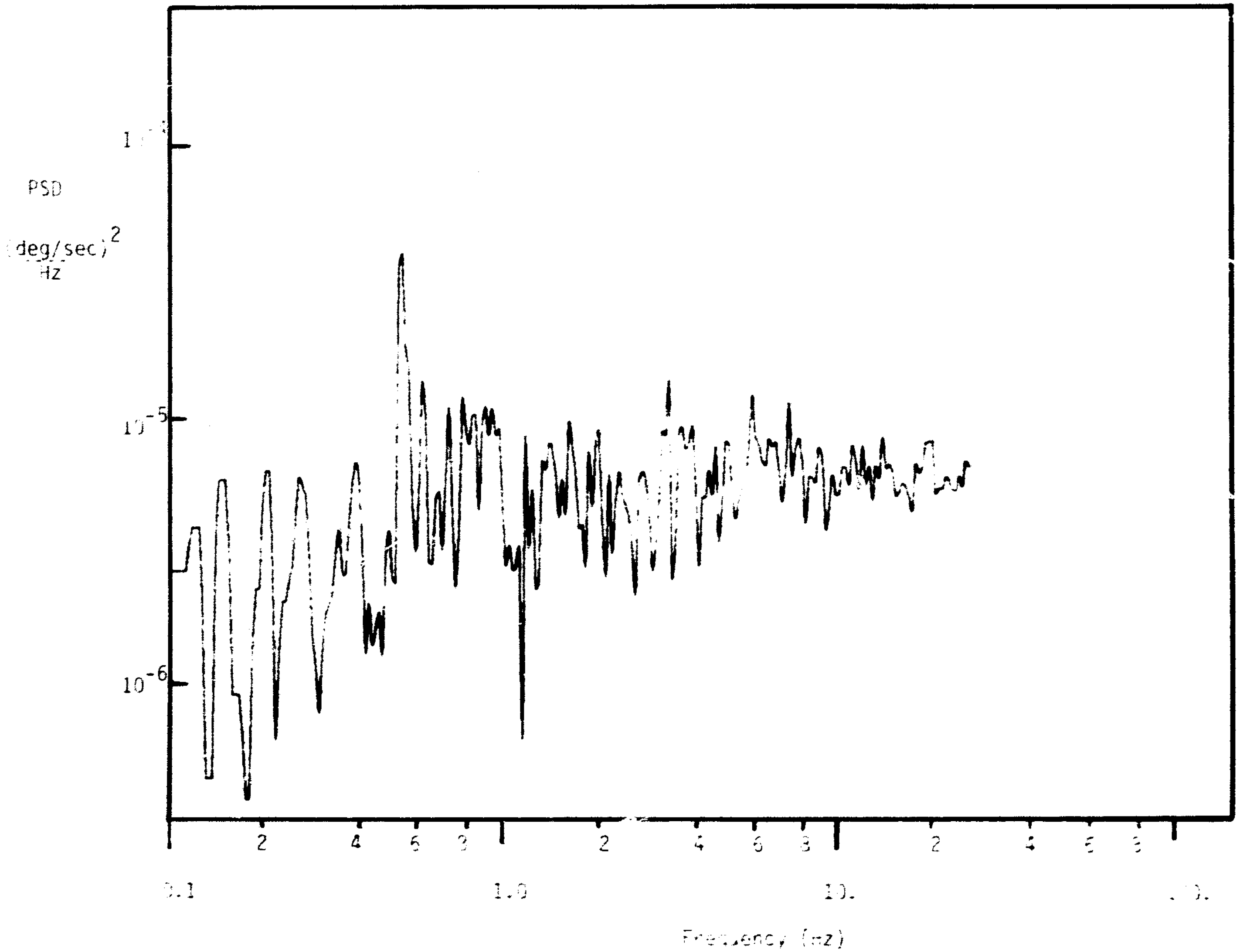

Figure 17. Gyro PSD (Engine Off)

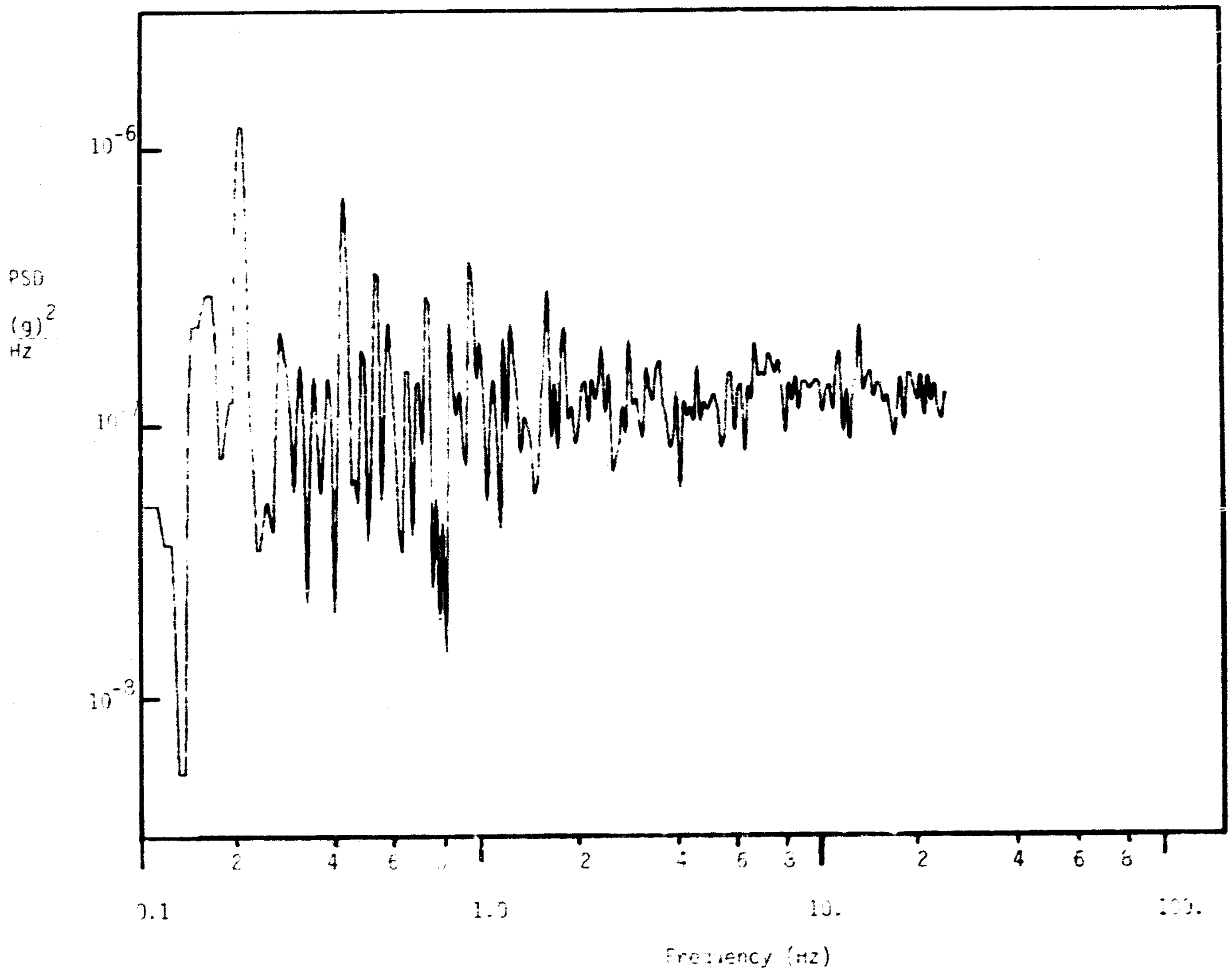

Figure 18. Accelerometer PSD (Engine Off)

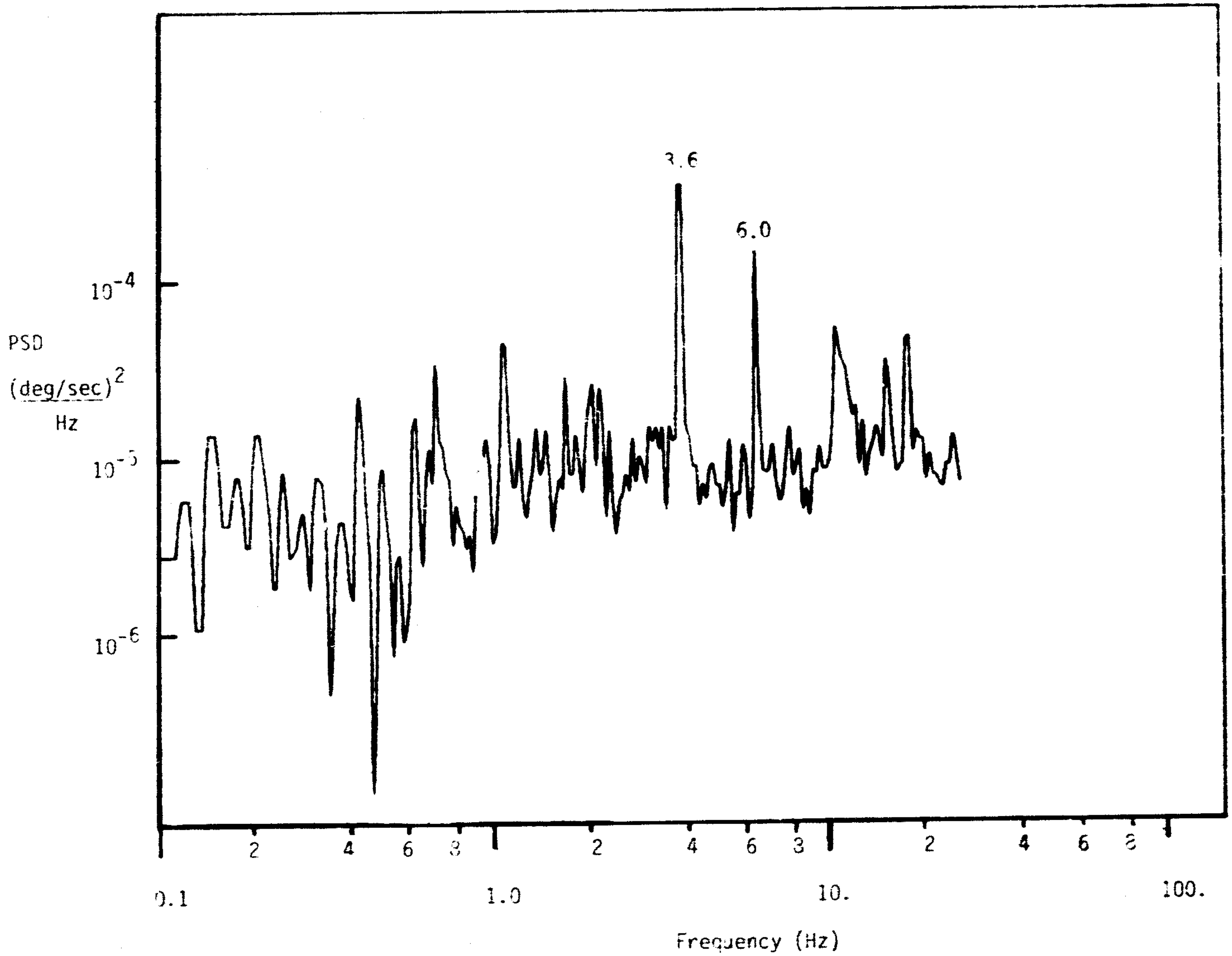

Figure 19. Gyro PSD (Engine Idle)

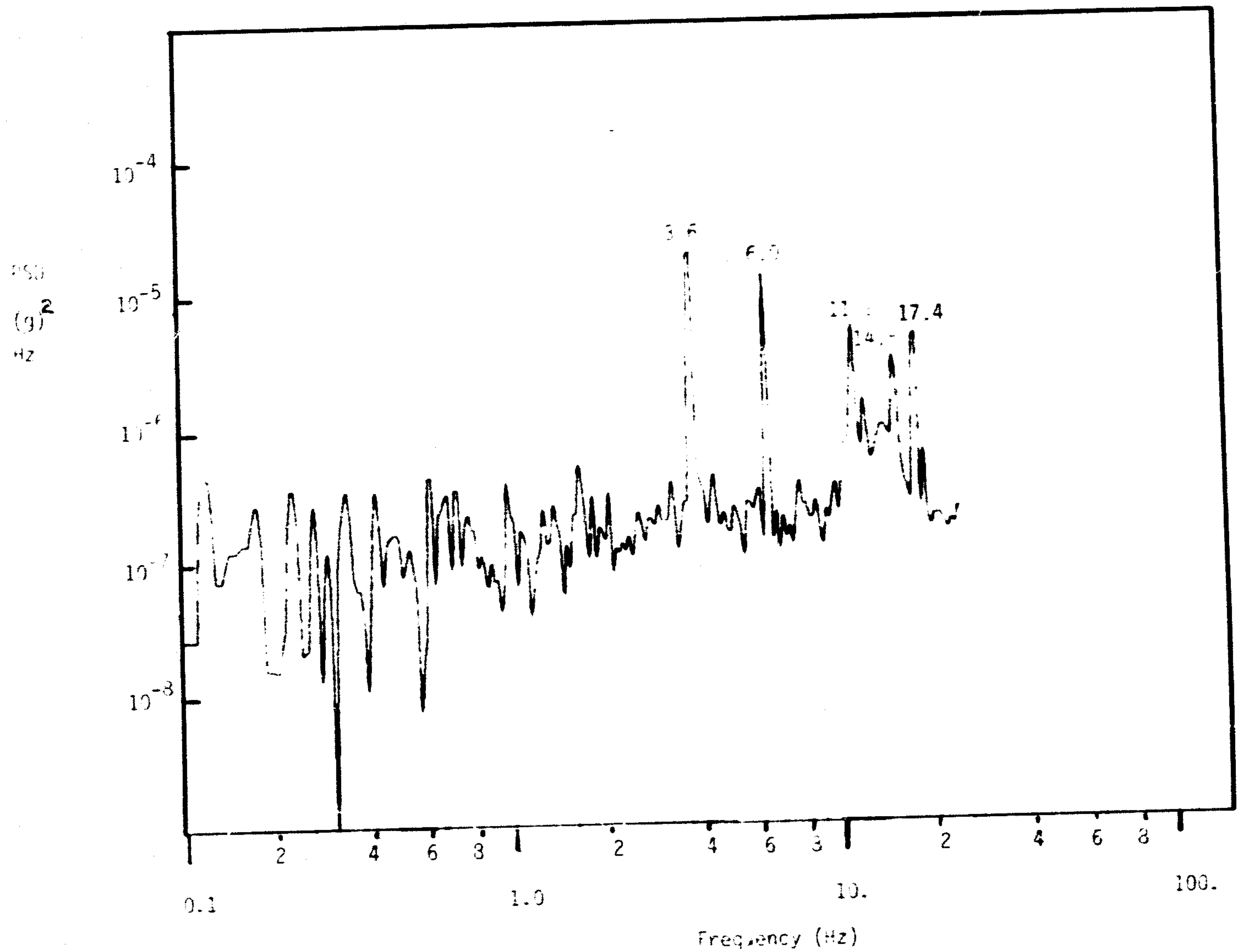

Figure 20. Accelerometer PSD (Engine Idle)

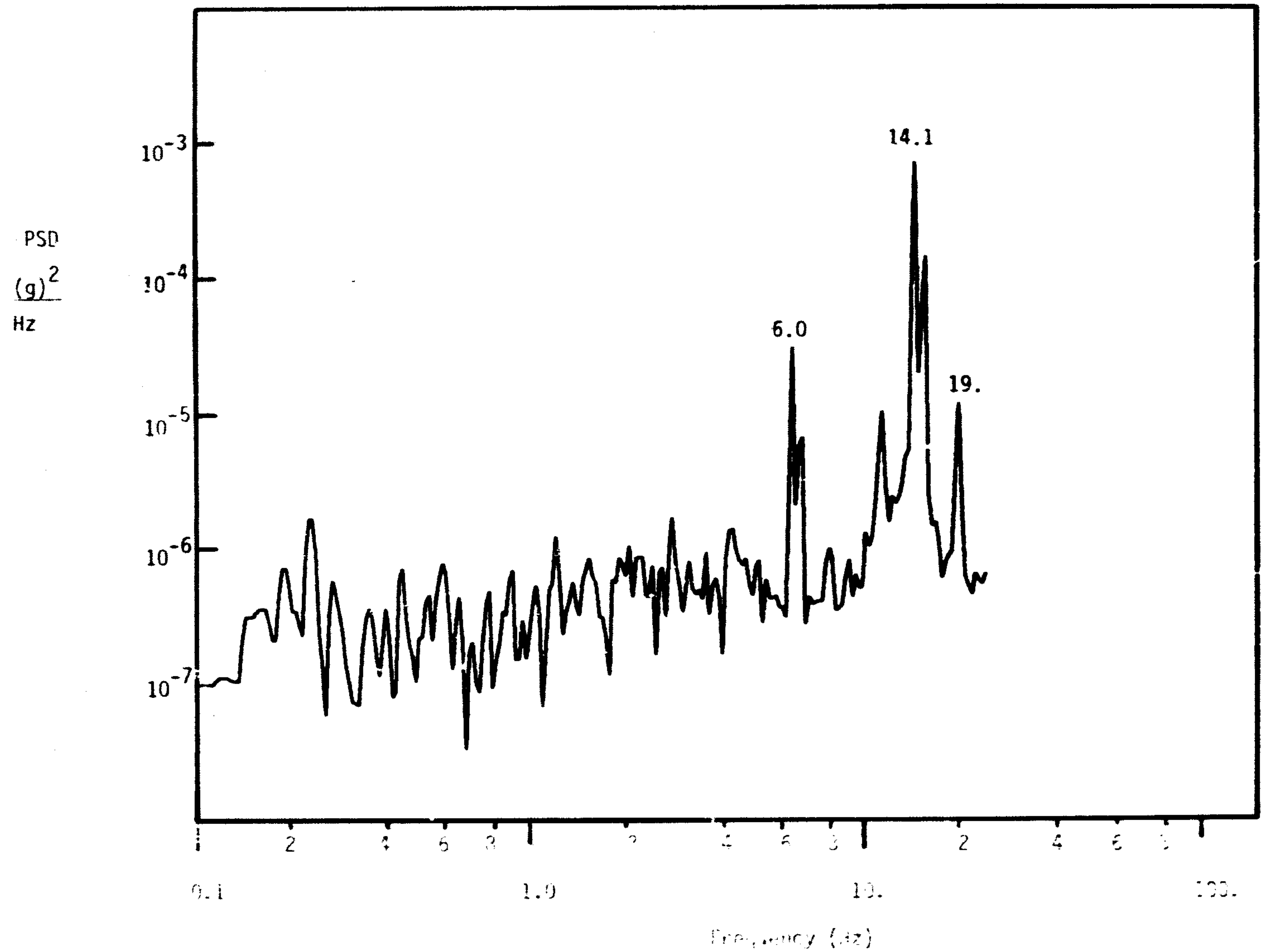

Figure 21. Gyro PSD (Engine 80 Percent RPM)

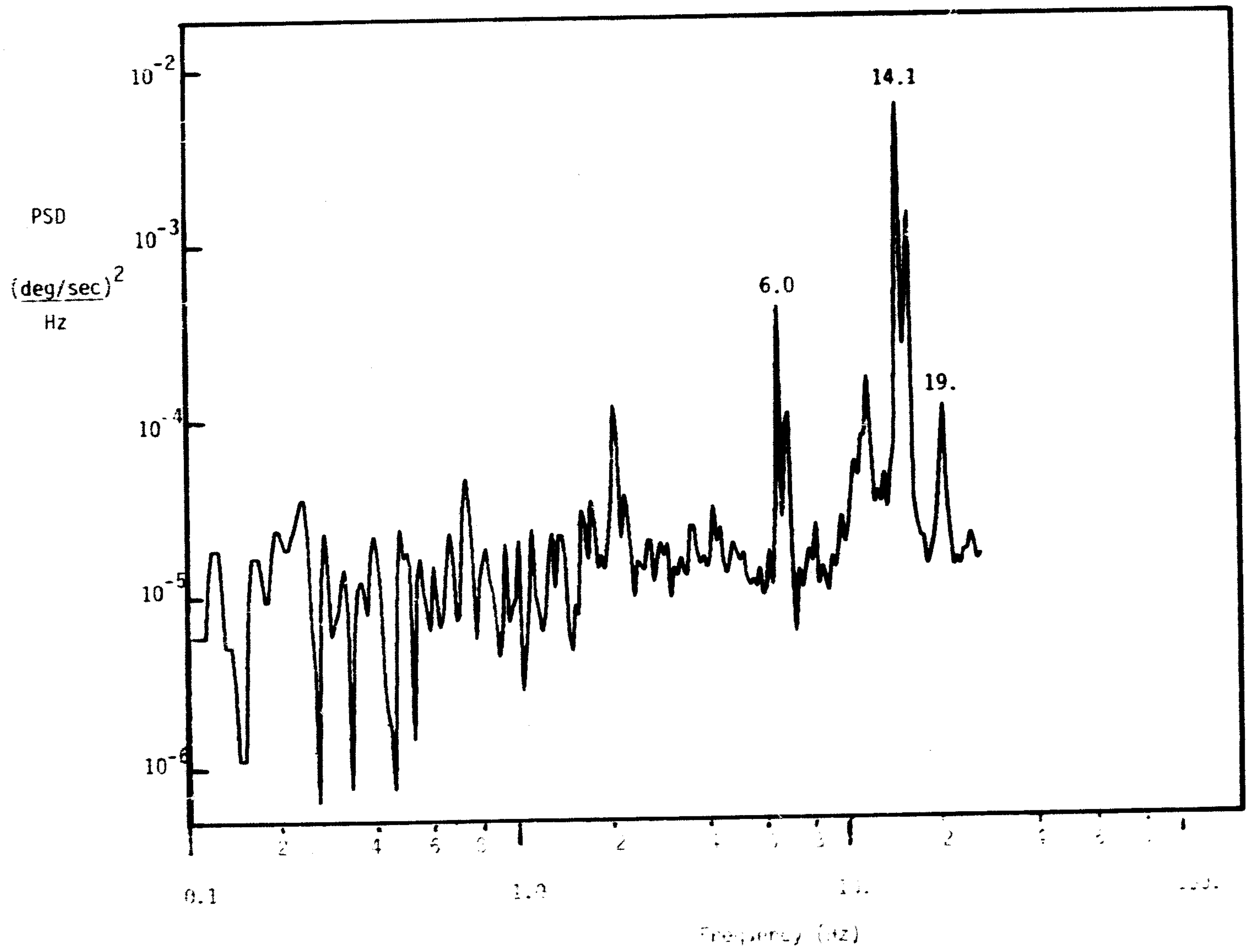

Figure 22. Accelerometer PSD (Engine 80 Percent RPM)

FLIGHT DATA

Sensor noise numbers applicable once the aircraft leaves the ground were deduced from Kalman filter residual histories, as generated during flight data parameter identification runs discussed in Section 6. These parameter identification runs used a general purpose identification program (GPMLE) to fit a best linear model to the flight data. The model extracts estimates of the (rigid body) sensor output, $\hat{y}_k$, leaving the residuals, $\nu_k = y_k - \hat{y}_k$, due to either internal sensor noise, unmodeled dynamics (e.g., structural modes), atmospheric turbulence, and mismatched rigid body motion. In the absence of turbulence and assuming a good model fit for rigid body motion, therefore, the residuals provide "effective" sensor noise time histories directly.

RMS noise levels from such residual histories are summarized in Table 15. Four maneuvers are shown, corresponding to flight data segments documented in Section 6. It is evident from this table that effective noise numbers in flight are substantially higher than both the hangar data and the ground test data. This is highlighted in Figures 23 and 24 which illustrate the data from all test conditions in graphical form. The figures clearly show that ground and hangar tests are inadequate indicators of airborne noise statistics. They also show that, while the constant statistics assumption made for PCMLE seems reasonably valid, the actual RMS levels used in the acceptance test should be modified somewhat to match the test aircraft sensors.

TABLE 15. STANDARD DEVIATION OF EFFECTIVE SENSOR NOISE: FLIGHT DATA

Maneuver	2:2	3:1	3:4	2:6
Altitude (feet)	20300	20129	19848	22500
Mach	0.44	0.566	0.85	1.12
GPMLE Residual Levels (RMS)				
Accelerometer (g's)	0.058	0.050	0.050	0.054
Gyro (deg/sec)	0.11	0.079	0.12	0.13

As a further evaluation of effective noise statistics, it would have been useful to repeat the analyses in Table 15 under turbulence conditions. There is some rationale to suggest that effective sensor noise should increase further with turbulence level because of increased unmodeled structural excitation. In the absence of turbulence data, we are forced to rely on conclusions from related noise modeling efforts conducted on the SAAB JA-37 aircraft (Reference 5). These suggest that effective noise increases due to turbulence are probably negligible.

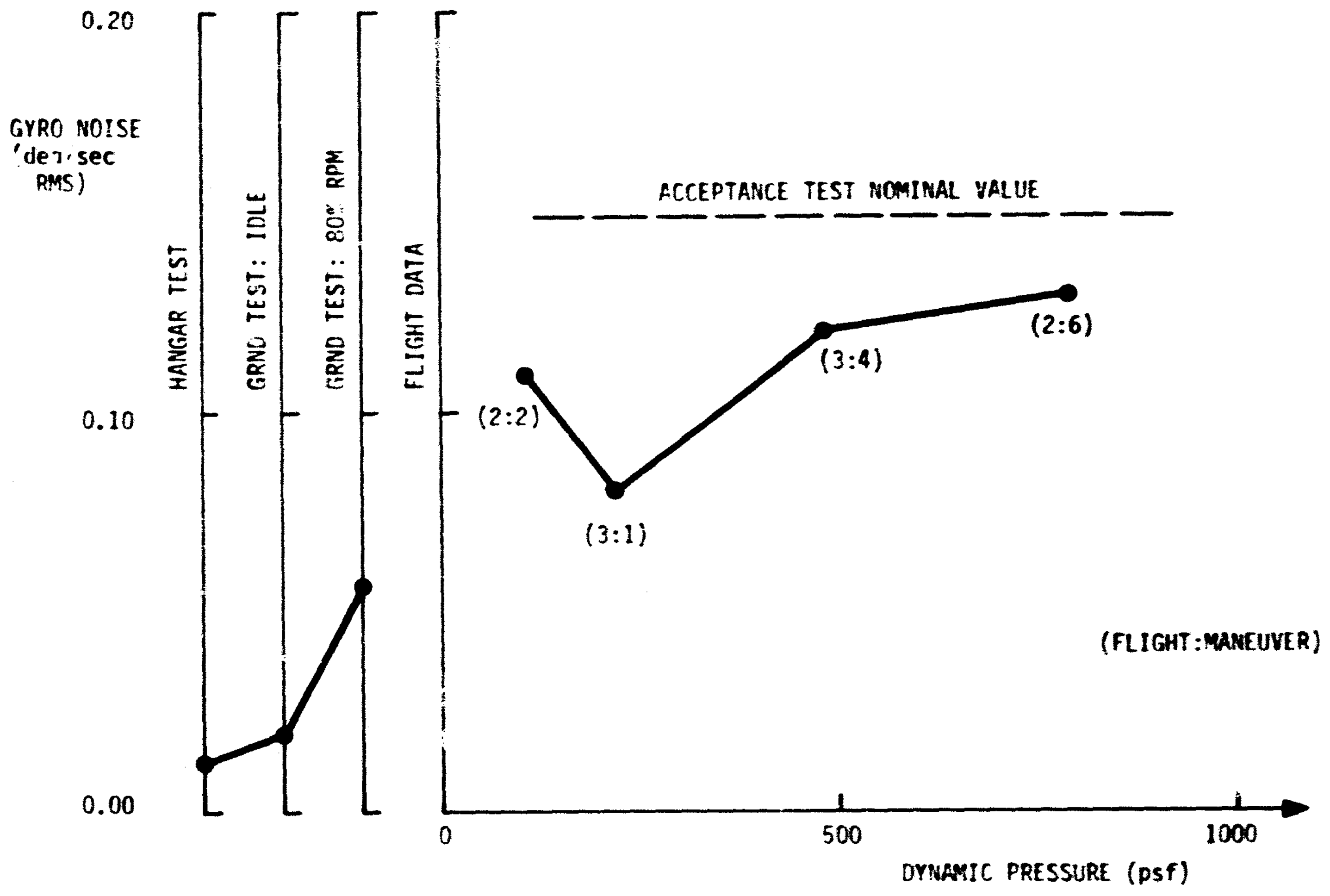

Figure 23. Gyro Noise Summary

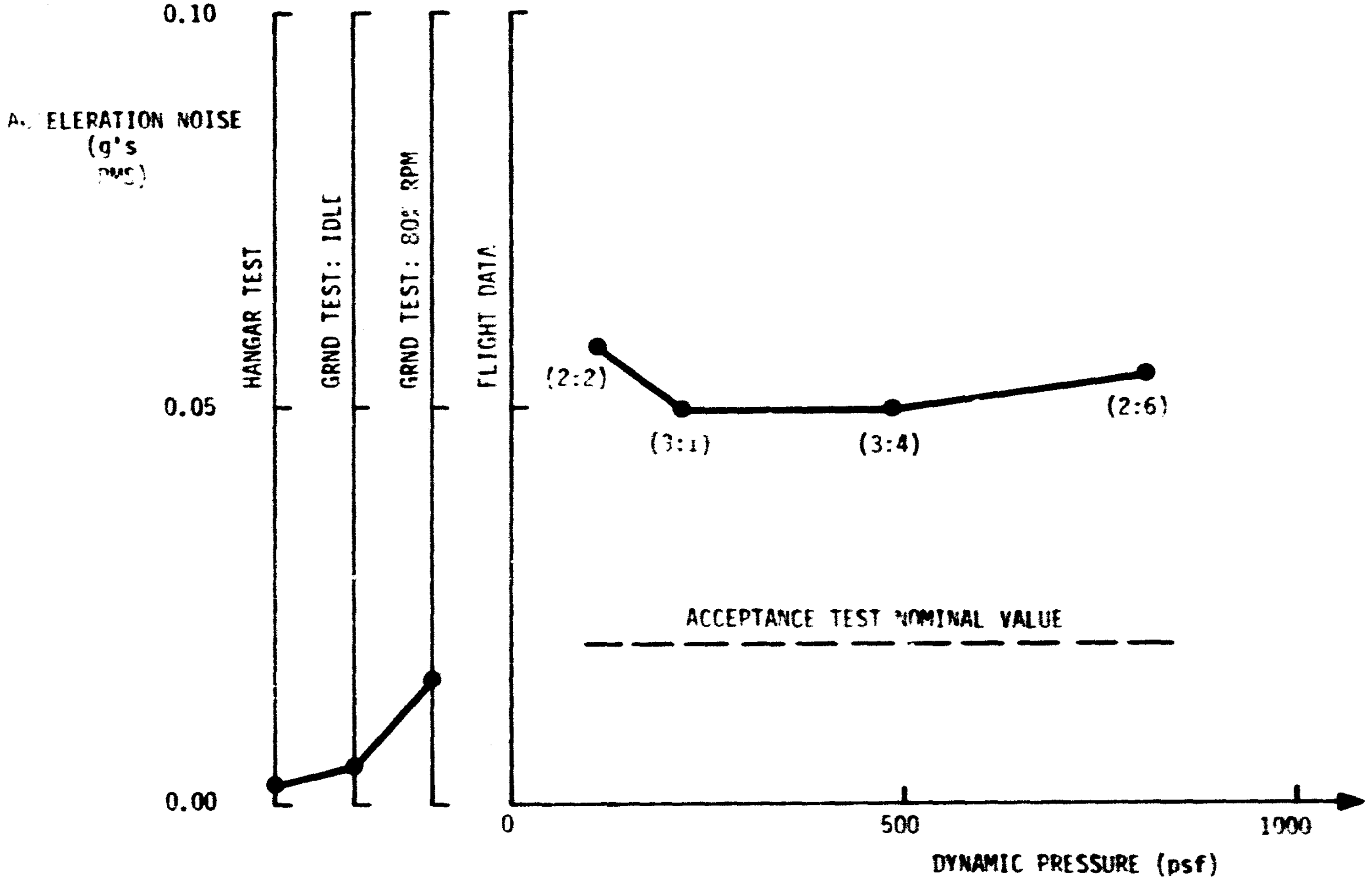

Figure 24. Accelerometer Noise Summary

SECTION 6

PARAMETER ESTIMATION WITH FLIGHT DATA

In order to gain increased confidence in the algorithm prior to flight test, PCMLE was exercised with recorded sensor outputs from F-8C flight tests. Since the flight recordings do not contain PCMLE's own test signal, data segments with large pilot commands were used to provide good conditions for identification. Results of these off-line exercises are very positive and provide a high level of confidence for successful closed-loop flight tests.

In addition to the PCMLE exercises, a general purpose maximum likelihood estimation (GPMLE) algorithm developed for the F-8C (Reference 1) was used to estimate all pitch axis parameters in a conventional iterative batch-processing mode. Results from both the PCMLE and GPMLE estimation are presented and compared in this section. They provide a data base for flight test recommendations made later in the report.

TEST POINTS

Flight conditions for which flight data were processed are plotted in Figure 25. This is an adequate number of conditions for checking PCMLE, although more data at 40,000 ft (12,195 M) would have been desirable. The flight records examined contain 15 pitch doublet maneuvers covering a dynamic range from 126 psf to 840 psf. These have all been processed with PCMLE.

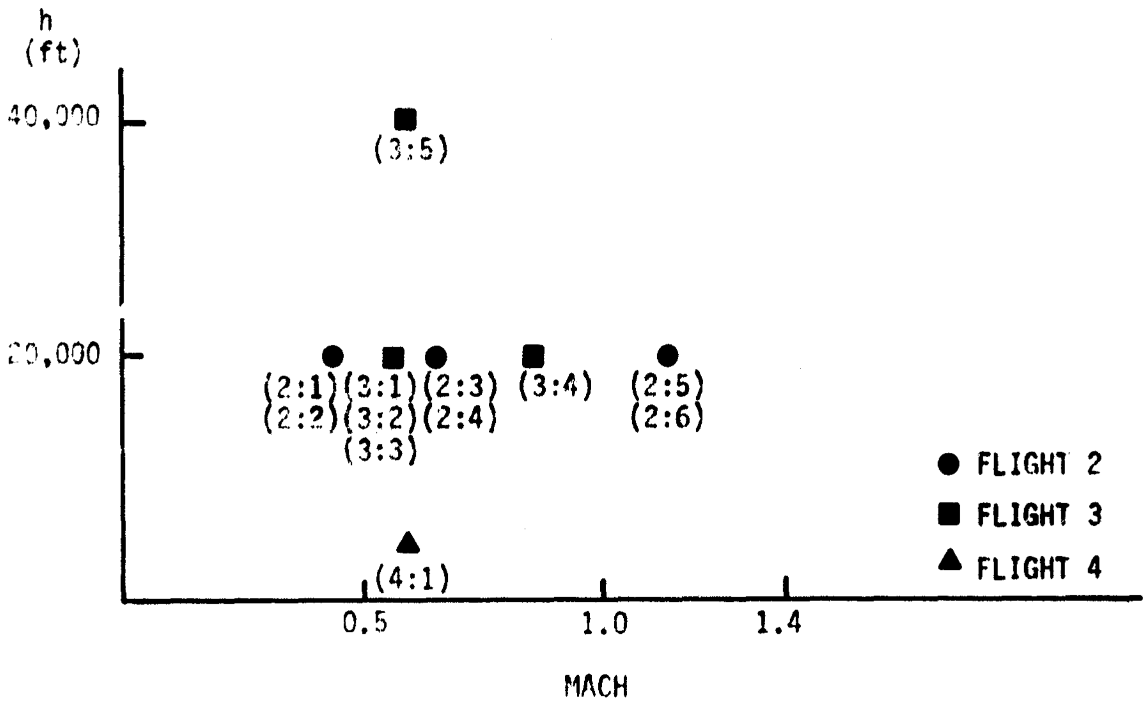

Figure 25. F-8C Flight Data Test Points

Several lateral maneuvers were also used as "disturbances" to PCMLE to evaluate the effect of lateral maneuvers on the pitch axis estimation. Finally, an acceleration run from Mach = 0.82 at 37,000 ft to Mach = 1.15 at 30,000 ft was processed.

The flight data for each test point consist of time histories for the three measurements needed to drive the PCMLE software. The time histories were sampled at 50 sps. Other related measurement parameters are given in Table 16. Note that the accelerometer was located at the c.g. Also, the quantization level of each sensor is higher than the ground data quantization used in Section 5.

c-2

TABLE 16. F-8C MEASUREMENTS

Measurement	Prefilter	Scale	Quantization
Pitch rate (q)	40 Hz	± 70 deg/sec	0.138 deg/sec
Normal acceleration	40 Hz	± 8 g	0.0156 g
Elevator position (δ_e)	40 Hz	+11.75°, -21.5°	0.0325 deg

Six longitudinal maneuvers (two consecutive pilot doublets each) were extracted from the Flight #2 data tape. Each maneuver is a 10.24-second segment. The maneuver start times are given in Table 17 for the time references of the tape. Five similar segments containing pitch axis pilot commands were extracted from the Flight #3 data tape. These are also identified in Table 17. For shorthand reference to all 12 data segments, the symbol "Maneuver i:j" will be used to designate Flight i, Maneuver j.

Plots of the maneuver time histories for all 11 maneuvers are shown in Figures A1 through A11 in Appendix A. Note that the accelerometer measurement on Maneuvers 2:5 and 3:5 are contaminated with low frequency oscillations.

PCMLE PERFORMANCE

The above maneuvers were used to exercise the baseline PCMLE algorithm (two parameters were identified using a single Newton-Raphson step) and also two of the software options:

TABLE 17. FLIGHT TEST POINTS

	Maneuver	Altitude (ft)	Mach	Start Time	Comments	Data Points (50 samples/sec)
Flight 2	1	20,485	0.43	09:54:13	2 doublets	512
	2	20,300	0.44	09:54:28	"	512
	3	20,485	0.645	09:57:14	"	512
	4	20,200	0.648	09:59:03	"	512
	5	22,700	1.113	10:04:20	"	512
	6	22,500	1.12	10:05:19	"	512
Flight 3	1	20,129	0.566	14:04:18	2 doublets	700
	2	19,987	0.57	14:04:45	"	750
	3	19,162	0.562	14:09:16	1 command	400
	4	19,848	0.85	14:15:55	2 doublets	630
	5	39,634	0.63	14:28:08	2 doublets	800
Flight 4	1	5,000	0.63	11:18:06	1 command	300

1. The second Newton-Raphson correction, and
2. Identification of additional parameters.

Since the algorithm for all these cases is nominally set up to operate with measured servo position, a modified actuator bandwidth parameter, ACTBW, was used to operate with the available measured surface position instead. The bandwidth was moved from 12.5 rad/sec to 100 rad/sec. In addition, the accelerometer noise parameter, SIGACCO, was increased from the nominal value of 0.02 g RMS to 0.04 g RMS, as suggested in Section 5. The distance parameter, DIST, was set to zero to match the c.g. location of the instrument. All other parameters remained at their nominal values in Table 5.

The Kalman filters in PCMLE use a parameterization based on "unflexed" M_δ because the functions are simpler. Therefore the parameters estimated by fitting data to the model will also be "unflexed."

Table 18 summarizes performance of the baseline algorithm for the 11 flight test points. Estimated variables in the table are the following:

$\hat{M}_{\delta_o}$ - PCMLE's estimate of surface effectiveness before quasi-state flexibility corrections.

$\hat{M}_{\delta_e}$ - Surface effectiveness estimate after quasi-state flexibility corrections.

$\hat{\sigma}_{M_\delta}$ - PCMLE's estimate of the one-sigma accuracy of its M_{δ_o} estimate. This tends to be an optimistic number because PCMLE does not recognize errors due to unidentified parameters.

$\hat{C}_2$ - Estimate of small perturbation parameter C_2 used to calculate pitching moment due to angle-of-attack.

TABLE 18. PERFORMANCE OF PCMLE ON FLIGHT DATA

Maneuver	Measured H (ft)	Measured V (ft/sec)	Measured Mach	$\hat{M}_o$	$\hat{M}_e$	$\hat{M}_q$	$\hat{C}_2$	$\hat{\sigma}_{C_2}$	$\hat{M}_\alpha$	$\hat{V}$ (ft/sec)	CH	Gust Level	SIGSQ
2:1	20,485	446	0.43	-5.26	-4.84	0.27	0.179	0.040	-4.07	459	2	Low	1.02
2:2	20,300	452	0.44	-5.38	-4.95	0.31	0.255	0.039	-4.55	464	2	High	0.[illegible]
2:3	20,485	667	0.645	-11.6	-9.78	0.95	0.151	0.034	-8.72	682	3	Low	0.762
2:4	20,200	672	0.648	-11.4	-9.59	0.822	0.228	0.0303	-9.42	674	3	Low	1.19
2:5	22,700	1144	1.113	-49.5	-33.7	4.41	0.570	0.099	-56.2	1830	5	High	0.702
2:6	22,500	1153	1.12	-33.1	-22.8	2.10	0.946	0.097	-49.0	1420	5	Low	0.706
3:1	20,129	586	0.566	-8.70	-7.62	0.638	0.204	0.0244	-6.94	590	3	Low	0.766
3:2	19,987	594	0.57	-8.61	-7.55	0.748	0.203	0.0315	-6.87	587	3	Low	1.05
3:3	19,162	584	0.562	-8.90	-7.78	0.925	0.473	0.0271	-6.95	597	3	Low	0.766
3:4	19,848	882	0.85	-28.1	-19.9	1.79	0.0801	0.0265	-19.2	1130	4	Low	0.662
3:5	19,634	610	0.63	-7.78	-6.90	0.455	0.0984	0.0537	-5.45	558	2	High	1.10
4:1	5,000	---	0.63	-28.02	-19.87	2.41	-0.235	0.0339	-16.48	1059	4	Low	1.043

SIGACC = 0.08 to compensate for large accelerometer oscillations.

$\hat{\sigma}_{C_2}$ - Estimate of the one-sigma accuracy of the C_2 estimate. Scaled up by $|M_{\delta_0}|$, this parameter gives a rough (optimistic) indication of the expected accuracy of PCMLE's M_α estimate.

$\hat{M}_\alpha$ - Estimate of pitching moment coefficient due to angle-of-attack, as computed from $\hat{M}_{\delta_0}$ and $\hat{C}_2$.

$\hat{V}$ - Estimate of velocity

CH - PCMLE's selected min-L channel.

Gust Level - PCMLE's estimate of random vertical gust level, either high (5 ft/sec RMS) or low (1 ft/sec RMS).

SIGSQ - Estimated scale factor on the residual magnitudes of the min-L channel. SIGSQ = 1 corresponds to nominal noise conditions.

Time histories of the min-L channel's gyro and accelerometer residuals, the estimated RMS error $\hat{\sigma}_{M_\delta}$, and the $\hat{M}_{\delta_0}$, $\hat{M}_{\delta_e}$, $\hat{M}_\alpha$ and $\hat{V}$ estimates themselves are shown for each maneuver in Figures B1 through B11 of Appendix B. Note that the starting transients include some drift in the estimates since PCMLE is not getting any information until pilot commands start. As mentioned earlier, the normal PCMLE test signal is not present in any of the flight data.

Compared with expected (simulation) parameter values for the test points in Table 17, all the estimates in Table 18 are reasonable except those for Maneuver 2:5. This case produces a more negative $\hat{M}_{\delta_0}$ estimate than expected, especially when compared to Maneuver 2:6 which is nearly the same flight condition. Looking at the raw data for Maneuver 2:5, we see that the accelerometer is particularly noisy for this maneuver and contains the unexplained low frequency oscillations noted earlier (about 3.25 Hz). This probably explains why PCMLE goes to the high gust estimate and selects a lower M_{δ_0} value. Note, however, that the amount of shift in M_{δ_0} (50 percent over the value on Maneuver 2:6) should cause no closed-loop stability or performance problems.

Following the above baseline runs, a selected subset of cases was rerun with a single channel located at the parameter estimates from the first run. This corresponds to a second Newton-Raphson correction performed in sequential fashion. Results of these experiments are summarized in Table 19. Their time histories are shown in Appendix C.

The results verify two properties of the PCMLE algorithm:

1. The first Newton-Raphson parameter correction achieves improved fit to the flight data. This is evident by comparing residual traces for the baseline cases with residual traces from the second iteration. The baseline residuals correspond to the min-L channels indicated in Table 18, while the second residuals correspond to channels located at corrected parameter values from the first Newton-Raphson steps. Note that the second residuals are smaller but still do not resemble white noise during the pilot input periods. This is because PCMLE's channel models ignore several aircraft parameters which are weakly identifiable under test signal conditions but can produce substantial residual errors under large pilot inputs.

TABLE 19. SECOND ITERATION PERFORMANCE (One Channel Located at Corrected Parameter Values from First Iteration)

Maneuver	$\hat{M}_{\delta_o}$	$\hat{\sigma}_{M_\delta}$	$\hat{C}_2$	$\hat{\sigma}_{C_2}$	$\hat{M}_{\delta_e}$	$\hat{M}_\delta$	V (ft/sec)	SIGSQ	Gust Channel
2:1	-5.24	0.308	0.249	0.0564	-4.83	-4.40	458	0.860	Low
2:2	-5.17	0.241	0.328	0.0519	-4.77	-4.72	455	0.882	Low
2:3	-10.9	0.820	0.567	0.0411	-9.30	-8.87	662	0.641	Low
2:4	-10.4	0.736	0.361	0.040	-8.88	-9.77	644	1.11	Low
2:5	-52.6	4.67	0.714	0.0679	-35.8	-66.7	1890	0.681	High
2:6	-35.7	2.60	0.824	0.0976	-24.4	-48.8	1550	1.09	Low

2. The first Newton-Raphson correction comes close to achieving a local minimum of the two-parameter likelihood function implemented in baseline PCMLE. This is evidenced by the fact that the second corrections in Table 19 do not move far from the first corrections in Table 18. Most changes are within one- or two-sigma units of the algorithm's own optimistic accuracy estimates. Hence, the second step is "satisfied" with the location found by the first. We note again that, because PCMLE's models ignore several other aircraft parameters, the location of this local minimum does not necessarily correspond to the true parameter values. According to our identifiability and design studies, however, it should be accurate to within 10 percent or so.

As a final experiment, the effects of estimating additional parameters were examined using Maneuvers 2:3 and 2:5. Results of these tests are summarized in Table 20. For each maneuver, two-, three-, and four-parameter identification trials were run. These show small changes (relative to PCMLE's accuracy estimates) of the original two parameters when additional parameters are estimated. The additional parameters themselves are found only crudely, as indicated by their corresponding accuracy estimates. For example, the expected one-sigma error on C_3 (small perturbation parameter for velocity) is greater than 35. The maximum variations of C_3 are known from wind tunnel data to be only ± 60. Similarly, the small perturbation parameter for $Z_\alpha V$ has expected one-sigma errors greater than 7.20. Its maximum variations are known to be $\pm$ 10.0. Hence, while PCMLE produces numbers for the additional parameters, their accuracy is hardly better than a priori knowledge. This is consistent with past identifiability and design studies.

TABLE 20. VARYING NUMBER OF PARAMETERS ESTIMATED (One Channel Located at Corrected Parameter Values from First Iteration)

Condition	$\hat{M}_{\delta_o}$	$\hat{\zeta}_M$	$\hat{C}_2$	$\hat{\zeta}_{C_2}$	C_3	$\hat{\zeta}_{C_3}$	$\hat{C}_4$	$\hat{\zeta}_{C_4}$	$\hat{M}_{\delta_e}$	$\hat{M}_{\alpha}$	$\hat{V}$ (ft/sec)	$Z_{\hat{V}}$
Maneuver 2:3												
NP = 2	-10.9	0.982	0.21	0.0411	---	---	---	---	-9.30	-8.87	662	-580
NP = 3	-11.0	0.983	0.228	0.0454	-60.0	35.3	---	---	-9.36	-9.055	465	-585
NP = 4	-13.6	1.33	0.00054	0.105	-60.0	37.7	-10.0	7.23	-10.9	-8.22	510	-583
Maneuver 2:5												
NP = 2	-49.5	4.31	0.570	0.099	---	---	---	---	-33.7	-56.2	1830	-2630
NP = 3	-49.9	4.7	0.571	0.099	69.3	52.0	---	---	-33.9	-56.6	1900	-2640
NP = 4	-51.4	5.54	0.469	0.256	65.5	53.1	-4.66	7.99	-35.9	-53.5	1900	-2490

Value limited to ± 60 by program.

PARAMETER ESTIMATION WITH GPMLE

Selected maneuvers from Table 18 were also used to conduct identification runs with a general purpose maximum likelihood algorithm (GPMLE). This software was used to do the original identifiability analyses which led to the PCMLE design (Reference 1). It uses a conventional iterative batch-processing approach to parameter estimation. The parameter estimates are updated with standard Newton-Raphson steps until the likelihood function ceases to improve. For this algorithm, the various gradients required are analytically computed.

Identification Models for GPMLE

The identification model used by GPMLE was a three-state pitch axis model with discrete measurements of pitch rate and normal acceleration. The model is

$$\frac{d}{dt} = \begin{bmatrix} q \\ \alpha_T \\ \alpha_g \end{bmatrix} = \begin{bmatrix} M_q & M_\alpha & 0 \\ 1 & Z_\alpha & -V/SL' \\ 0 & 0 & -V/SL \end{bmatrix} \begin{bmatrix} q \\ \alpha_T \\ \alpha_g \end{bmatrix} + \begin{bmatrix} M_{\delta_e} \\ Z_{\delta_e} \\ 0 \end{bmatrix} \delta_e + \begin{bmatrix} 0 \\ \sigma_\alpha \sqrt{\frac{2V}{L}} \\ \sigma_\alpha \sqrt{\frac{2V}{L}} \end{bmatrix} \xi + \begin{bmatrix} M_o \\ g/V \\ 0 \end{bmatrix}$$

$$\begin{bmatrix} q_m \\ N_{z_m} \end{bmatrix} = \begin{bmatrix} 1 & 0 & 0 \\ dM_q & M_\alpha - Z_\alpha V & 0 \end{bmatrix} \begin{bmatrix} q \\ \alpha_T \\ \alpha_g \end{bmatrix} + \begin{bmatrix} 0 \\ dM_\delta - Z_\delta V \end{bmatrix} \delta_e + \begin{bmatrix} \sigma_q^2 & 0 \\ 0 & \sigma_{n_z}^2 \end{bmatrix} \eta$$

where

ξ, η = white noise

d = acceleration displacement from c.g.

Model Parameterization

One of the features of the PCMLE algorithm that allows it to work well while estimating a small number of parameters is its method of parameterization. The coefficients appearing in the above model are computed from one dominant parameter C_5 (which is M_{δ_o}) plus other small perturbation parameters (C_1 through C_4, C_6) as shown in Table 21.

TABLE 21. F-8C MODEL PARAMETERIZATION

$$M_q = -0.23 + (0.028 - 0.017\,C_2)\,C_5 + C_1$$

$$M\alpha = (0.61 + 0.92\,C_2)\,C_5$$

$$V = (200 + C_3)\sqrt{-C_5}$$

$$Z_\alpha V = (53 + C_4)\,C_5$$

$$M_{\delta_o} = C_5$$

$$Z_\delta V_o = (7.7 + C_6)\,C_5$$

Correction for quasi-static flexibility:

$$M_{\delta_e} = M_{\delta_o}(1 + 0.016\,M_{\delta_o} + 0.0002\,M^2_{\delta_o})$$

$$Z_\delta V = (Z_\delta V_o)\,M_{\delta_e}/M_{\delta_o}$$

GPMLE Results

The parameter estimates obtained with GPMLE are summarized in Table 22. Estimates of M_q, M_α, V, $Z_\alpha V$, and $Z_\delta V$ are plotted against M_{δ_e} in Figures 26 through 30. The figures are the original scatter plots used in the model analysis on the F-8C adaptive study (Reference 1). The x's and o's represent the model parameter values at 25 flight conditions which were used to establish the PCMLE functions given in Table 21. The functions are plotted as solid lines. The four flight data points from Table 22 are plotted as Δ's.

Comparison of the flight data with the original linear models shows that the model fits quite well for M_α, V, and $Z_\delta V$ (Figures 27, 28, and 30). However, the aircraft seems to have more damping (M_q, Figure 26) and larger c.g. acceleration due to surface deflection ($Z_\delta V$, Figure 30) than indicated by the model. Moreover, there does not appear to be a need for the quasi-static flexibility correction used in Table 21. The original model data in Figures 27 through 30 are plotted as a function of "unflexed" surface effectiveness, M_{δ_o}, while the flight data is plotted as a function of actual ("flexed") M_{δ_e}.

Since these plots are compatible (except for the scale factor changes on M_q and $Z_\delta V$ already mentioned), it follows that M_{δ_o} may just as well be interpreted as M_{δ_e}.

TABLE 22. GPMLE PARAMETER ESTIMATION SUMMARY

Parameter	Test Points (Flight-Maneuver)														
	2:2			2:6			3:1			3:4			3:5		
	Estimate	Estimated Accuracy		Estimate	Estimated Accuracy		Estimate	Estimated Accuracy		Estimate	Estimated Accuracy		Estimate	Estimated Accuracy	
		[illegible]	( )		[illegible]	( )		[illegible]	( )		[illegible]	( )		[illegible]	( )
M_q	-0.4742	0.028	5.9	-0.767	0.028	3.6	-0.769	0.045	5.9	-1.578	0.048	3.0	-0.586	0.041	7.0
M_{α}	-3.916	0.0516	1.3	-43.52	0.16	0.4	-6.51	0.109	1.7	-18.9	0.174	0.9	-4.22	0.056	1.3
N	386	[illegible]	4.9	934	11.3	1.2	536	30	5.5	834	19.0	2.3	792	91.8	11.6
Z_N	-295.6	[illegible]	1.9	-2052	8.5	0.4	503.2	10.3	2.0	-1436	12.5	0.9	-292	14.9	5.1
M	-5.66	0.151	0.9	-32.27	0.24	0.7	-10.1	0.15	1.5	-26.75	0.32	1.2	-5.78	0.078	1.4
Z N	-83.86	[illegible]	3.9	-518	11.6	2.3	-125.6	6.65	5.3	-329.4	14.3	4.5	-42.4	4.3	10.2

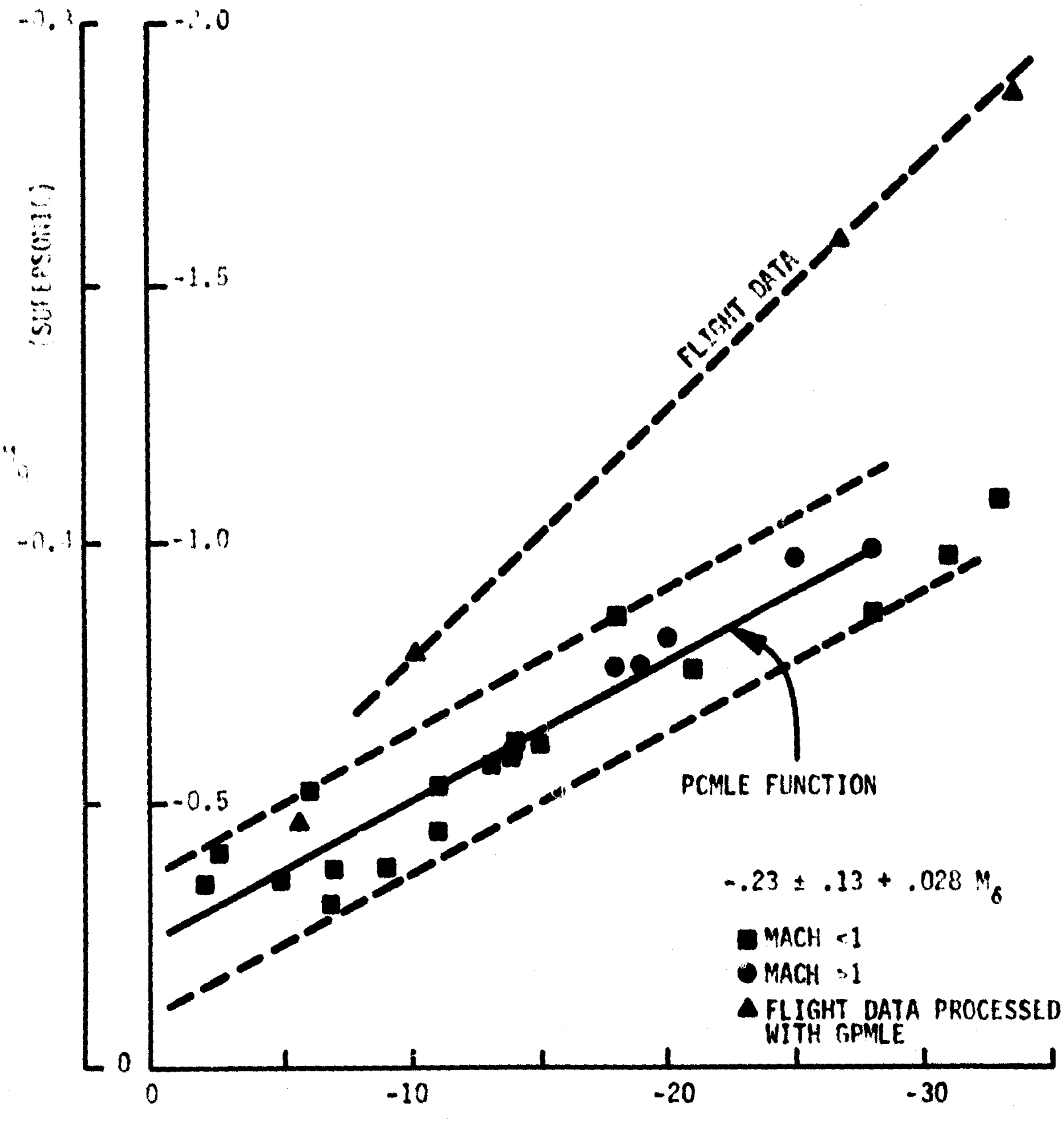

Figure 26. M_q vs. M_δ

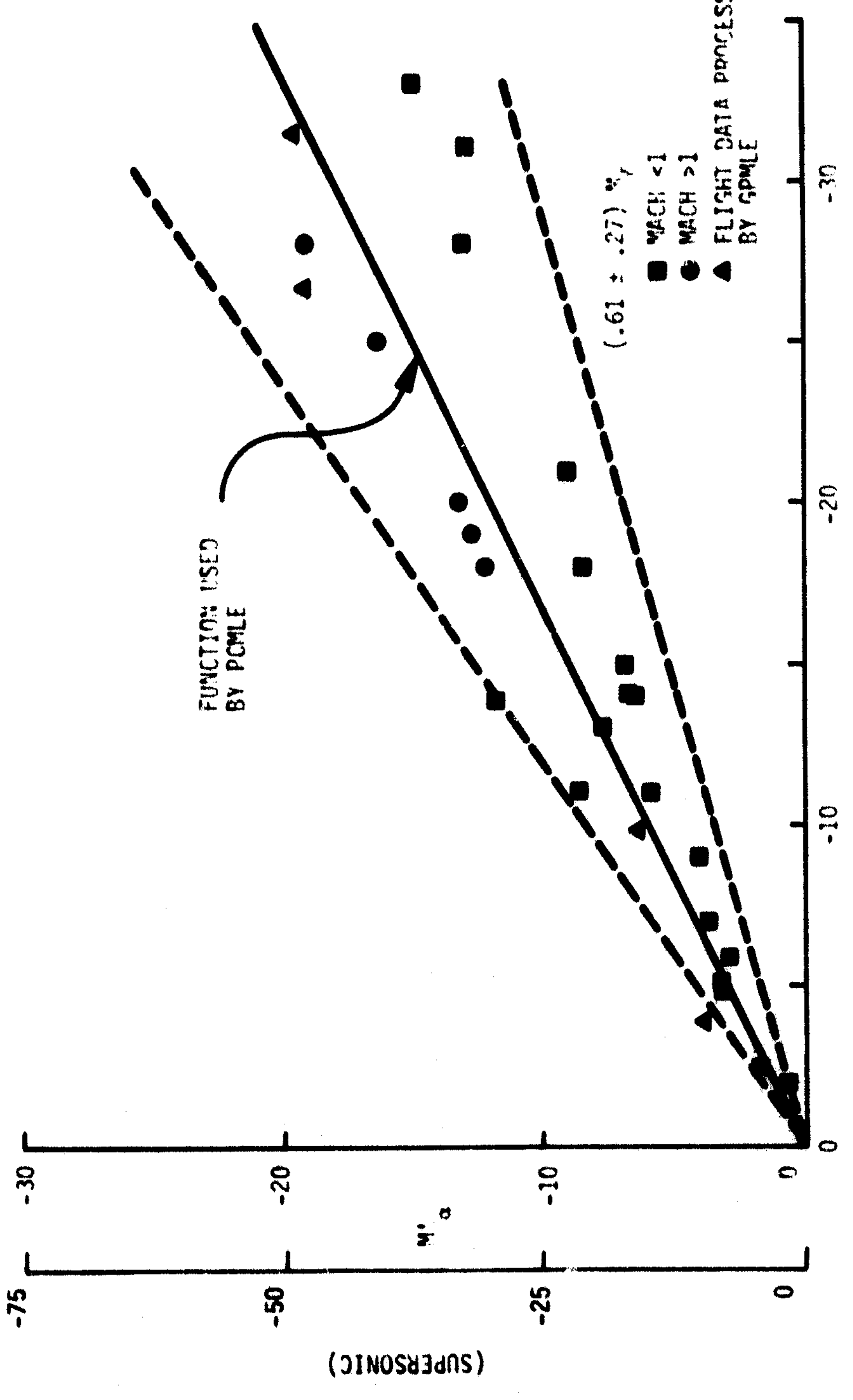

Figure 27. M_{α} **vs.** M_{δ}

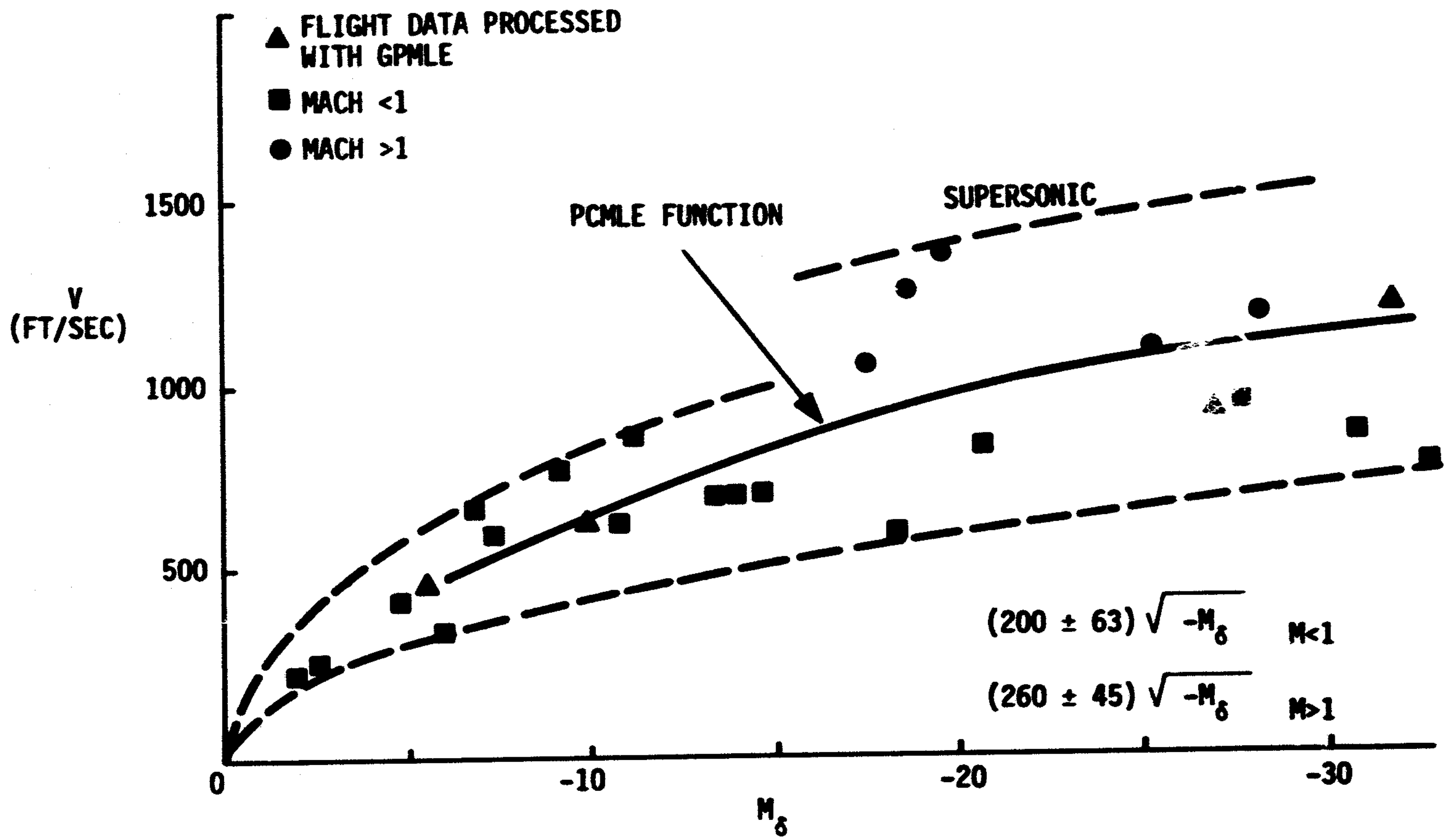

Figure 28. V vs. M_δ

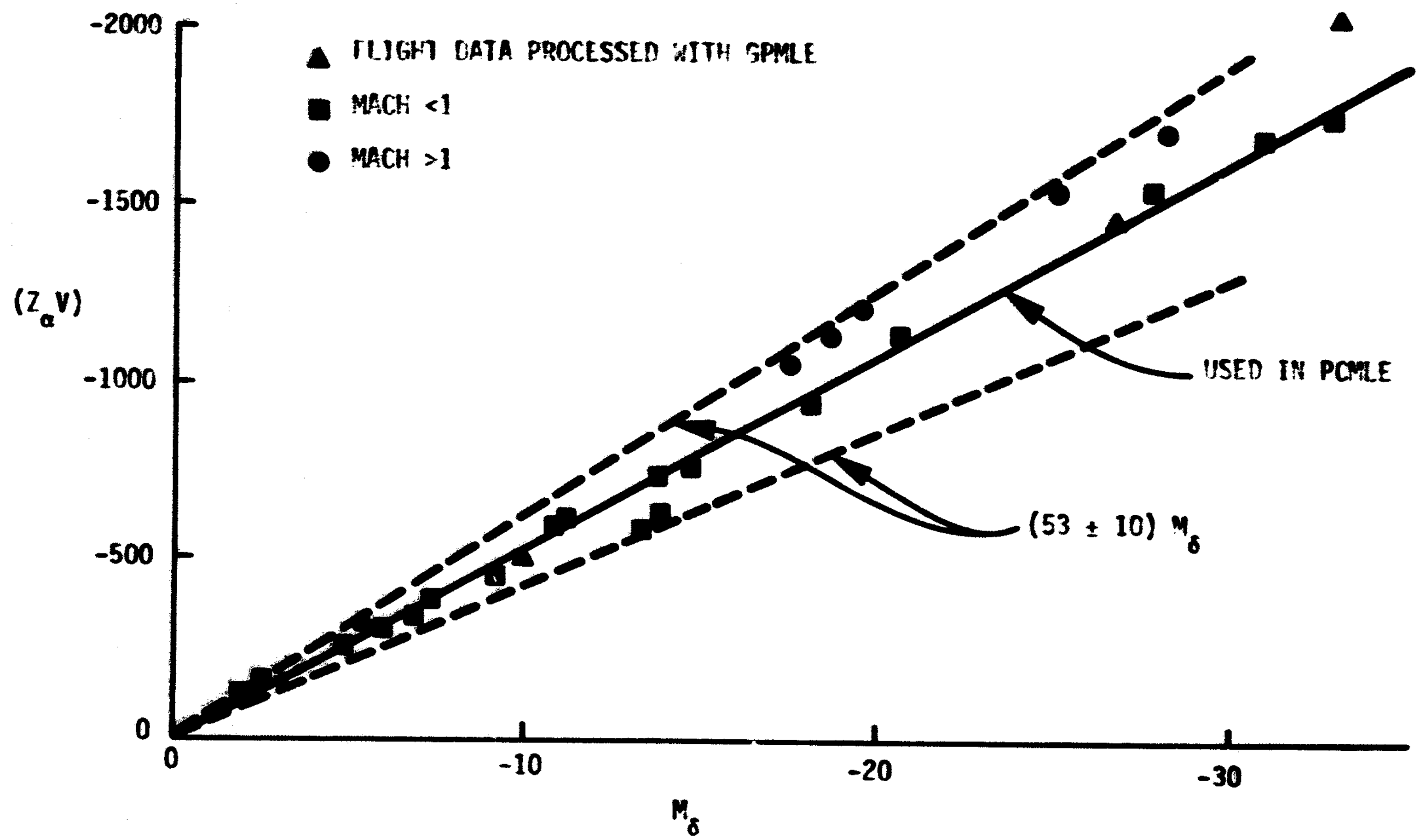

Figure 29. $(Z_\alpha V)$ vs. M_δ

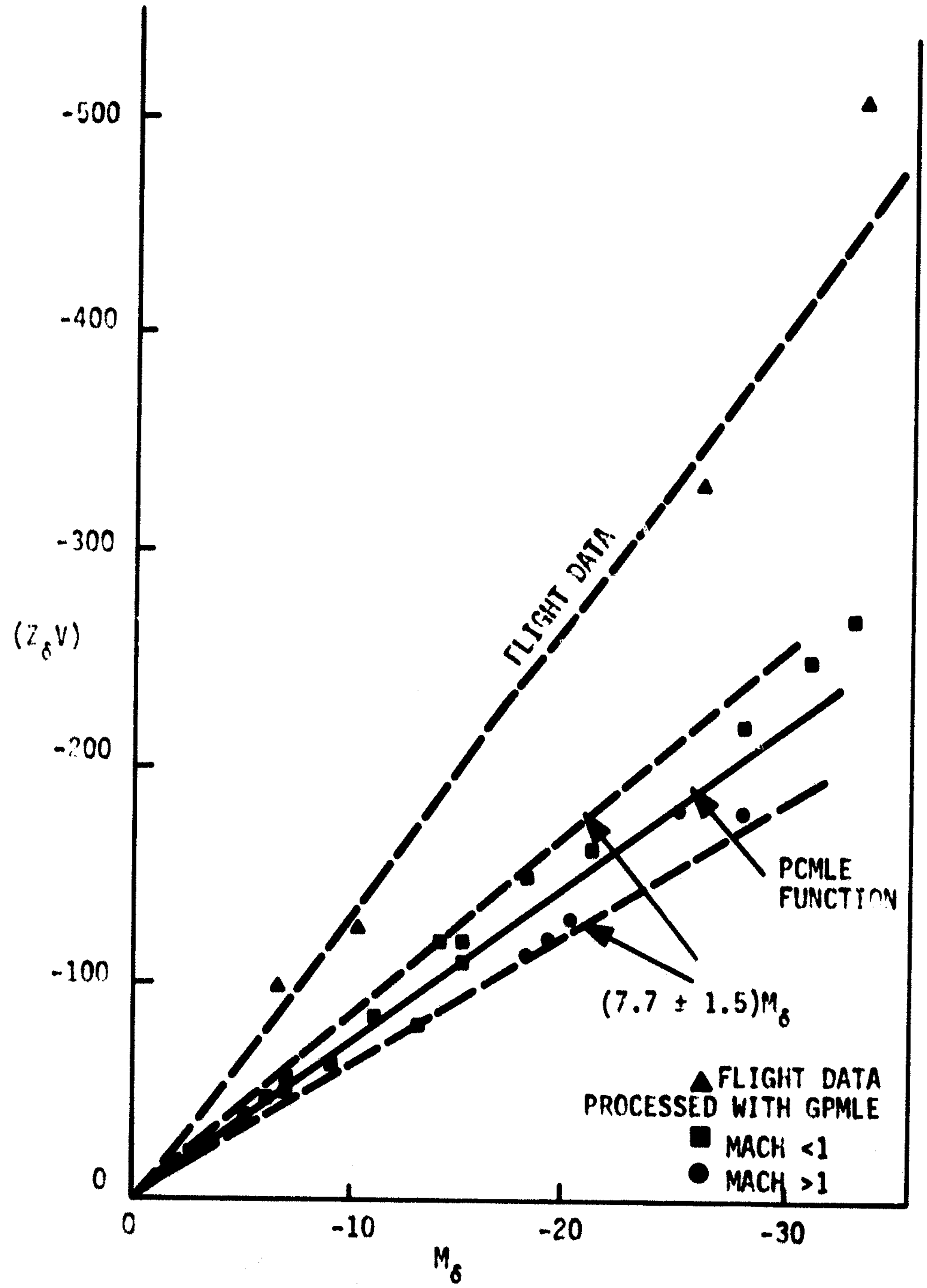

Figure 30. $Z_\delta V$ vs. M_δ

GPMLE and PCMLE Comparisons

A comparison of PCMLE and GPMLE estimates for a subset of maneuvers is given in Table 23. For the M_δ and M_α parameters, a percent difference is also shown which indicates that the two estimation procedures agree to within reasonable percentages. True values of these parameters are, of course not known. For the V estimate, on the other hand, a measured air data value is available. This value falls somewhere between the GPMLE and PCMLE estimates. The GPMLE velocity estimate does not improve over the PCMLE estimate at two test points (2:2 and 3:1). Both the percentage differences and the differences between estimated and measured values are consistent with theoretical performance predicted during the PCMLE design program.

Representative comparisons of GPMLE and PCMLE residual time histories ($\nu = y - \hat{y}$) are shown in Figure 31. These traces correspond to the residuals from the last iteration of GPMLE (a Kalman filter located at the parameter values in Table 22) as compared with the residuals from the min-L channel of PCMLE (a Kalman filter located at one of the nominal channel locations given in Table 6). Both filters fit the raw signals quite well. However, it is clear that the GPMLE filter should (and does) fit better because it includes several aircraft model parameters not recognized by the PCMLE filters. The net effects of this improved fit are the 10 to 20 percent parameter differences already noted in Table 23.

MANEUVERING FLIGHT

The performance of PCMLE during a maneuver is shown in Figure 32. The top five traces show the response of the aircraft. The maneuver, lasting about 135 seconds, is an acceleration from Mach = 0.85 to Mach = 1.15

TABLE 23. GPMLE/PCMLE COMPARISONS

Test Point	$\hat{M}_{\delta}$			$\hat{M}_{\alpha}$			$\hat{V}$		
	GPMLE	PCMLE	% Δ	GPMLE	PCMLE	% Δ	GPMLE	PCMLE	Measured
2:2	-5.66	-5.38	4.9	-3.92	-4.55	-16.1	386	464	452
3:1	-10.1	-8.70	13.9	-6.51	-7.62	-17.1	536	590	586
3:4	-26.7	-28.1	-5.2	-18.9	-19.2	-1.6	834	1132	882
2:6	-32.3	-33.1	-2.5	-43.5	-49.0	-12.6	934	1418	1153

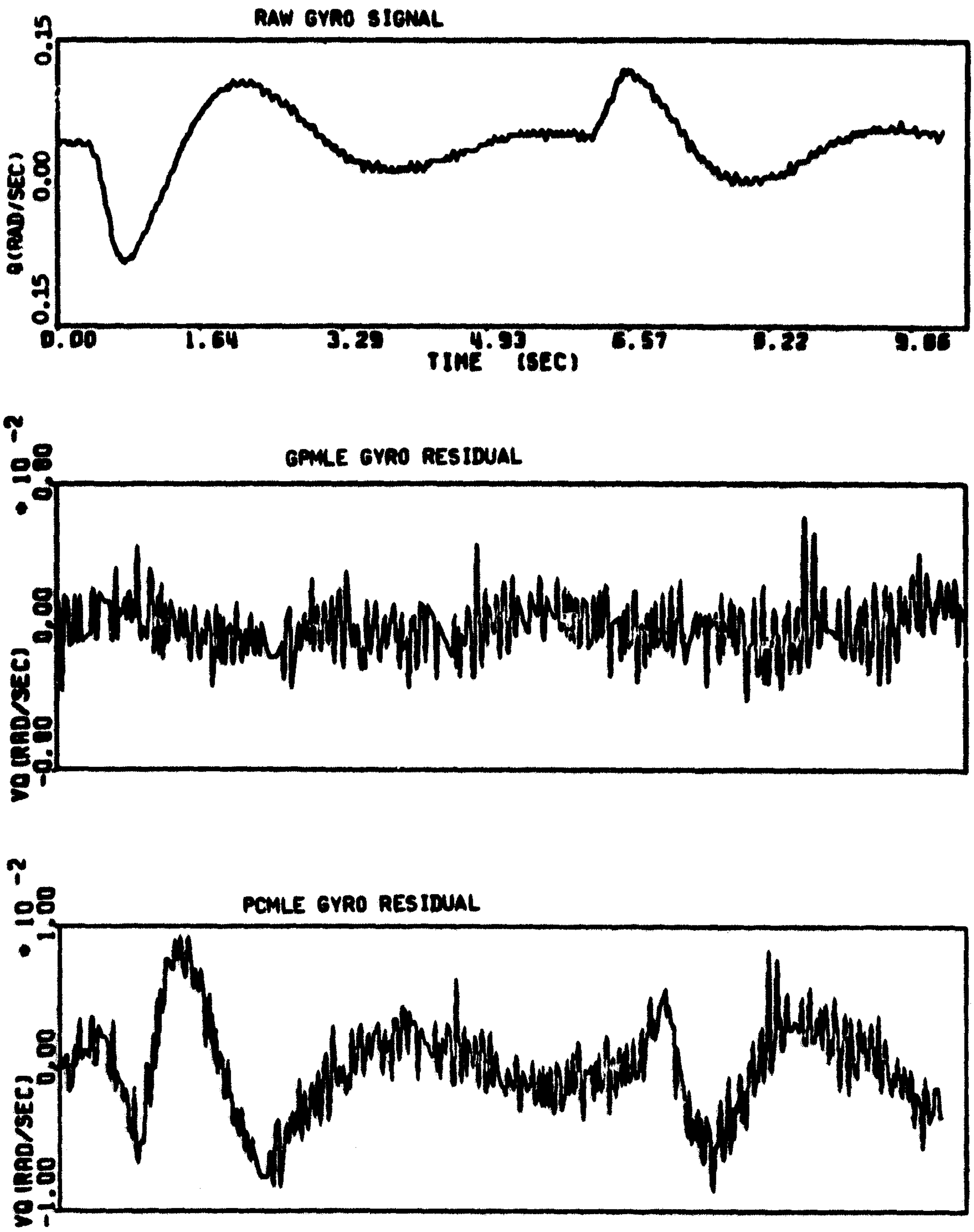

Figure 31. GPMLE/PCMLE Residual Comparisons

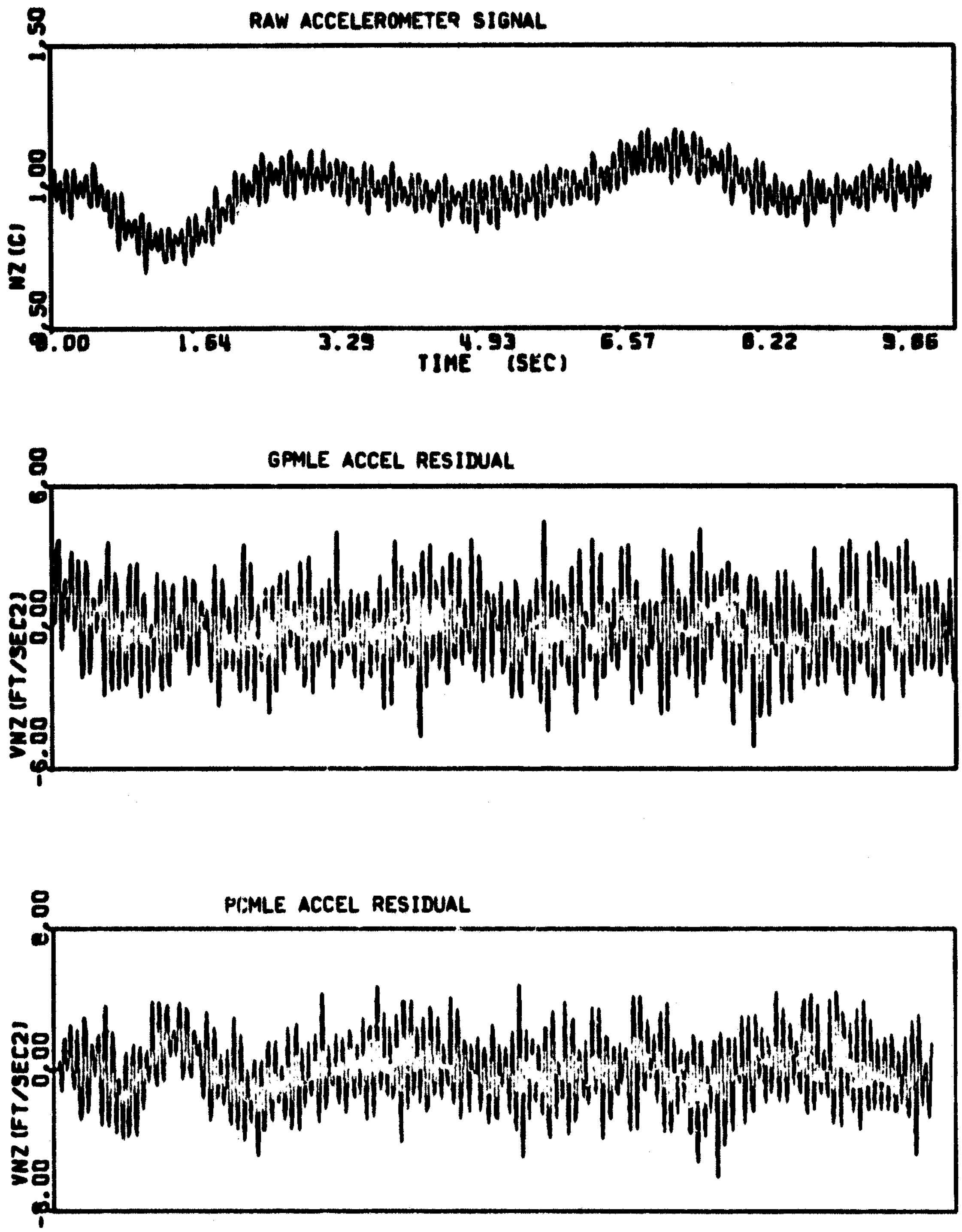

Figure 31. GPMLE/PCMLE Residual Comparisons (concluded)

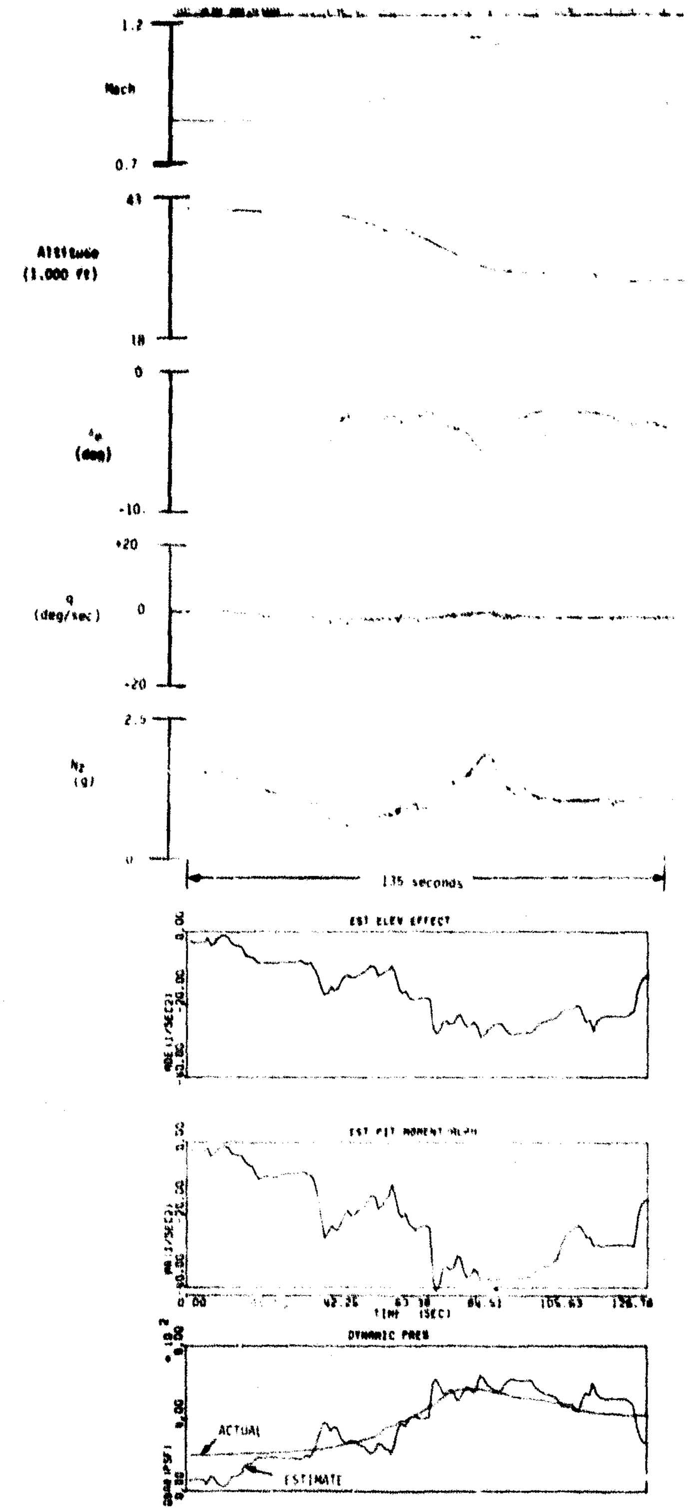

Figure 32. PCMLE Performance in Maneuvering Flight

during which the altitude decreases from 41,000 feet to 23,000 feet. This is immediately followed by a deceleration back to Mach = 0.89. The F-8C is supersonic for about 57 seconds during this maneuver.

The next two traces show the $\hat{M}_{\delta_e}$ and $\hat{M}_\alpha$ estimates from PCMLE. Note how $\hat{M}_\alpha$ goes sharply more negative (as it should) as the aircraft goes supersonic. The $\hat{M}_{\delta_e}$ estimate was used to produce an estimated dynamic pressure $\hat{\bar{q}}$. In the bottom trace of Figure 32, this estimate is compared to a dynamic pressure ($\bar{q}_a$) computed from the measured altitude and mach number. The $\bar{q}$ error is initially large (for 10 seconds or so) because there is no pilot activity. (This maneuver does not contain any test signal.) During the remainder of the maneuver the RMS error is about 20 percent.

SECTION 7

FLIGHT TEST RECOMMENDATIONS

Based on the acceptance test and flight data processing results discussed in previous sections, the PCMLE software is judged to be ready for flight test evaluation. Recommended nominal parameters, test inputs, and evaluation experiments which should be incorporated in the flight tests are discussed in this section.

NOMINAL PCMLE PARAMETERS

The flight tests should be initiated with the same nominal PCMLE parameters recorded in Table 5, except for the following modifications:

1. Modified PCMLE model parameterization

MQ1	=	0.044	(old value 0.028)
ZDV1	=	13.8	(old value 7.7)
FX1	=	0.	(old value 0.016)
FX2	=	0.	(old value 0.0002)

The first two changes alter the pitch damping function and the acceleration due to surface deflection function in PCMLE's models. The remaining changes remove quasi-static flexibility. These are justified by GPMLE results in Section 6.

2. Modified sensor noise

SIGACCO = 0.06 (old value 0.02)

This change increases the accelerometer noise level to the value found in Section 5.

TEST SIGNALS

Test inputs for PCMLE flight evaluation should include normal pilot inputs and flight disturbances, plus random test signals generated by the filter network shown in Figure 33.

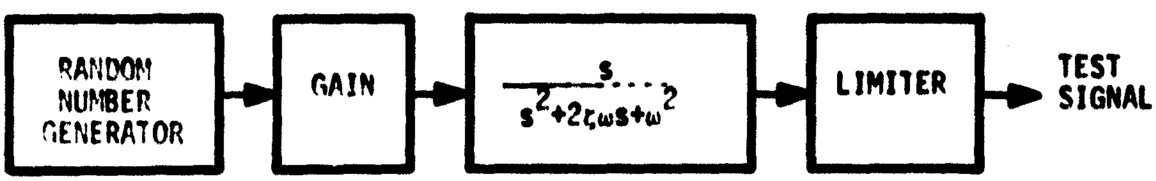

Figure 33. Test Signal Generation

This filter is mechanized as a subroutine of PCMLE and corresponds to the same test signal routine used for simulator design evaluation at Langley Research Center. The output should be applied as a C*-command to the pitch axis control augmentation system. The random number generator provides a uniform distribution from -0.5 to +0.5. The frequency and damping of the filter are adjustable, as is the RMS level of the test signal.

Provisions have been added to produce sine wave and square wave test signals with the same software. To do this the input and damping are set to zero and initial conditions on the filter are defined to produce a sine wave. By limiting the sine wave, a suitable square wave can be realized.

A FORTRAN coded version of the test signal subroutine is shown in Table 24. The various parameters are communicated through labeled common (UTEST). Typical values are given in Table 25.

TABLE 24. FORTRAN CODE FOR TEST SIGNAL

```
      SUBROUTINE TSIG(MODE,UT)
      COMMON/UTEST/DT,SEED,WUT,DUT,SIGUT,UT10,UT20,UTMAX
C     UT/INPUT = S*SIGUT/(S*S + 2*DUT*WUT*S + WUT*WUT)
C     INPUT = RANDOM NO WITH 0 MEAN  UNIFORM  -0.5 TO  0.5
C     UT1,UT2  STATES IN SECOND ORDER FILTER
      GO TO (1,2) MODE
C     INITIALIZATION
    1 W2UT=-WUT*WUT*DT
      TZWUT=-2.*WUT*DUT*DT
      GAMUT0=SQRT(-24.*TZWUT)
      UT1=UT10
      UT2=UT20
      RETURN
    2 SEED=AMOD(3125.*SEED,34359738368.)
      S=0.291038304567E-10*SEED - 0.5
      S=W2UT*UT1 + TZWUT*UT2 + GAMUT0*SIGUT*S
      UT1=UT1 + DT*UT2
      UT2=UT2 + S
      UT=UT2
      IF(ABS(UT).GE.UTMAX) UT=SIGN(UTMAX,UT)
      RETURN
      END
```

TABLE 25. TEST SIGNAL PARAMETERS

ω (WUT)	= 6.0	--Frequency	
ζ (DUT)	= 1.25	--Damping ratio	
SIGUT	= 4.0	--RMS level	
Initial Values:			
SEED	= 3051758125	--Random number generator seed	
UT10	= 0	--Initial test signal	
UT20	= 0	--Initial test signal rate	
UTMAX	= 10	--Test signal magnitude limit	

FLIGHT EXPERIMENTS

Recommended flight test experiments with the PCMLE software are summarized in Table 26. They fall into seven major groups which should be completed in sequential fashion in order to maximize safety and experimental value. An eighth group of experiments which involves off-line processing of data from other groups is also recommended. These off-line runs can be conducted as data become available. They serve to maximize the experimental value of available flight hours. A brief description of each experimental group is given in the following pages.

TABLE 26. RECOMMENDED PCMLE FLIGHT EXPERIMENTS

GROUP	FUNCTION	CONTROL MODE	PCMLE MODE	FLIGHT CONDITIONS*	INPUTS	OBSERVATION
1	Test signal Acceptability	Pitch CAS with Air Data $\bar{q}$	Open loop nominal 5 channels standard Newton-Raphson update	2-2, 2-6, 3-1, 3-4, 3-5 as a minimum	Test signal varied from 0 to 10 ft/sec^2	Detectability and acceptability of test signal
2	Open Loop RAV operation in real-time	Same as 1	Same as 1 but no test signal	Same as 1	Pilot doublets as used in recorded maneuvers	Repeat results for selected maneuvers (2-2, 2-6, 3-1, 3-4, 3-5,
3	Open Loop RAV operation	Same as 1	Same as 1	Same as 1	Test signal	Estimation accuracy as function of test signal size compare with simulator results
4	Closed Loop RAV Operation	Pitch CAS with adaptive $\bar{q}$ schedule	Same as 1 but closed loop	Same as 1	Test signal plus pilot commands	Compare with results of group 2 and 3
5	Flight Transitions	Same as 4	Same as 4	• Maneuvering flight using power changes • Constant attitude banking turns	Test signal	Parameter tracking ability
6	All Attitude Maneuvers	Same as 4	Same as 4	All-attitude maneuvers --full rolls and loops Configuration changes --gear, flaps, wing transitions	Test signal	Parameter tracking ability
7	Flight in turbulent air	Same as 4	Same as 4	Repeat 4 as practical in turbulent air. Fly near buffet boundary using wind up turns	Same as 4	Same as 4
8	Off-line data processing	-	Redo selected experiments from groups 1-7 with various PCMLE options	-	-	-

Group 1: Test Signal Acceptability

These experiments can be conducted with the standard air-data scheduled C*-command control mode. The random test signal should be mechanized as shown above and inserted at the C*-command point. With several different pilots and at several straight and level trimmed conditions, the RMS test signal level should be slowly increased by a ground-based experimenter from zero to 10 ft/sec. The pilot should be asked to indicate when he first detects the signal and when it becomes unacceptable. The corresponding levels should be noted by the experimenter. We recognize that the definitions of detectability and acceptability must necessarily remain vague and that the entire experiment will at best be "informal" in the human factors sense. More sophisticated experimentation is not justified unless the test signal level turns out to be a crucial design and performance issue.

Group 2: Open-Loop RAV Operation

These experiments repeat selected maneuvers from this report in the real-time RAV environment but with uplink data unused (i.e., control gains should be set by the air-data schedule). Each experiment should qualitatively match estimation results presented in this report. This will verify proper real-time downlink/RAV/PCMLE operation. The received uplink gain parameters (unused) should be compared via telemetry with on-board air-data scheduled gains and with PCMLE's sent uplink parameters. This verifies proper uplink and gain-scheduled operation.

Group 3: Open-Loop RAV Operation With Test Signals

These experiments examine estimation accuracy in straight and level "hands off" flight at several test signal levels. The aircraft should be in the standard air-data scheduled C*-Command Mode, and PCMLE should be in its baseline configuration. The test signal level should range from less than detectable to barely acceptable, as determined from Group 1 experiments.

Group 4: Closed-Loop RAV Operation

These experiments repeat selected maneuvers from this report with the RAV loop closed. That is, the aircraft should be in the Adaptive C*-Command Mode, and PCMLE should be in Baseline. Cases with pilot commands only and with pilot commands plus selected test signal levels (from Group 3) should be run and should qualitatively match estimation results presented in this report. Closed-loop handling qualities should be judged by the pilot and should closely approximate the scheduled C*CAS mode ratings. If these flight results are positive, other test points not covered in this report should be evaluated as available.

Group 5: Flight Transitions

These experiments examine PCMLE's tracking capability in closed-loop RAV operation. Cases should be run with test inputs only and with occasional (normal) pilot inputs.

Group 6: All-Attitude Maneuvering Flight

These experiments evaluate PCMLE performance during various flight maneuvers and configuration changes. The aircraft should remain in the Adaptive C*-Command Mode throughout, and PCMLE should be in Baseline with a test signal level judged acceptable from previous flights.

Group 7: Flight in Turbulent Air

PCMLE performance should be evaluated in turbulent flight environments as available.

Group 8: Off-Line Data Processing

These experiments use selected flight data from Groups 1 through 7 to evaluate various PCMLE options. Using prerecorded data for this purpose serves two functions. First, it makes more effective use of available flight hours, and, second, it provides a baseline run over the same data against which to make performance comparisons.

The options which show greatest promise include:

- Channel Reconfiguration
  - More or fewer channels
  - More channels without Newton-Raphson parameter corrections
- Kalman Parameter Corrections
  - Unaided (as presently mechanized)
  - Aided with other data (as discussed in Reference 2)

- **Sample Skipping**

Indications to date are that the second Newton-Raphson step option and the option to find additional parameters have little promise and hence should be of lower priority. Two recommended channel reconfiguration options are given in Table 27. One uses only three channels and hence relies heavily on the Newton-Raphson parameter correction step for accurate estimation. The other uses ten channels. It should be evaluated with and without a Newton-Raphson parameter correction step and also in combination with sample skipping. Both procedures would offset the increased computing time needed to handle the large number of channels.

Additional details on the recommended experiments in each of the above groups can be found in Table 26. We note that these experiments are not intended to represent a rigid protocol for flight experimentation with PCMLE; rather, they should be viewed as a rough experimental outline to be enhanced and modified as the opportunities of the moment permit.

TABLE 27. CHANNEL RECONFIGURATIONS
(C_4 = 0 for All Channels)

CHANNEL	M_{δ_e}	C_2	C_3
1	-5.0	0	0
2	-20.0	0	0
3	-26.7	1.	60.
1	-3.25	0	0
2	-4.67	0	0
3	-6.76	0	0
4	-9.69	0	0
5	-13.9	0	0
6	-20.1	0	0
7	-28.9	0	0
8	-41.7	0.	0.
9	-28.9	1.	60.
10	-41.7	1.	60.

SECTION 8

CONCLUSIONS

The goal of this program was to refine the PCMLE design and prepare it for flight evaluation on DFRC's Remotely Augmented Vehicle facility.

The refinement includes several steps:

1. The addition of a number of options to enhance the research value of flight tests by permitting easy modification to the baseline configuration (such as adding channels, varying the sample rate, etc.). Proper operation of these features has been verified on the F-8C Iron Bird.

2. The determination of sensor noise statistics from ground tests and in-flight recordings. Results show that the statistics are reasonably constant over the flight envelope. Specific values recommended for the PCMLE algorithm are based on time histories of Kalman filter residuals from the flight records. The assumption that sensor noise does not have to be identified on-line was confirmed.

3. Identification performance was checked using the flight data. These estimates were cross-checked with batch MLE identification and compared with wind tunnel data. The estimates are consistent. Overall performance on flight data correlates well with theoretical predictions and simulation results.

The PCMLE design is now ready for flight test. Specific experiments are recommended in Section 7. Successful flight demonstration of the design signifies renewed vitality of adaptive flight controls in modern digital implementations.

APPENDIX A

FLIGHT DATA TIME HISTORIES

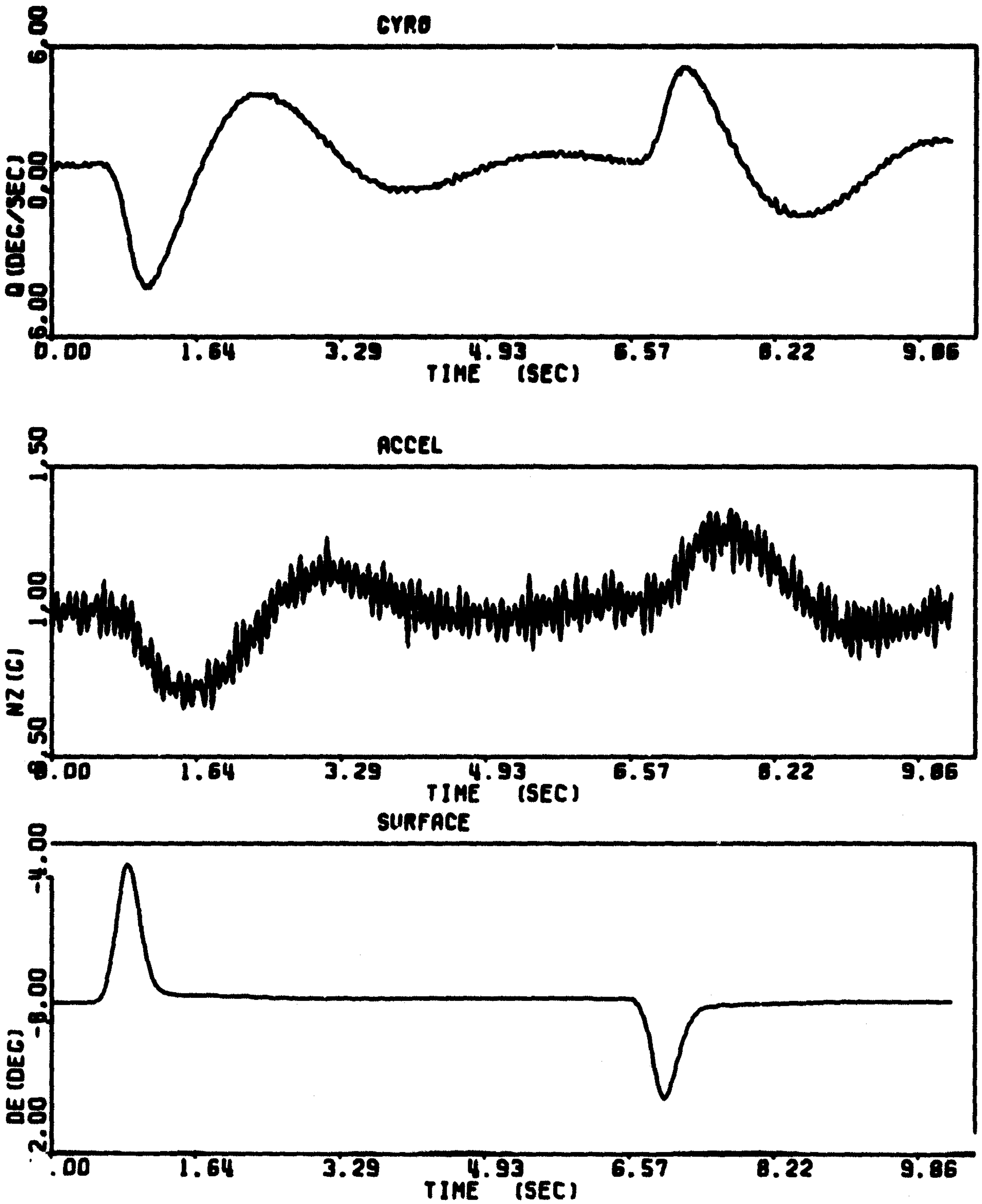

Figure A1. Maneuver 2:1

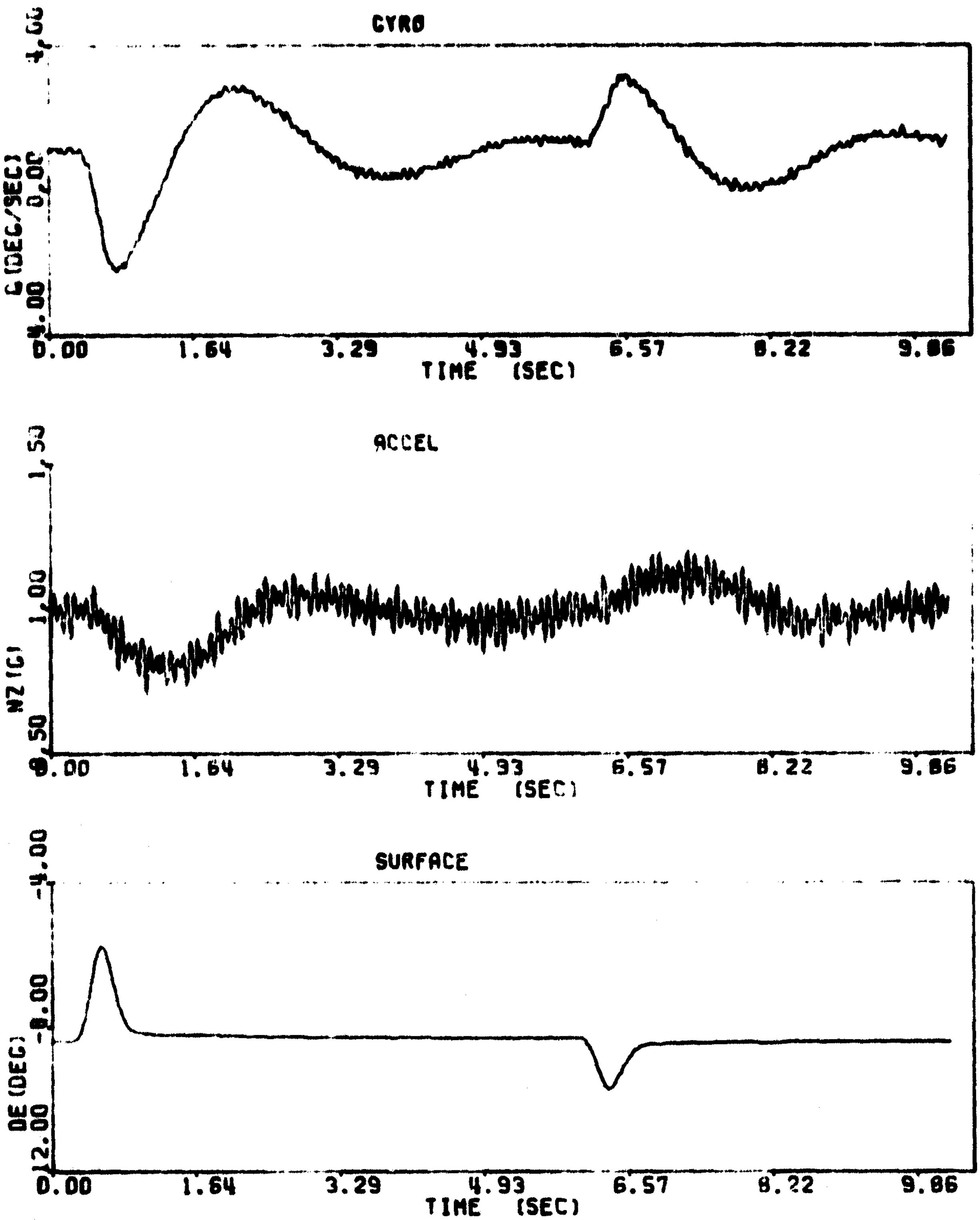

Figure A2. Maneuver 2:2

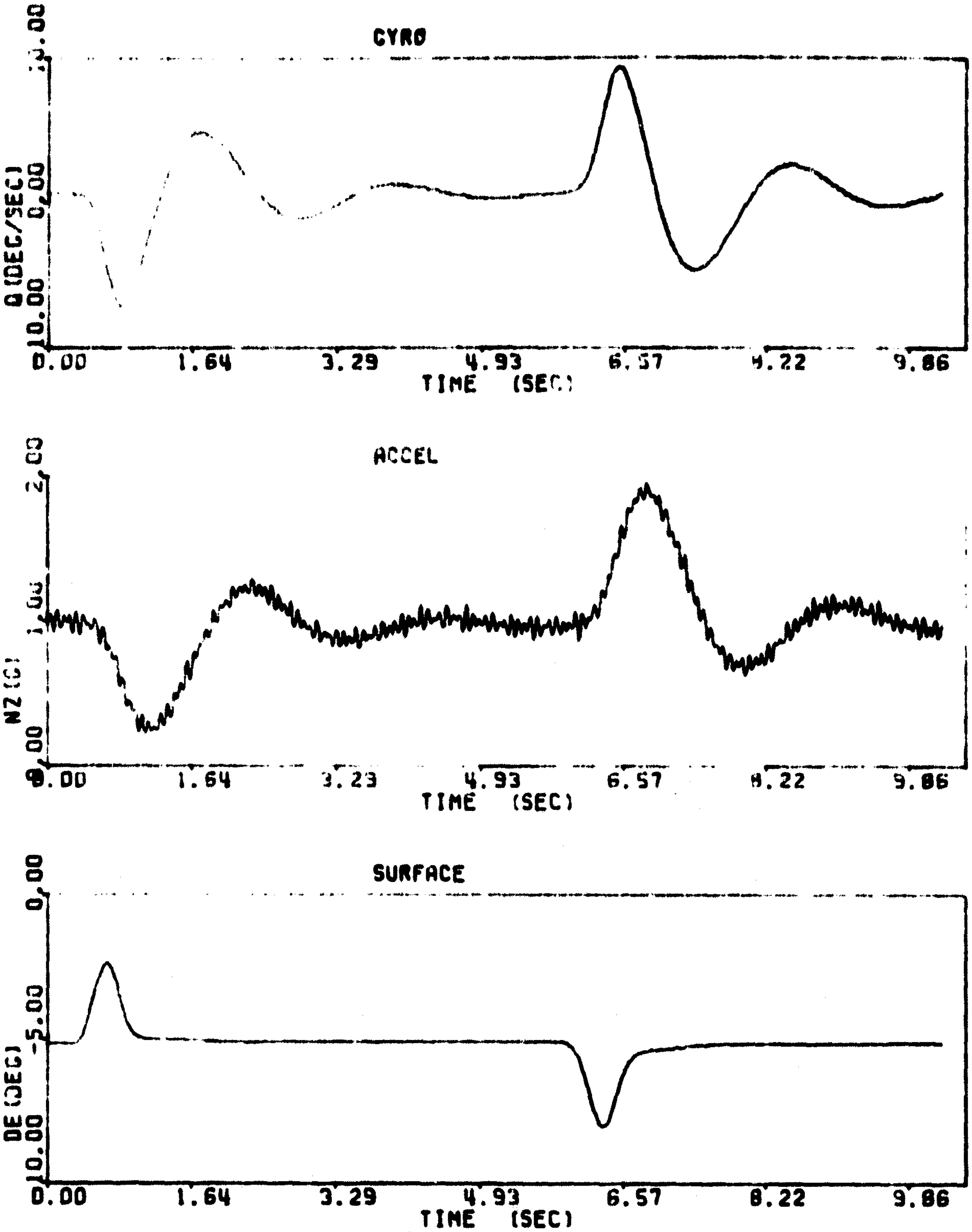

Figure A3. Maneuver 2:3

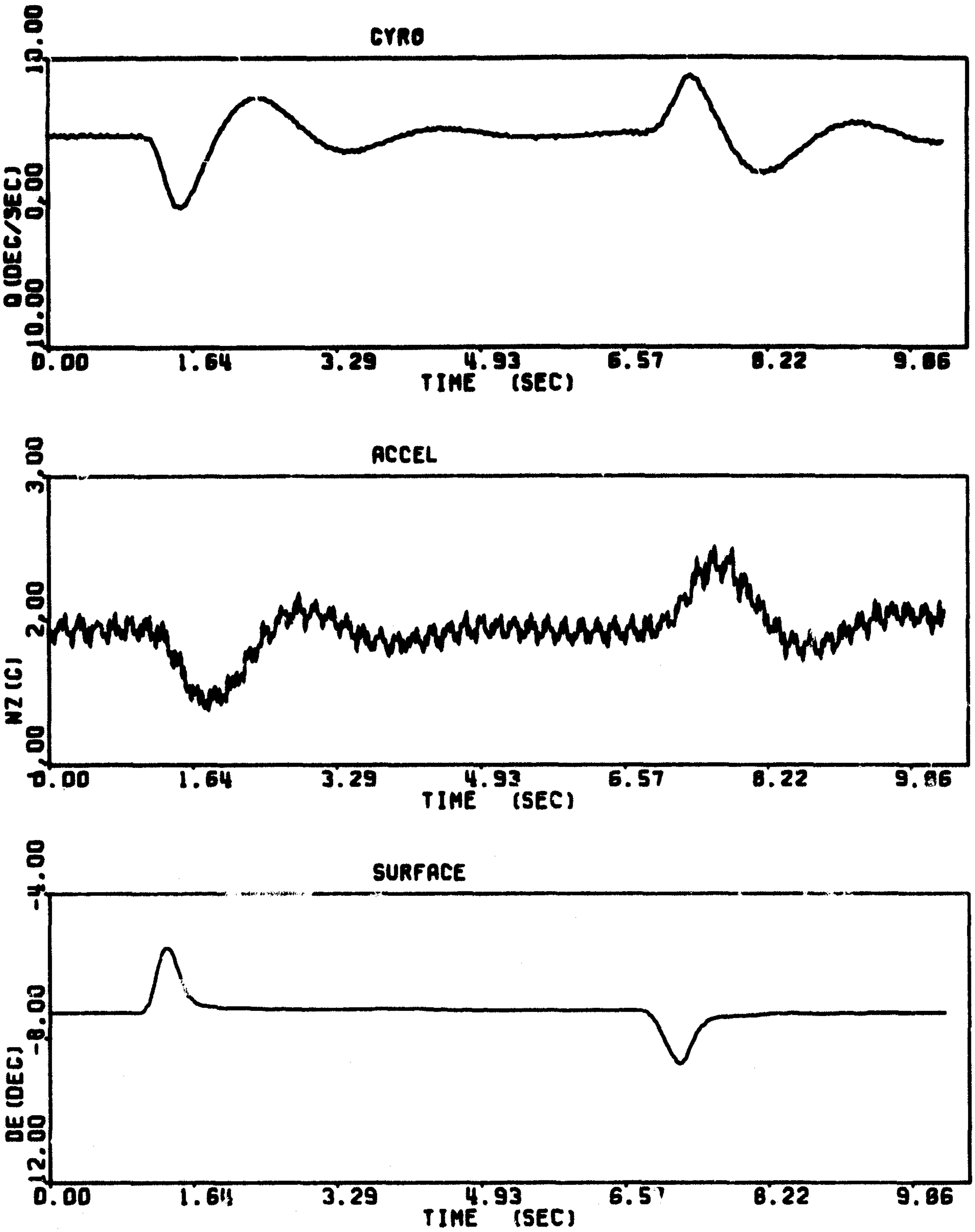

Figure A4. Maneuver 2:4

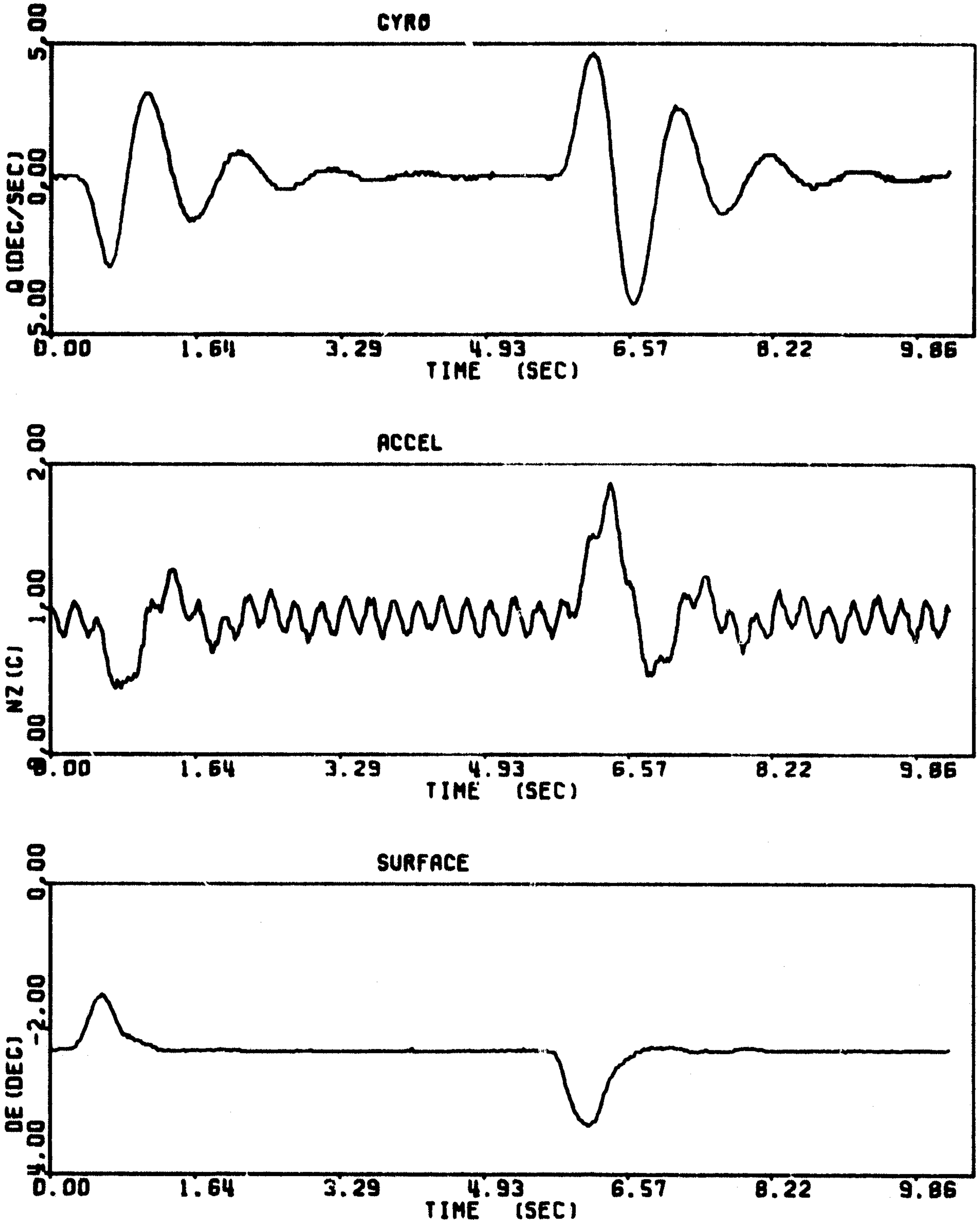

Figure A5. Maneuver 2:5

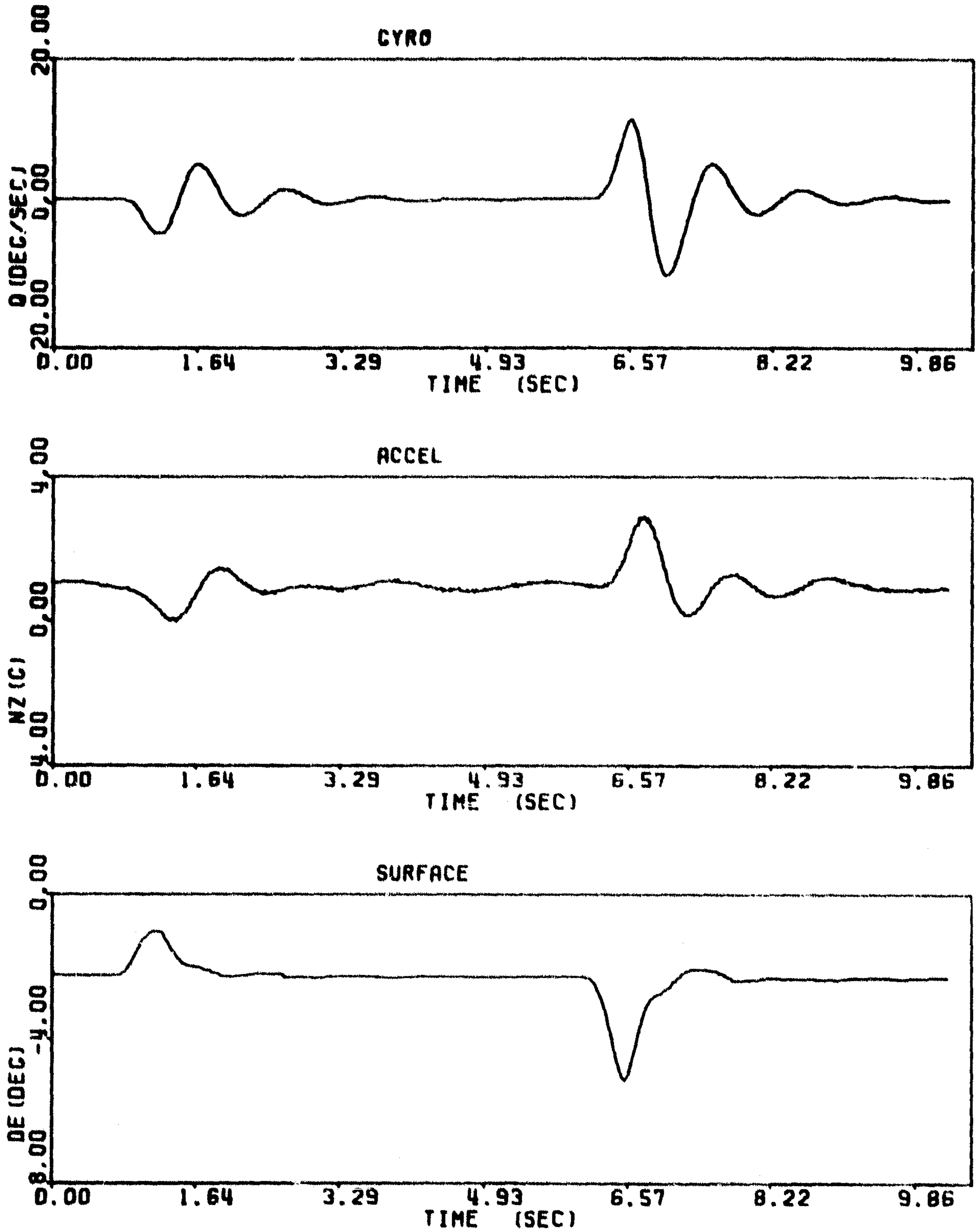

Figure A6. Maneuver 2;6

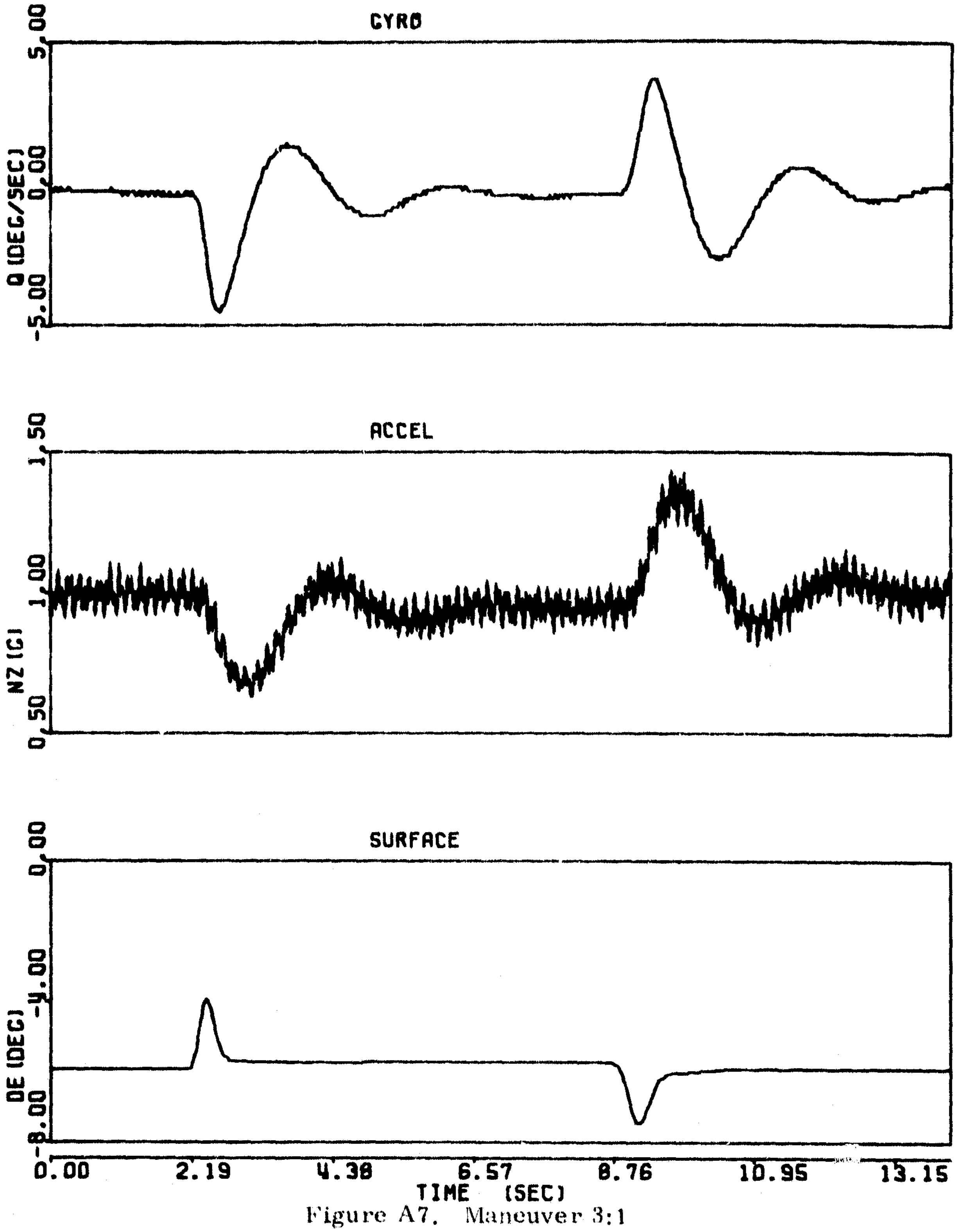

Figure A7. Maneuver 3:1

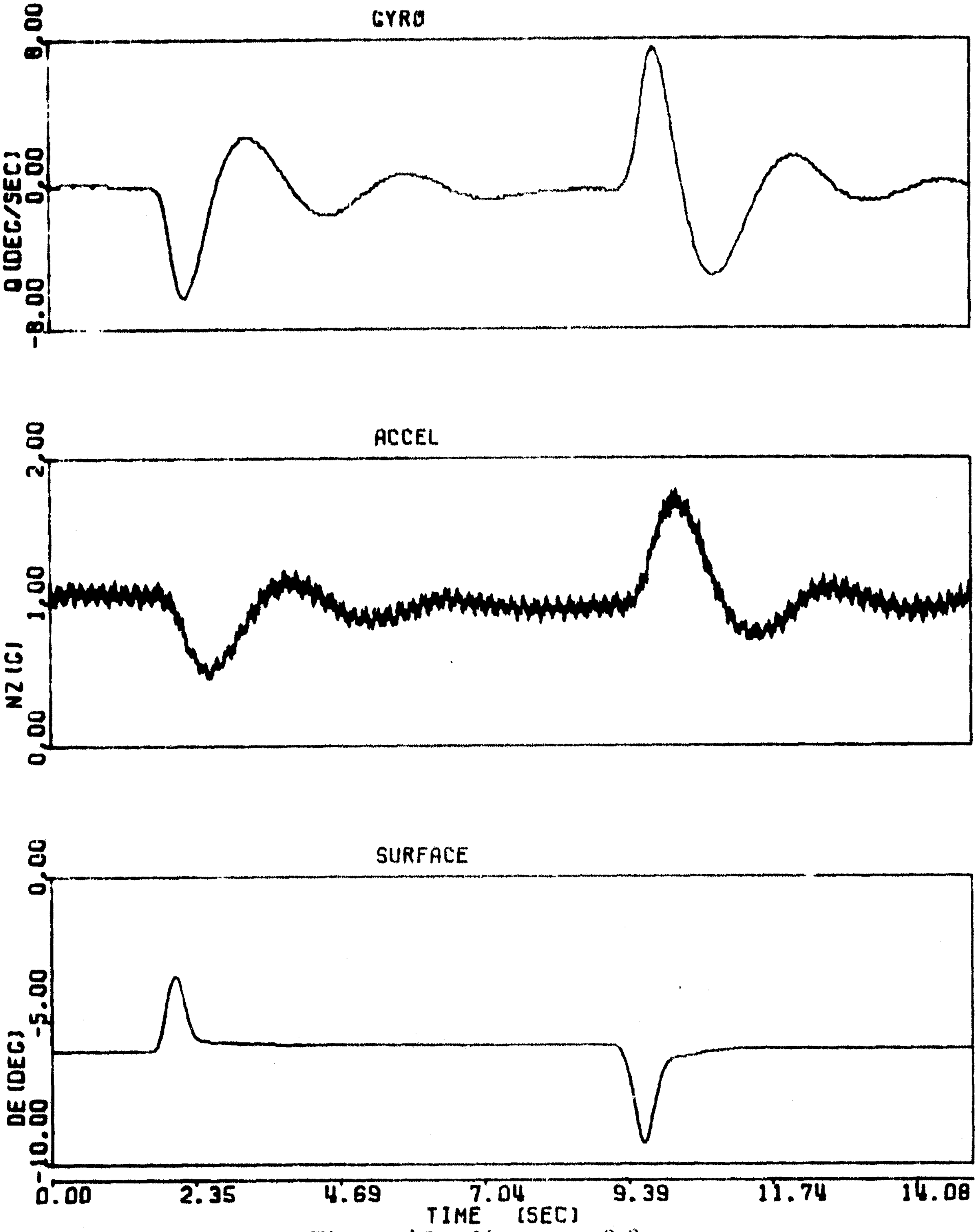

Figure A8. Maneuver 3:2

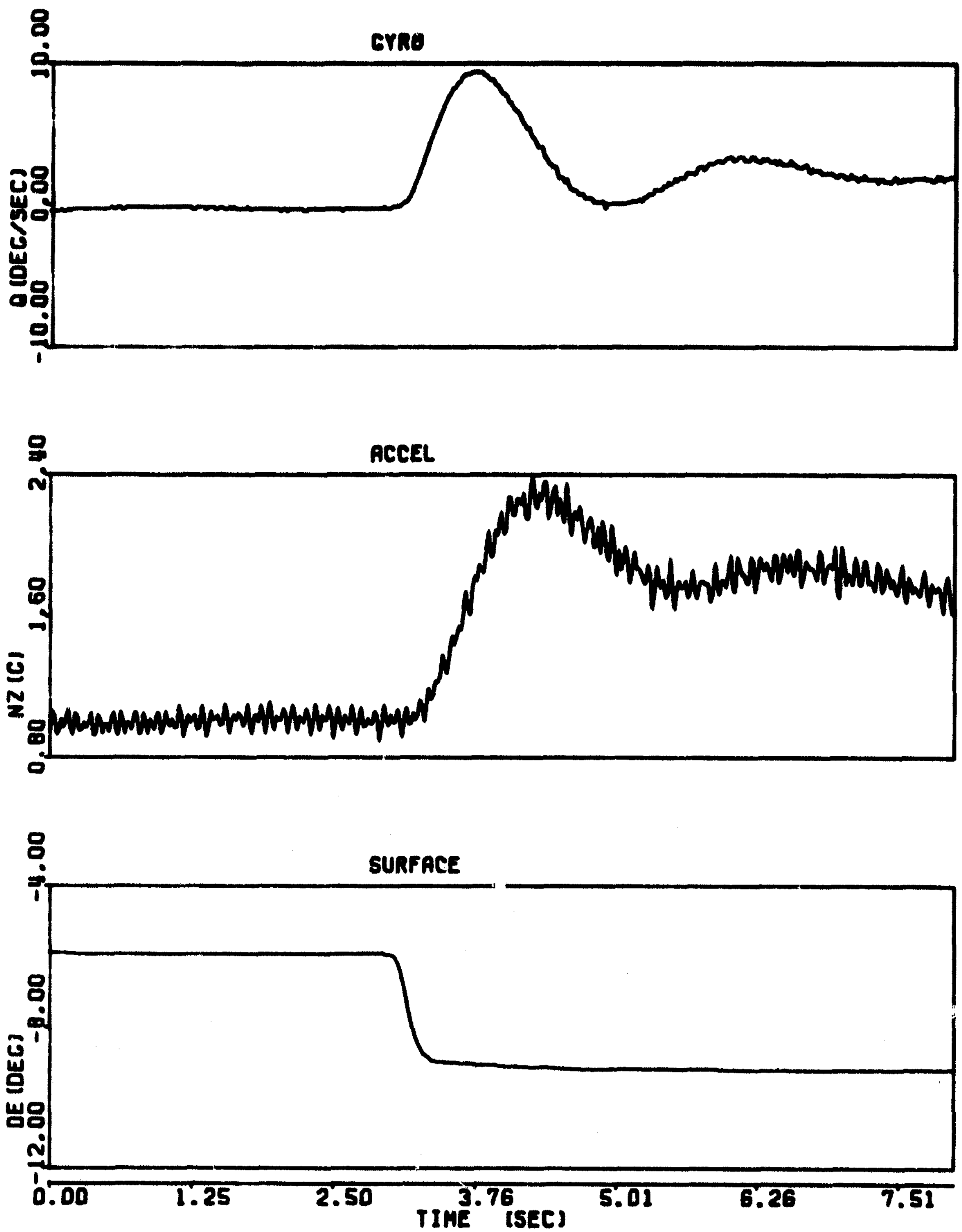

Figure A9. Maneuver 3:3

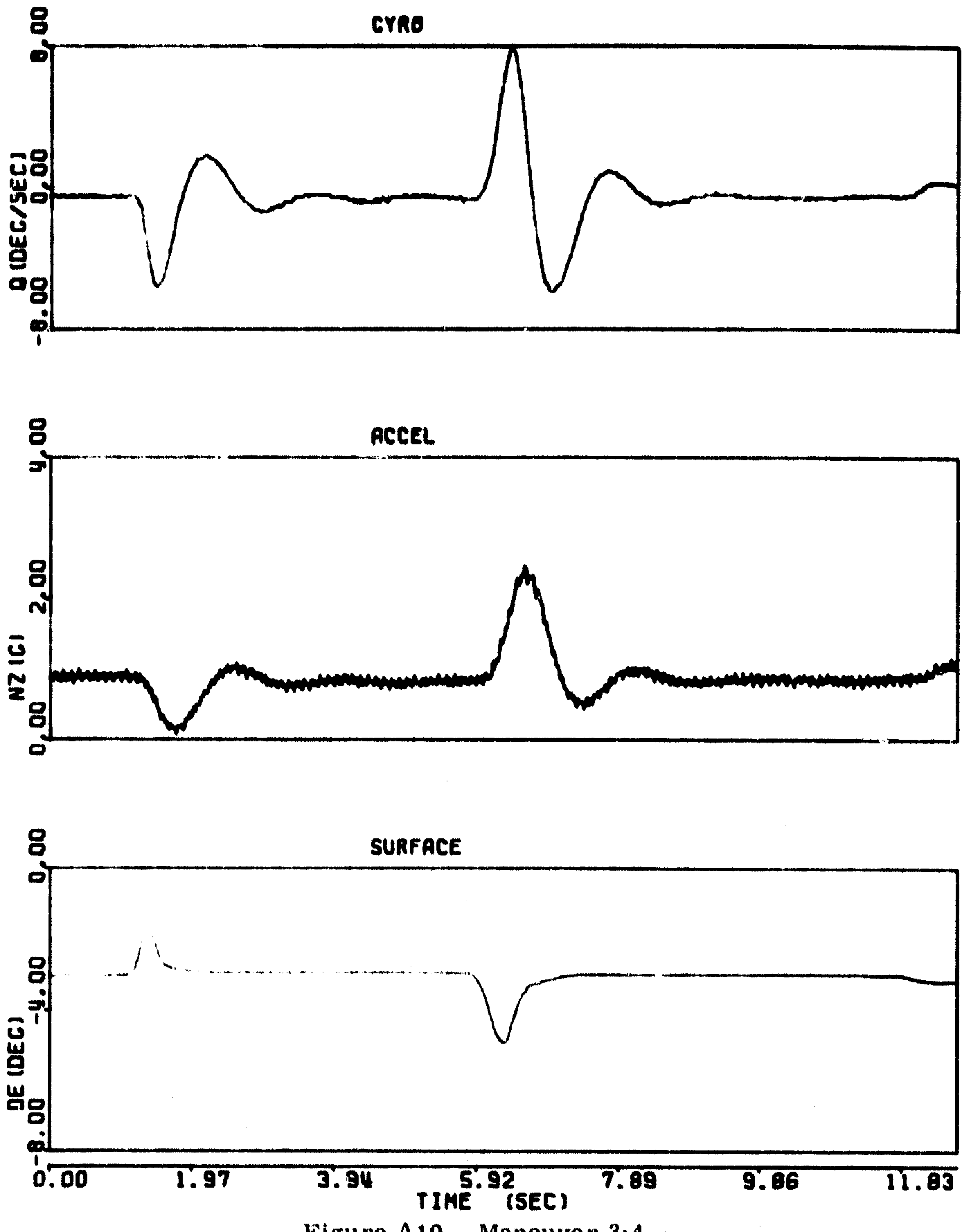

Figure A10. Maneuver 3:4

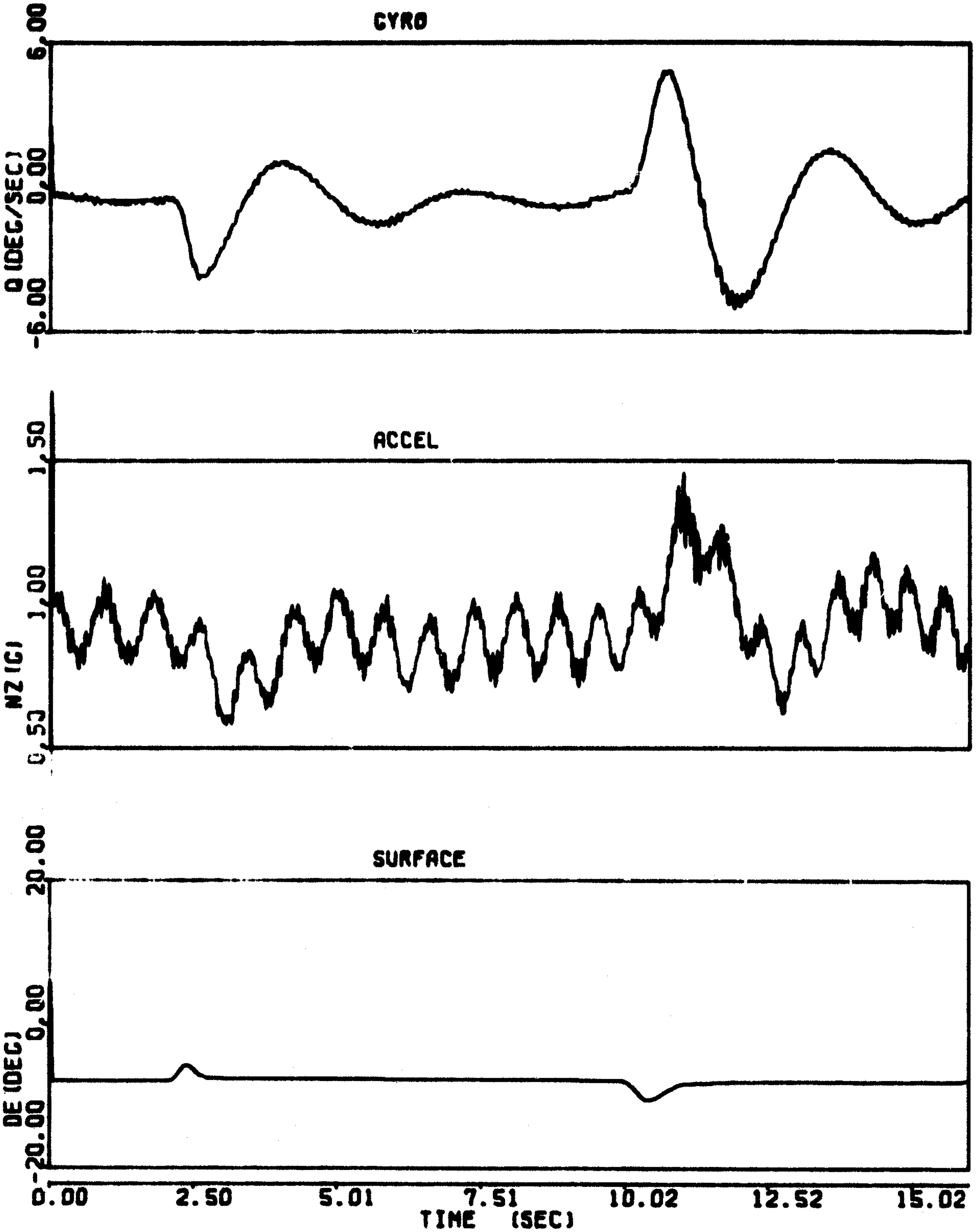

Figure A11. Maneuver 3:5

APPENDIX B

PCMLE PERFORMANCE TIME HISTORIES: BASELINE ALGORITHM

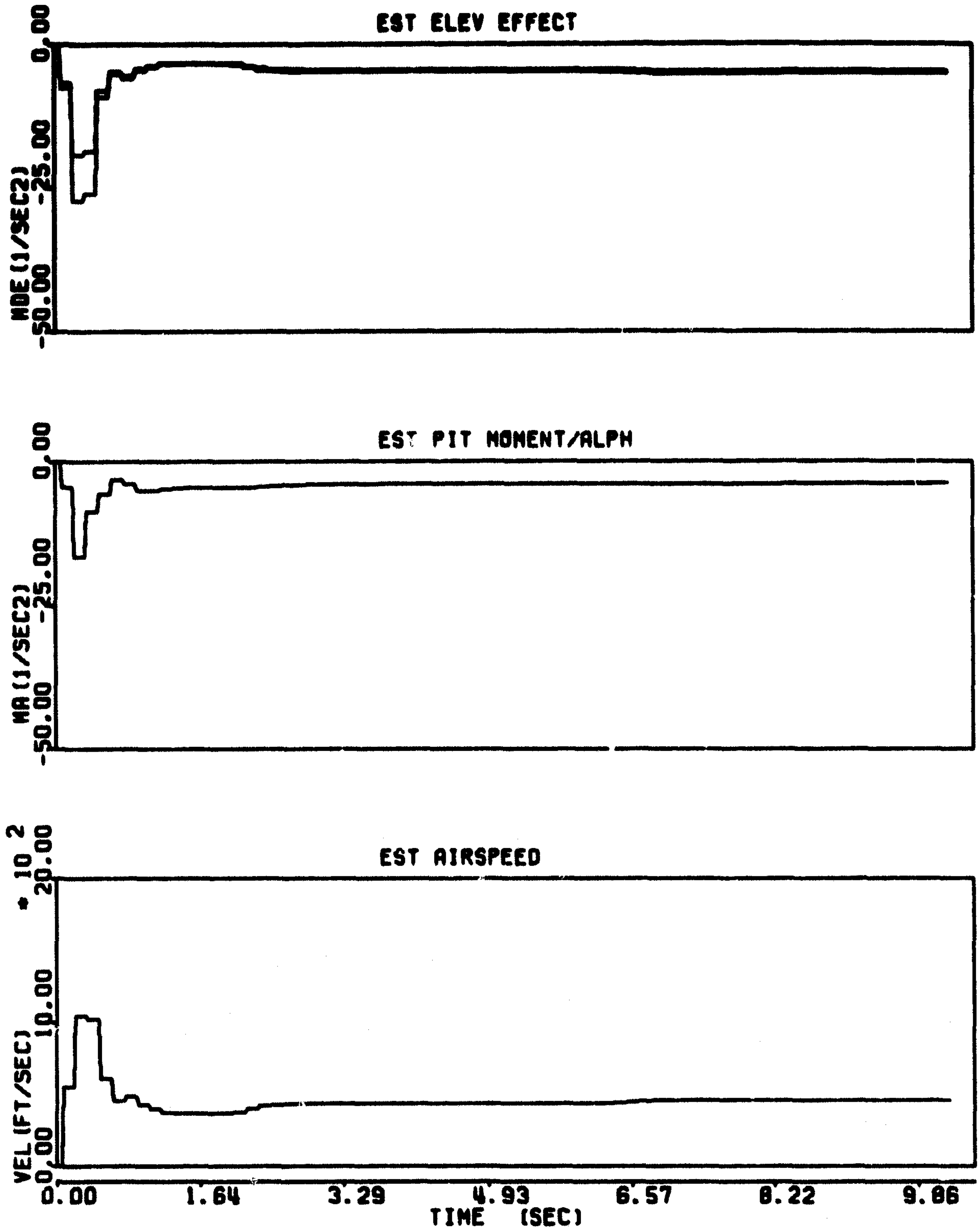

Figure B1. PCMLE Performance, Maneuver 2:1

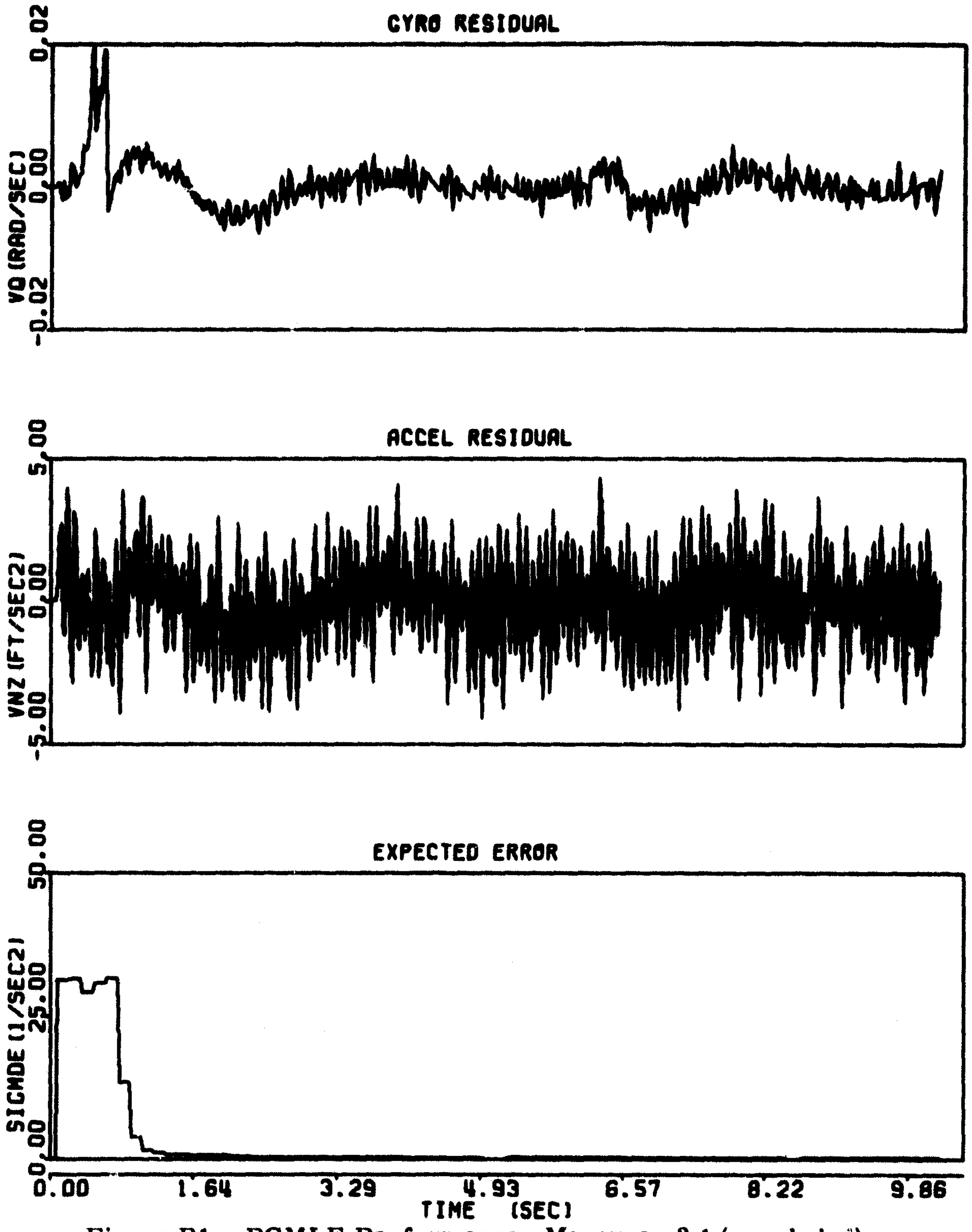

Figure B1. PCMLE Performance, Maneuver 2:1 (concluded)

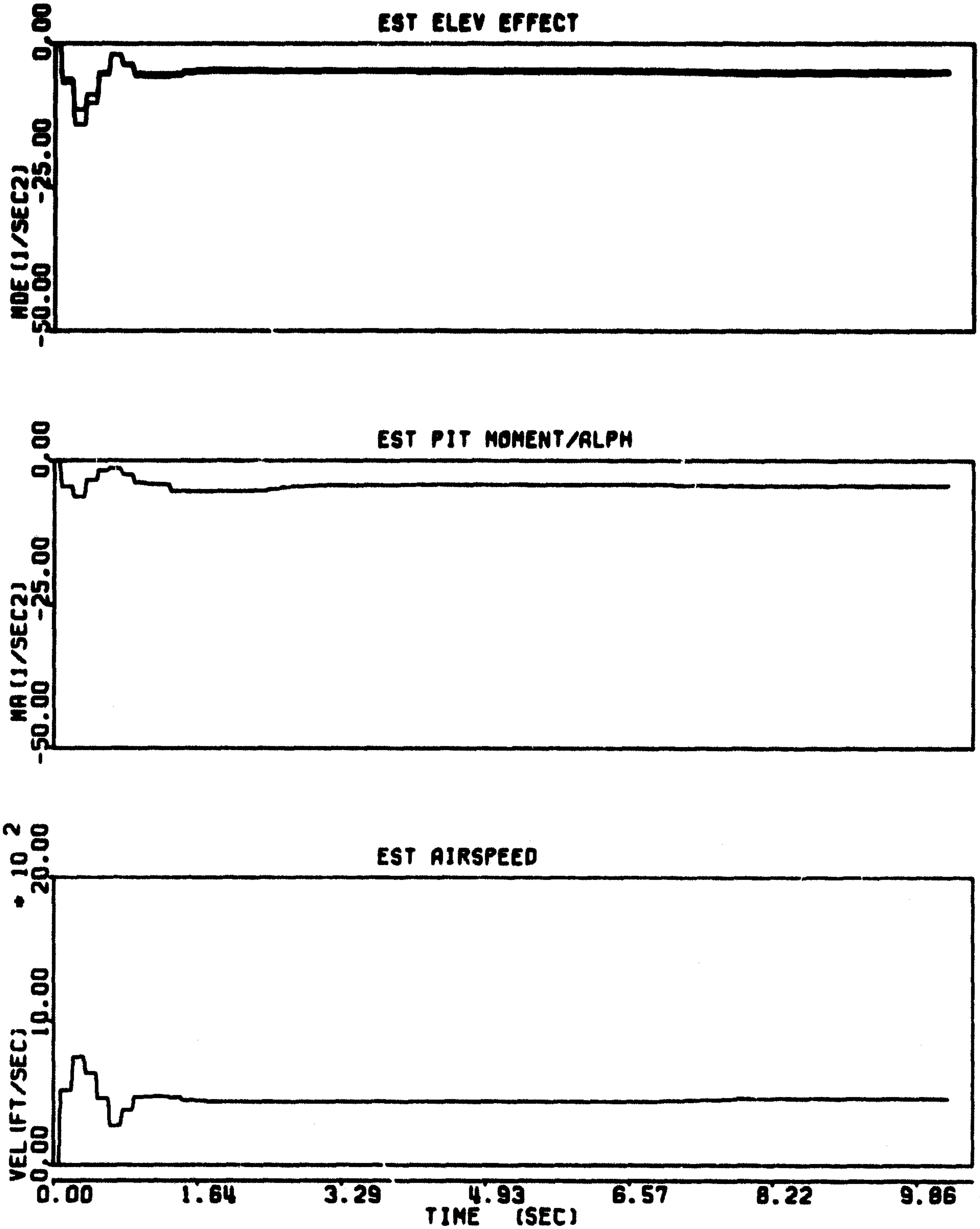

Figure B2. PCMLE Performance, Maneuver 2:2

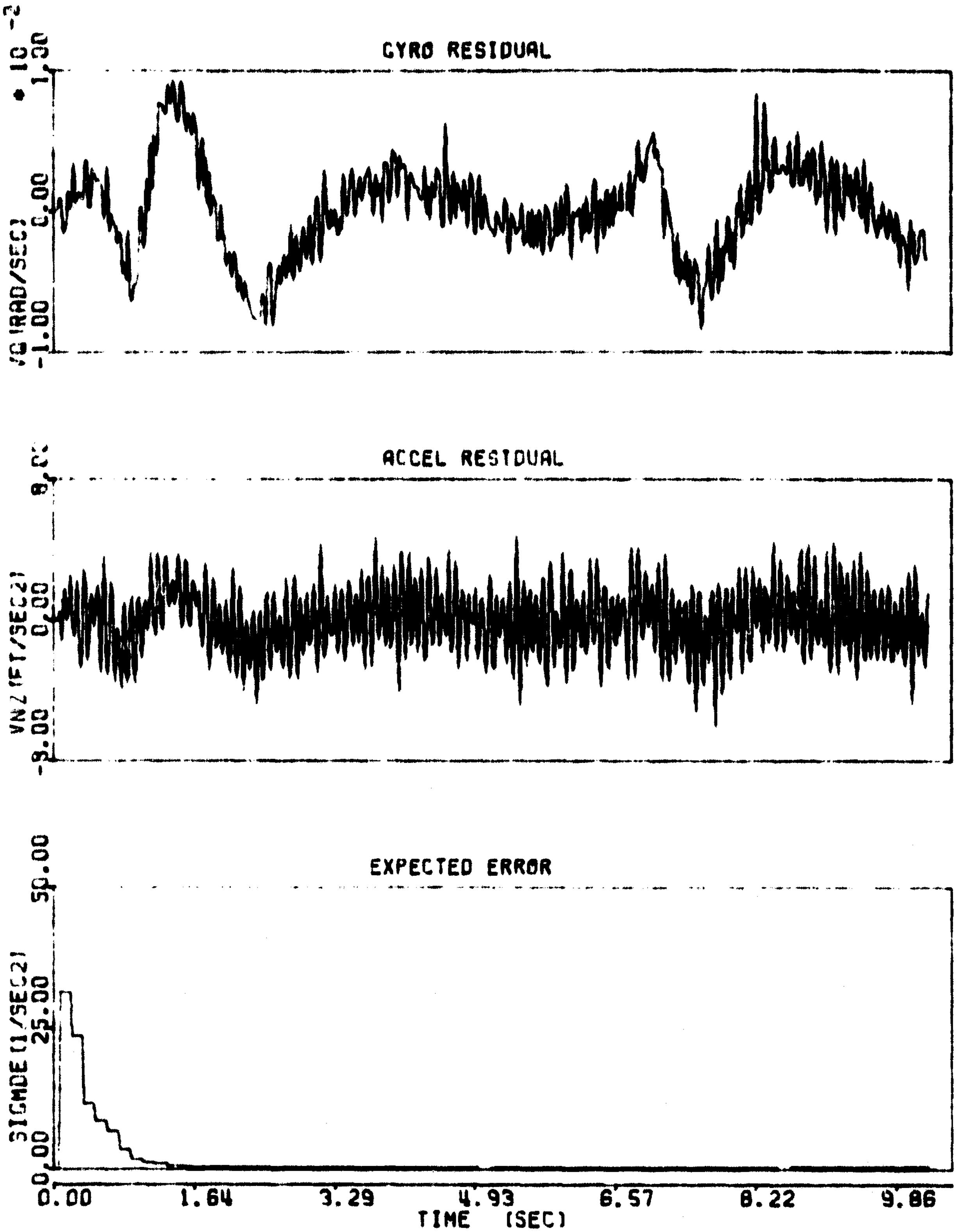

Figure B2. PCMLE Performance, Maneuver 2:2 (concluded)

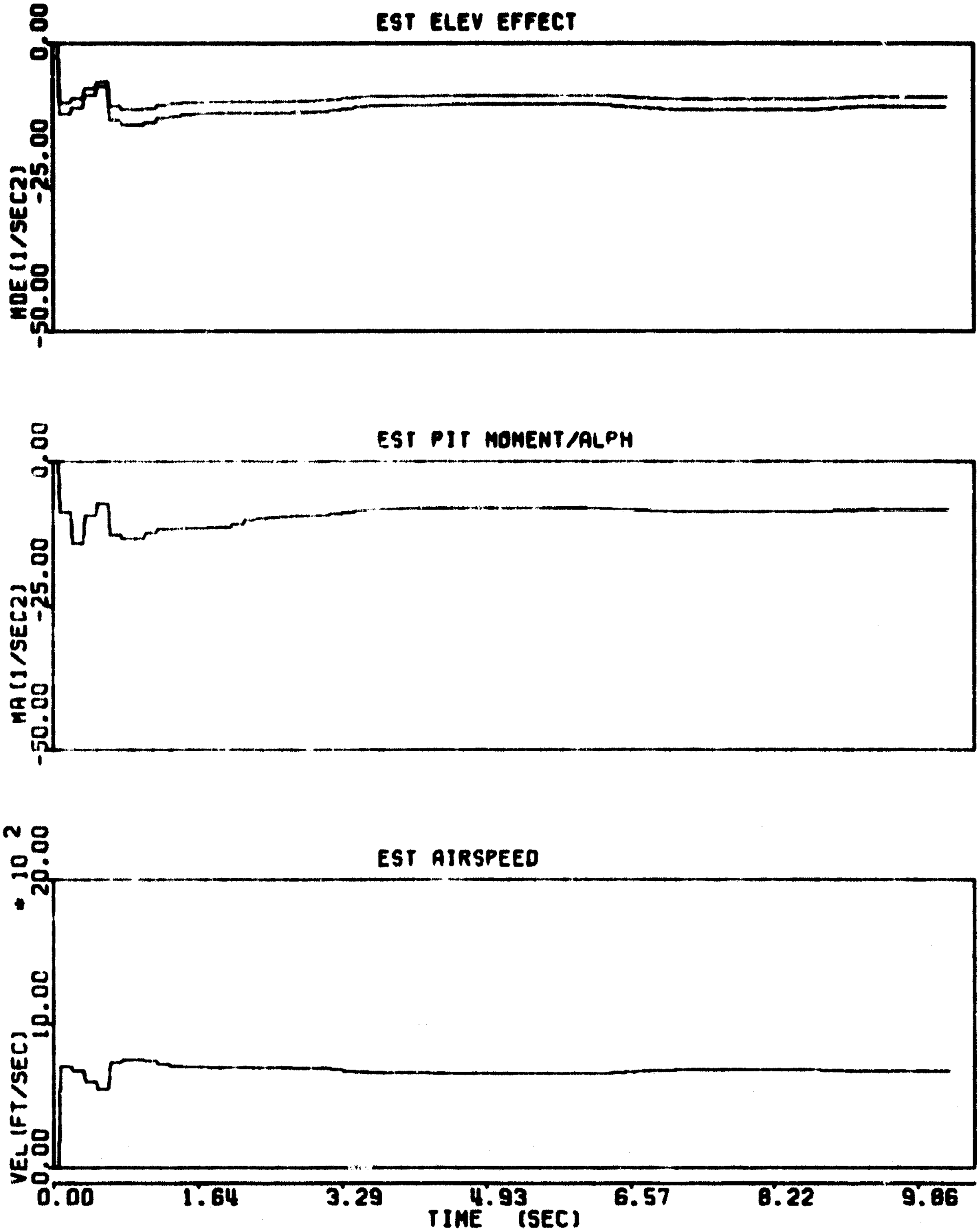

Figure B3. PCMLE Performance, Maneuver 2:3

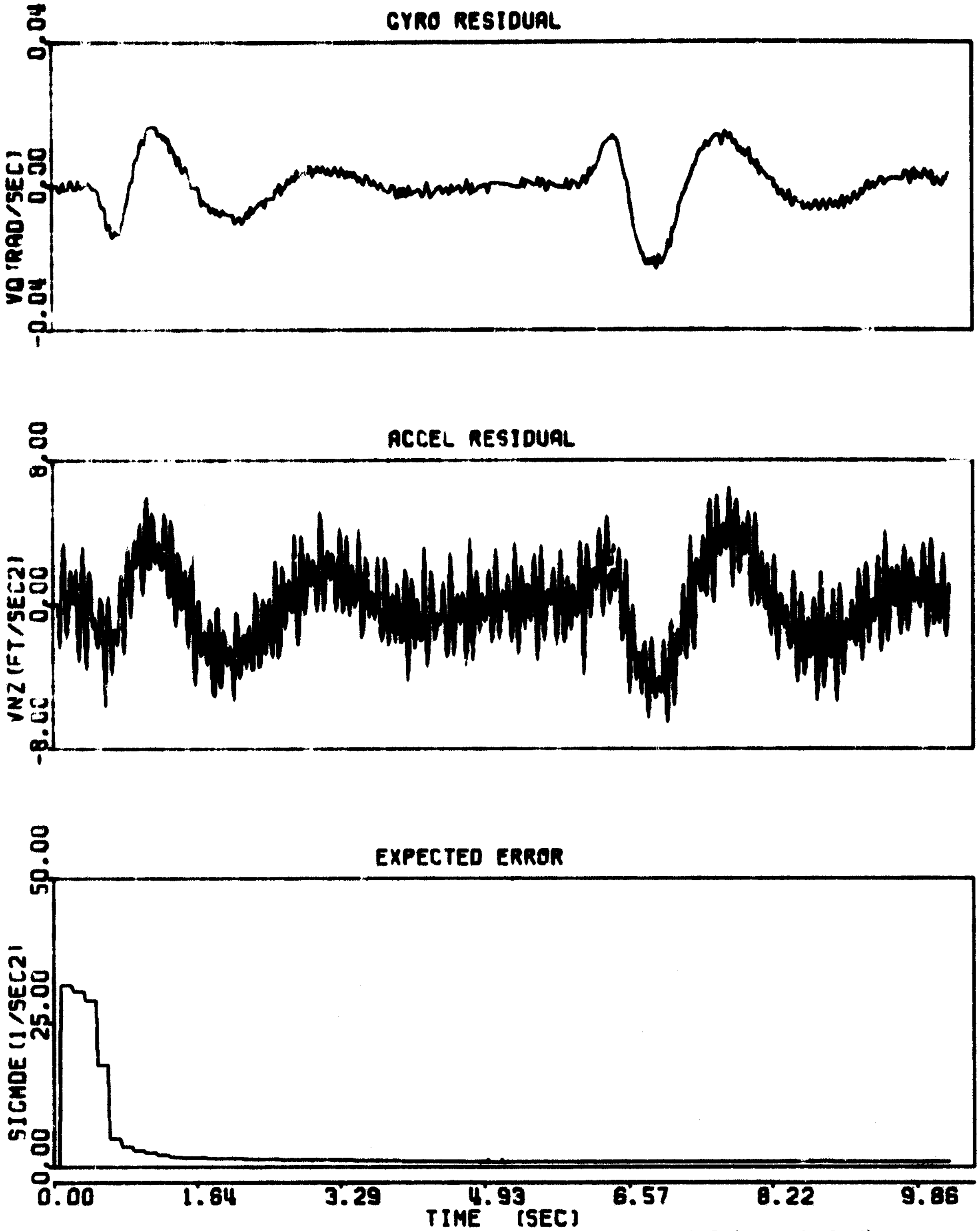

Figure B3. PCMLE Performance, Maneuver 2:3 (concluded)

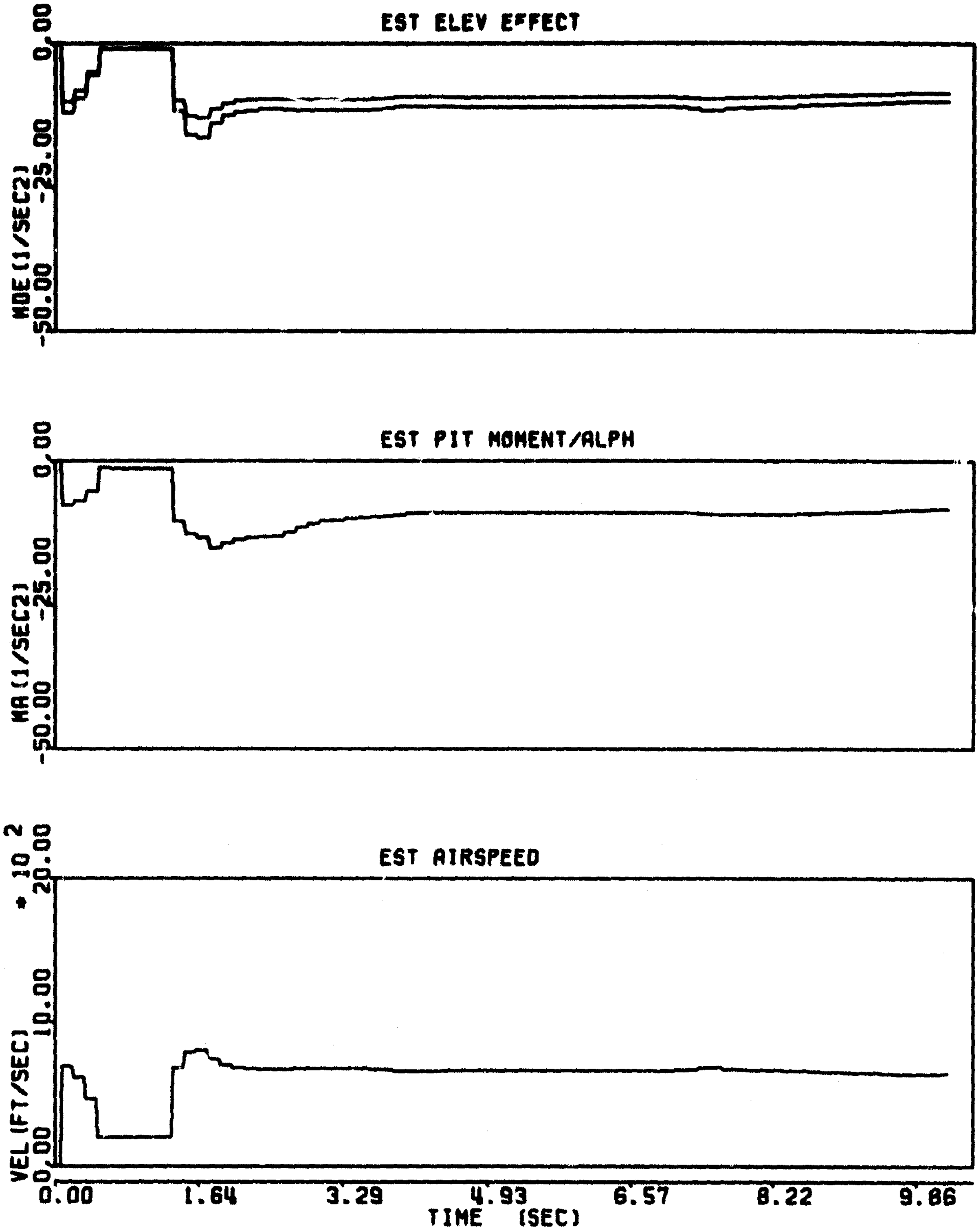

Figure B4. PCMLE Performance, Maneuver 2:4

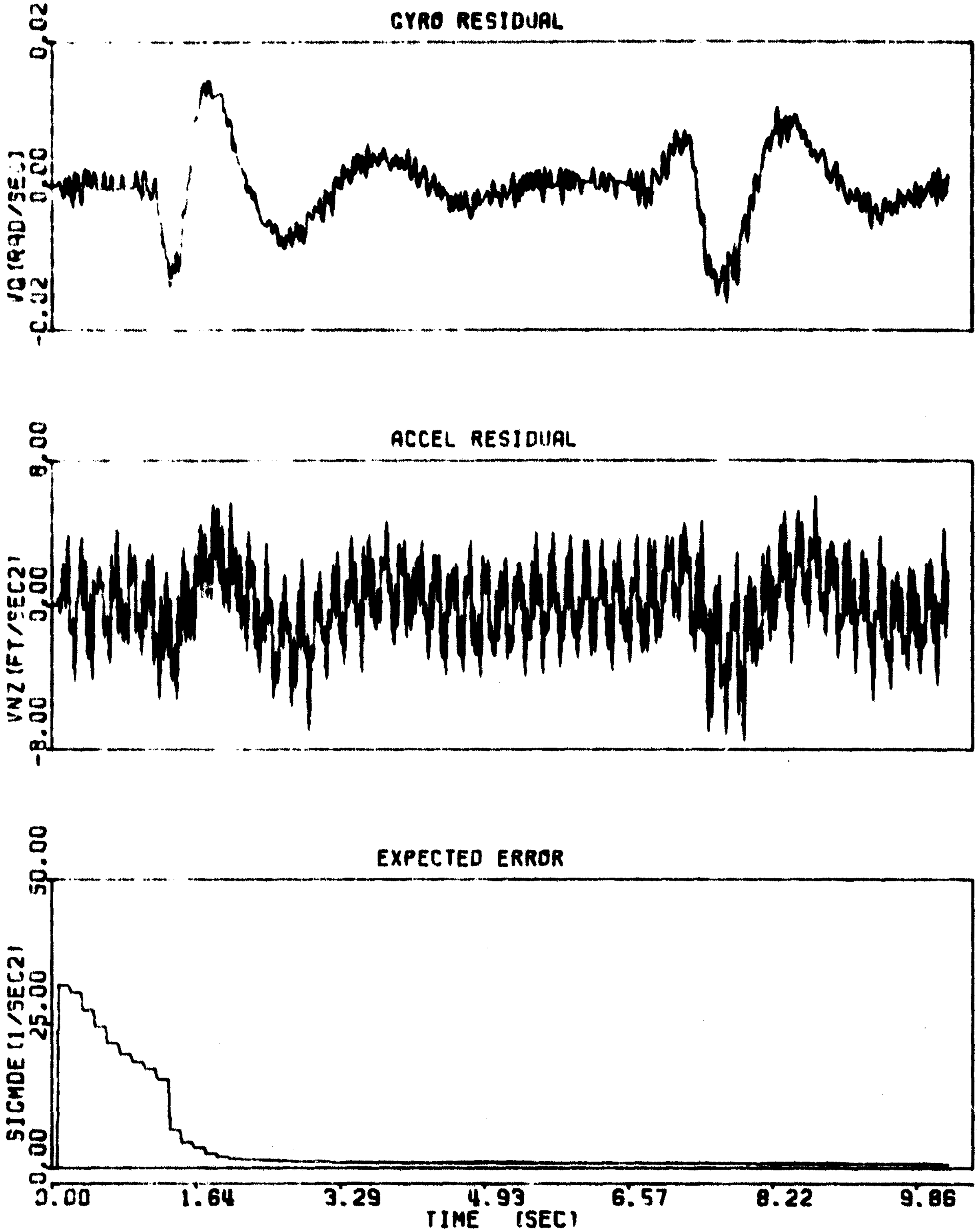

Figure B4. PCMLE Performance, Maneuver 2:4 (concluded)

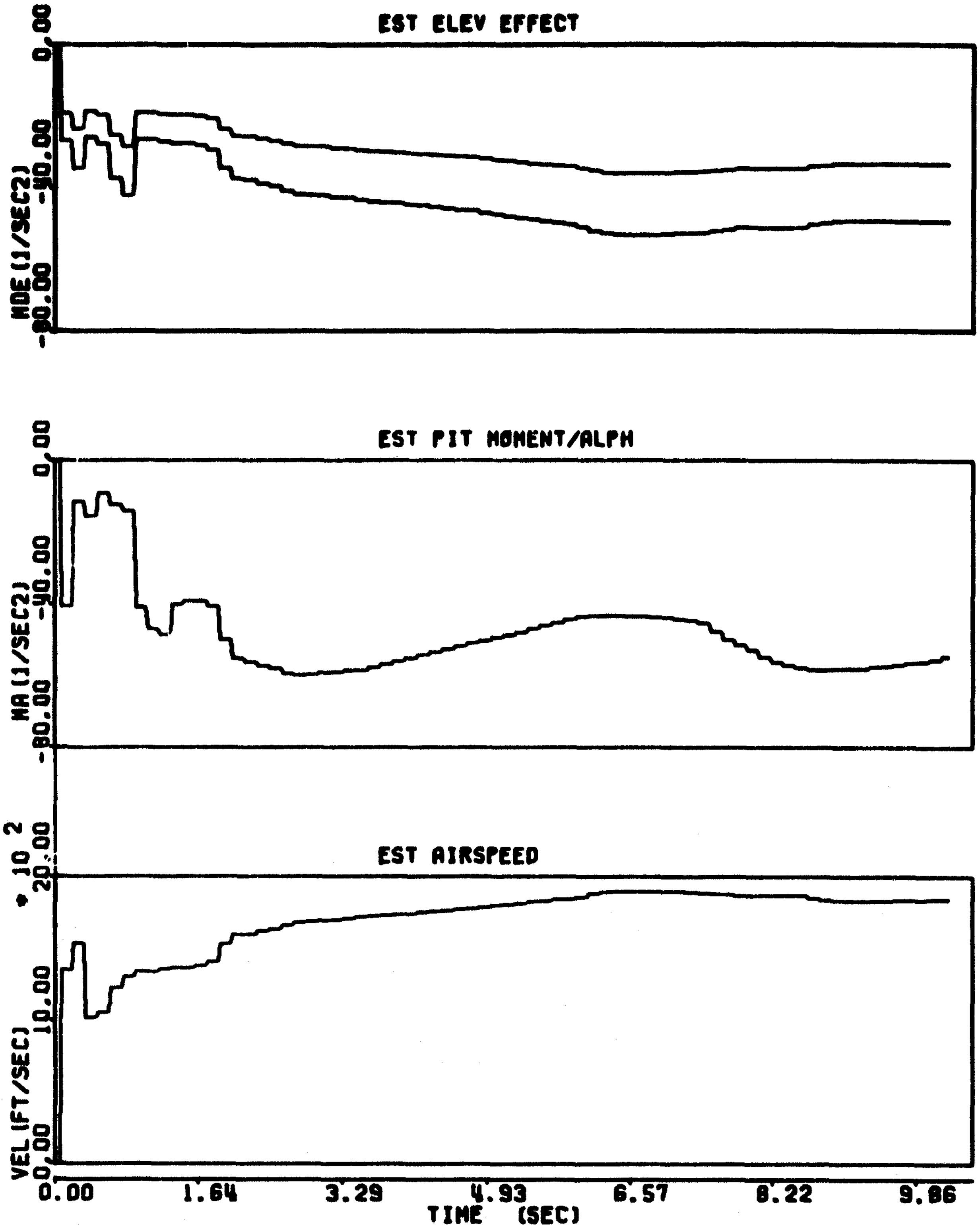

Figure B5. PCMLE Performance, Maneuver 2:5

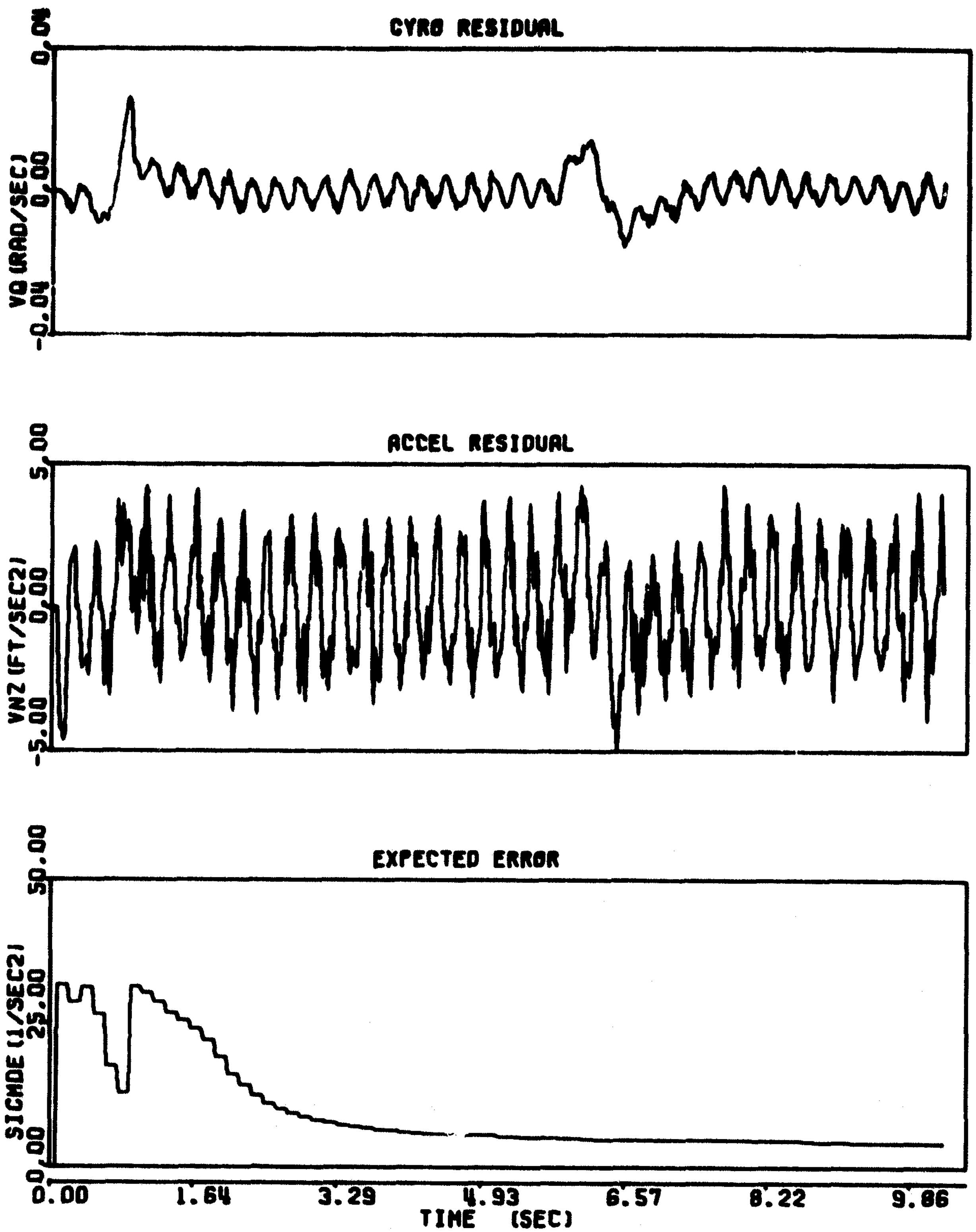

Figure B5. PCMLE Performance, Maneuver 2:5 (concluded)

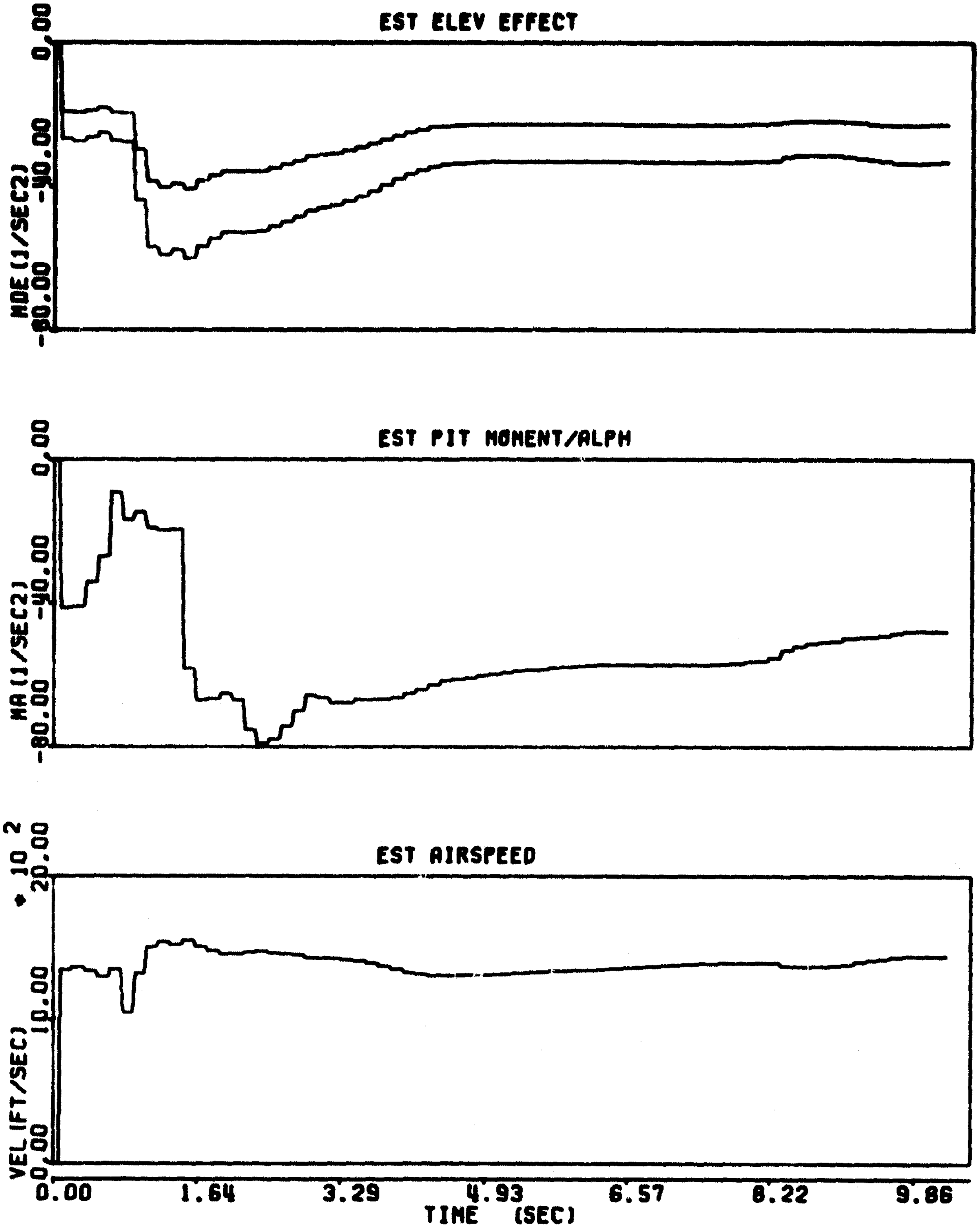

Figure B6. PCMLE Performance, Maneuver 2:6

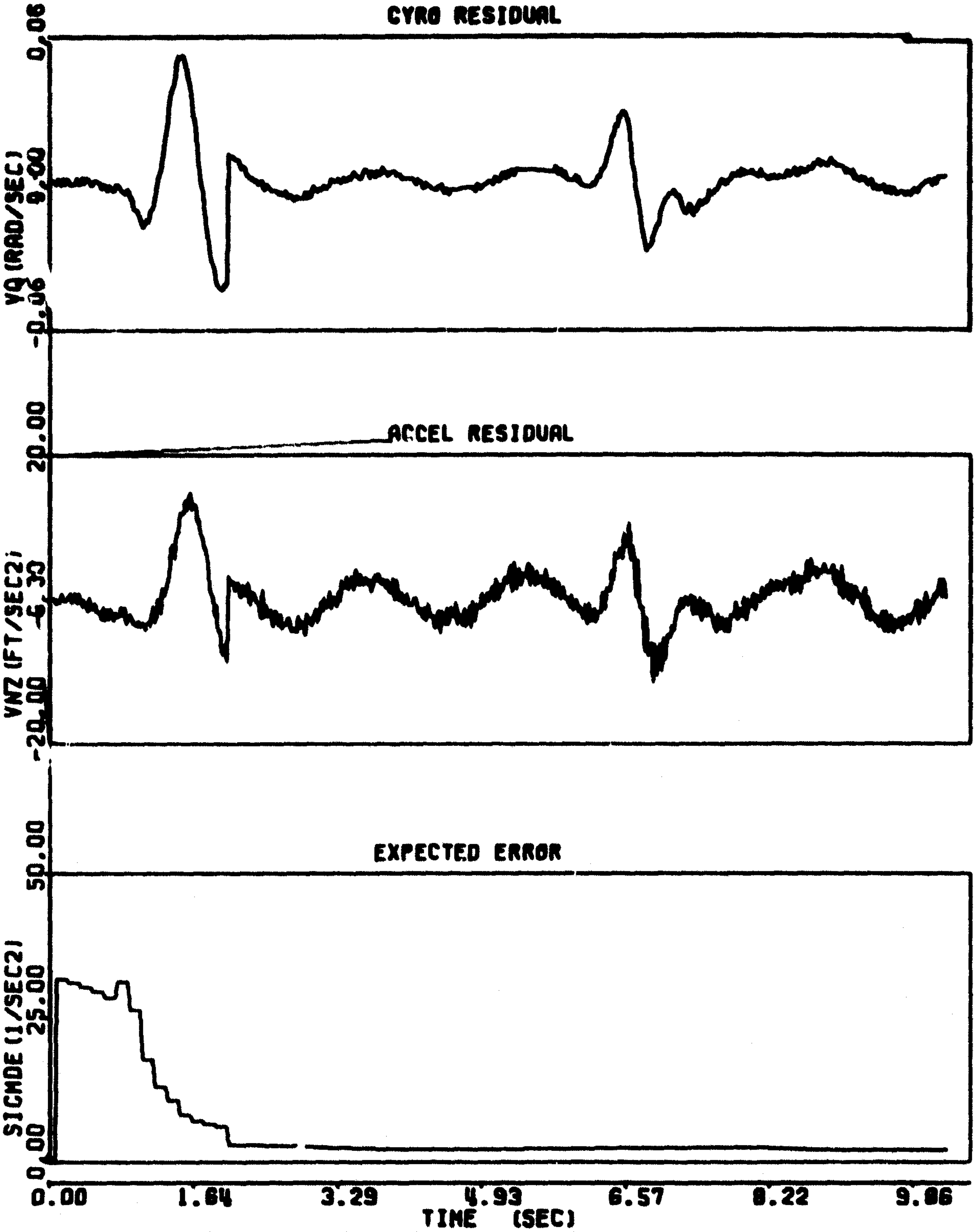

Figure B6. PCMLE Performance, Maneuver 2:6 (concluded)

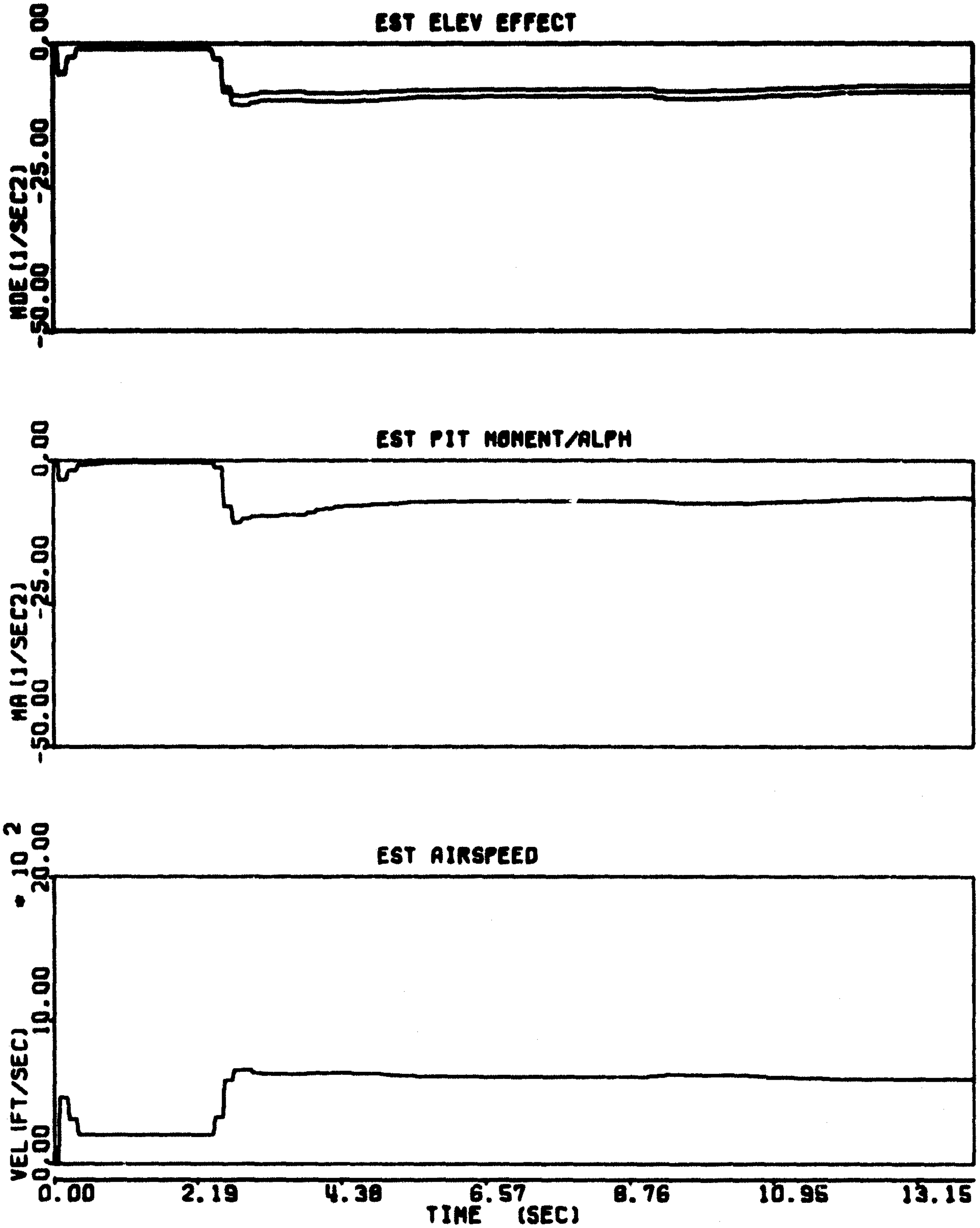

Figure B7. PCMLE Performance, Maneuver 3:1

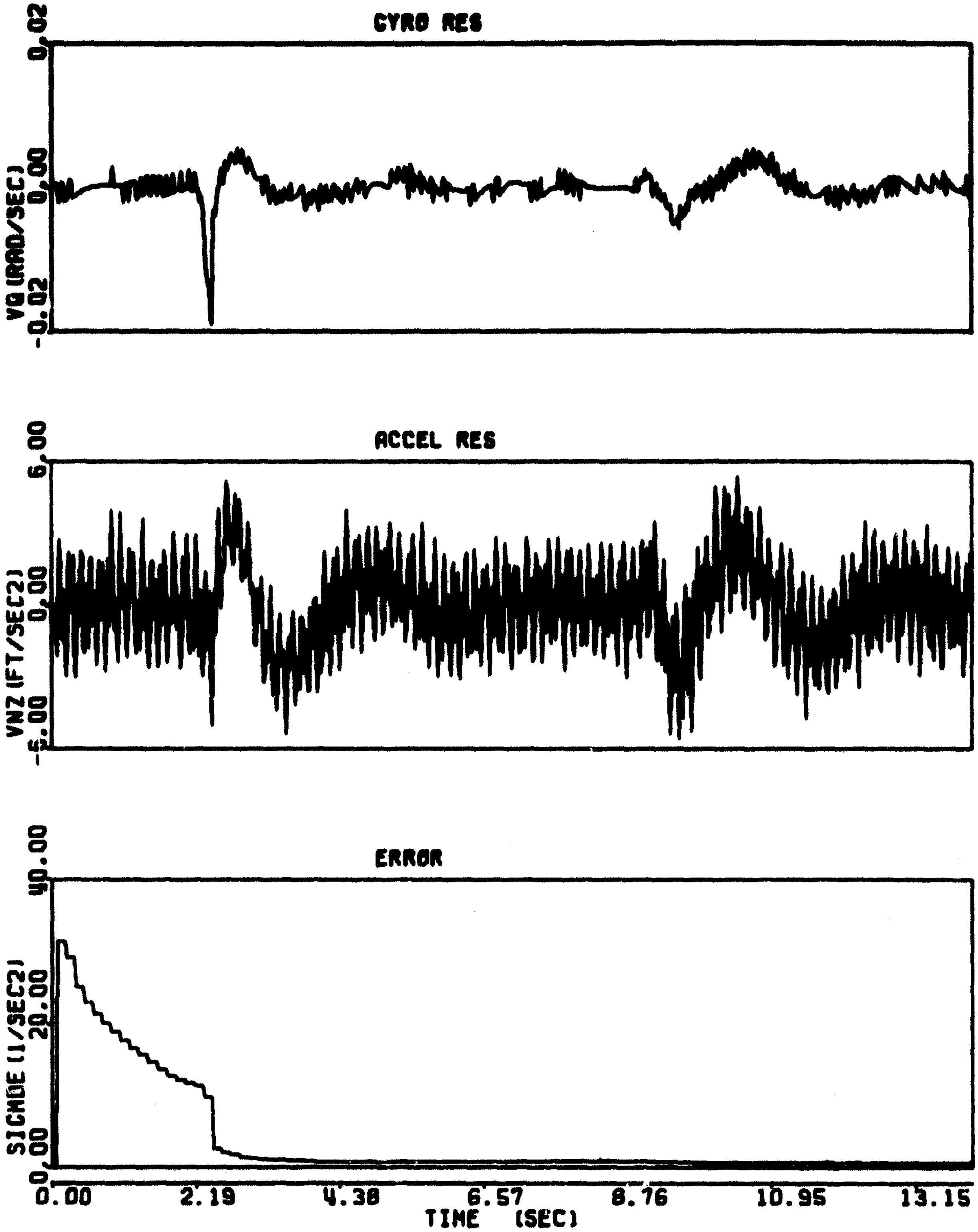

Figure B7. PCMLE Performance, Maneuver 3:1 (concluded)

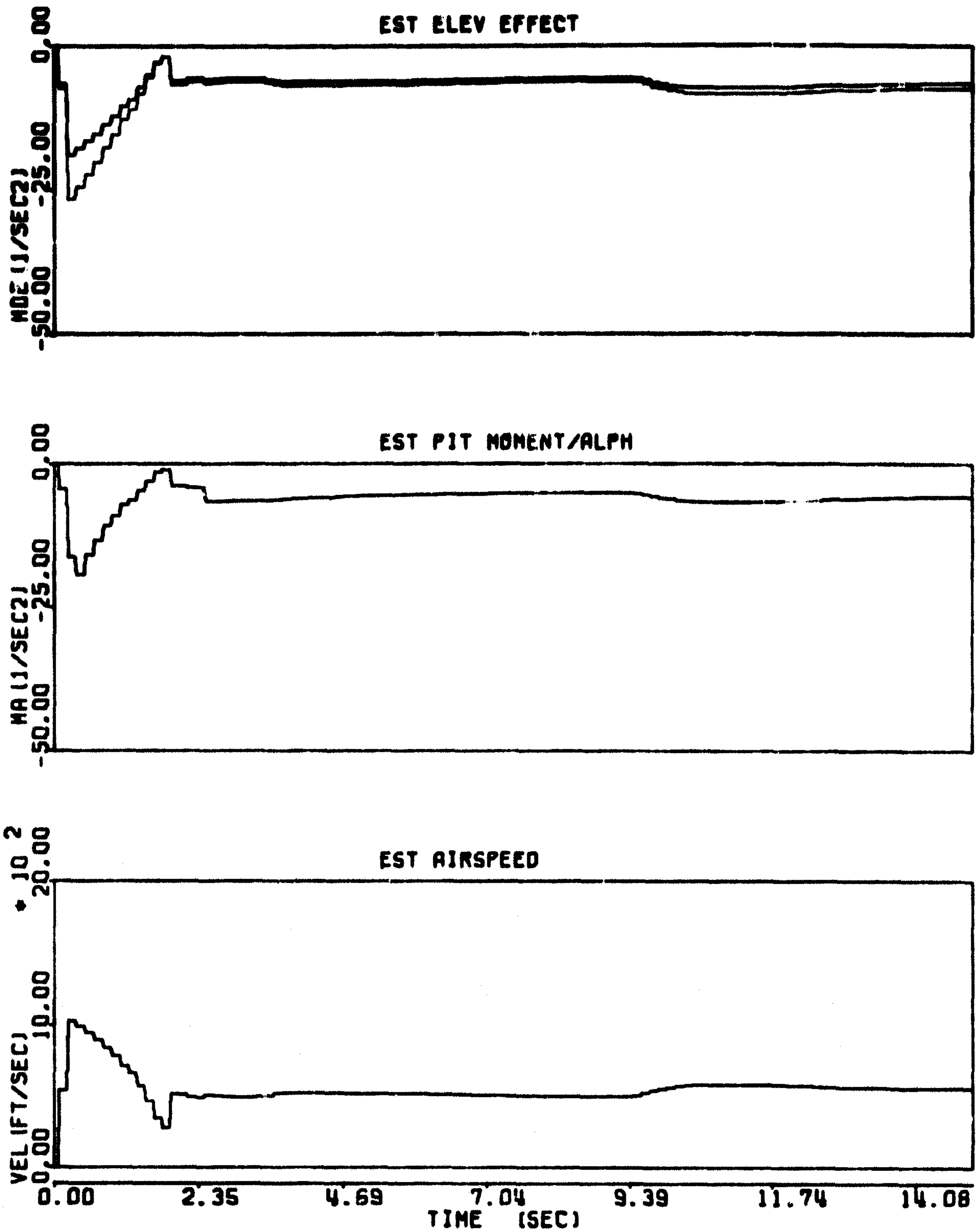

Figure B8. PCMLE Performance, Maneuver 3;2

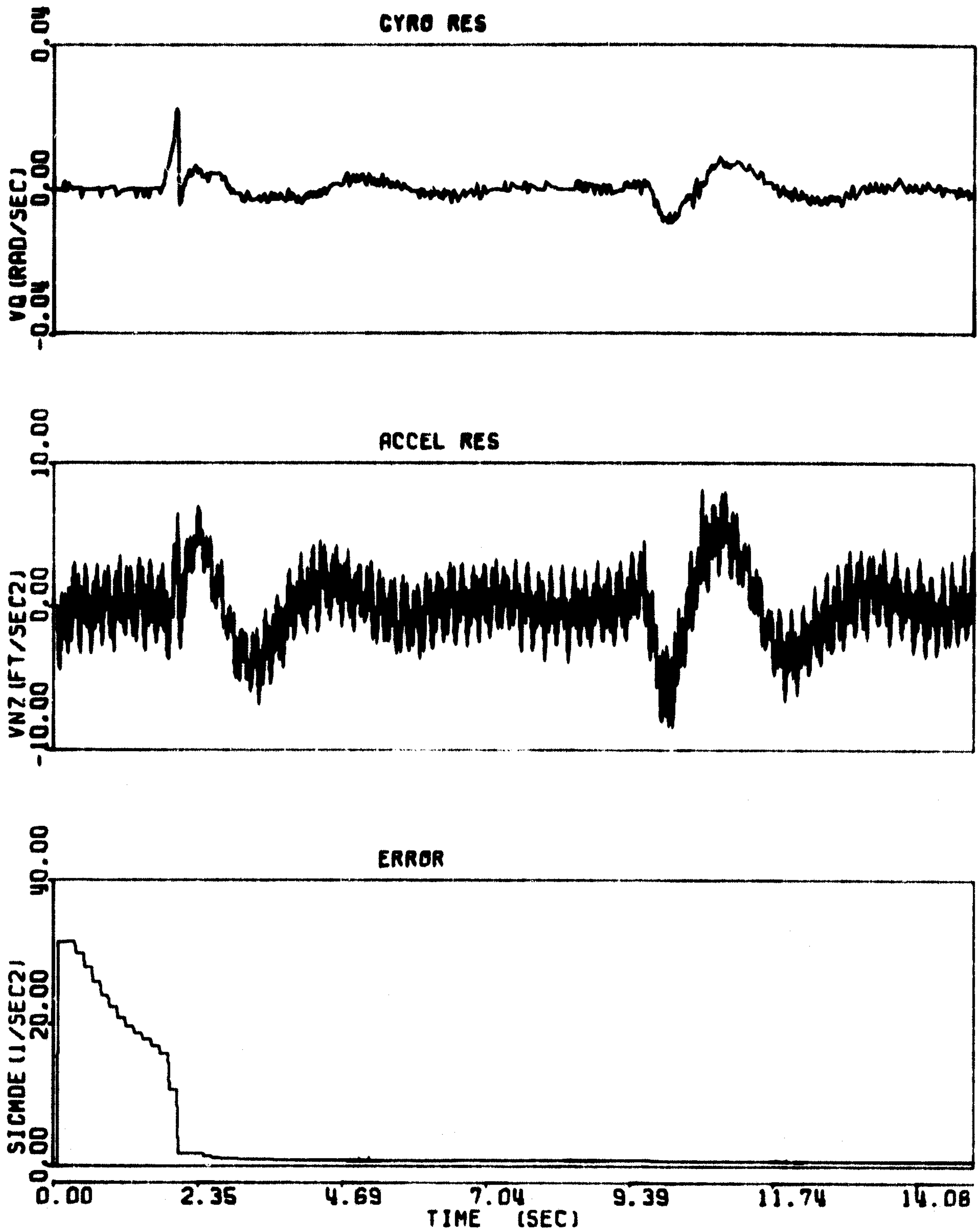

Figure B8. PCMLE Performance, Maneuver 3:2 (concluded)

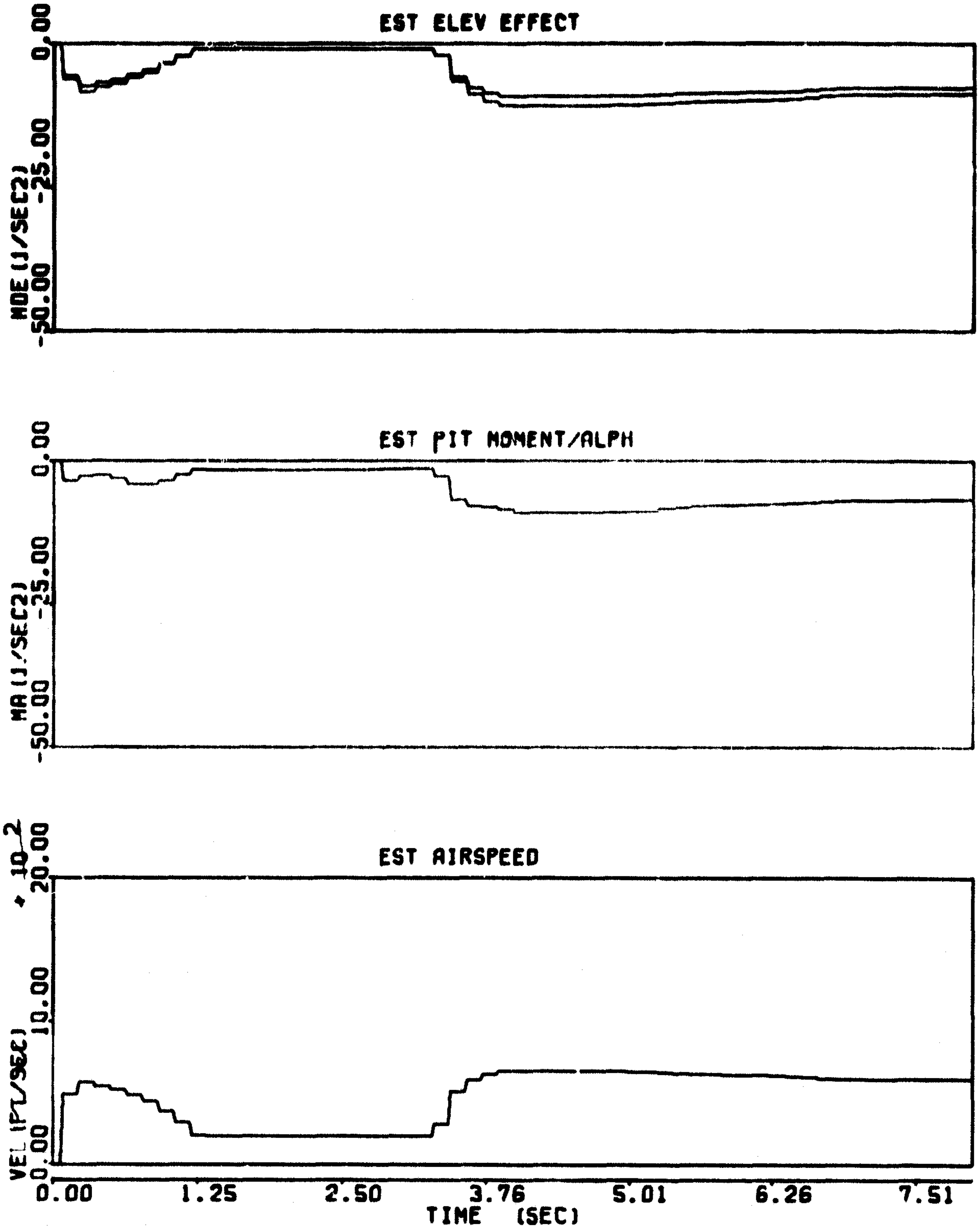

Figure B9. PCMLE Performance, Maneuver 3:3

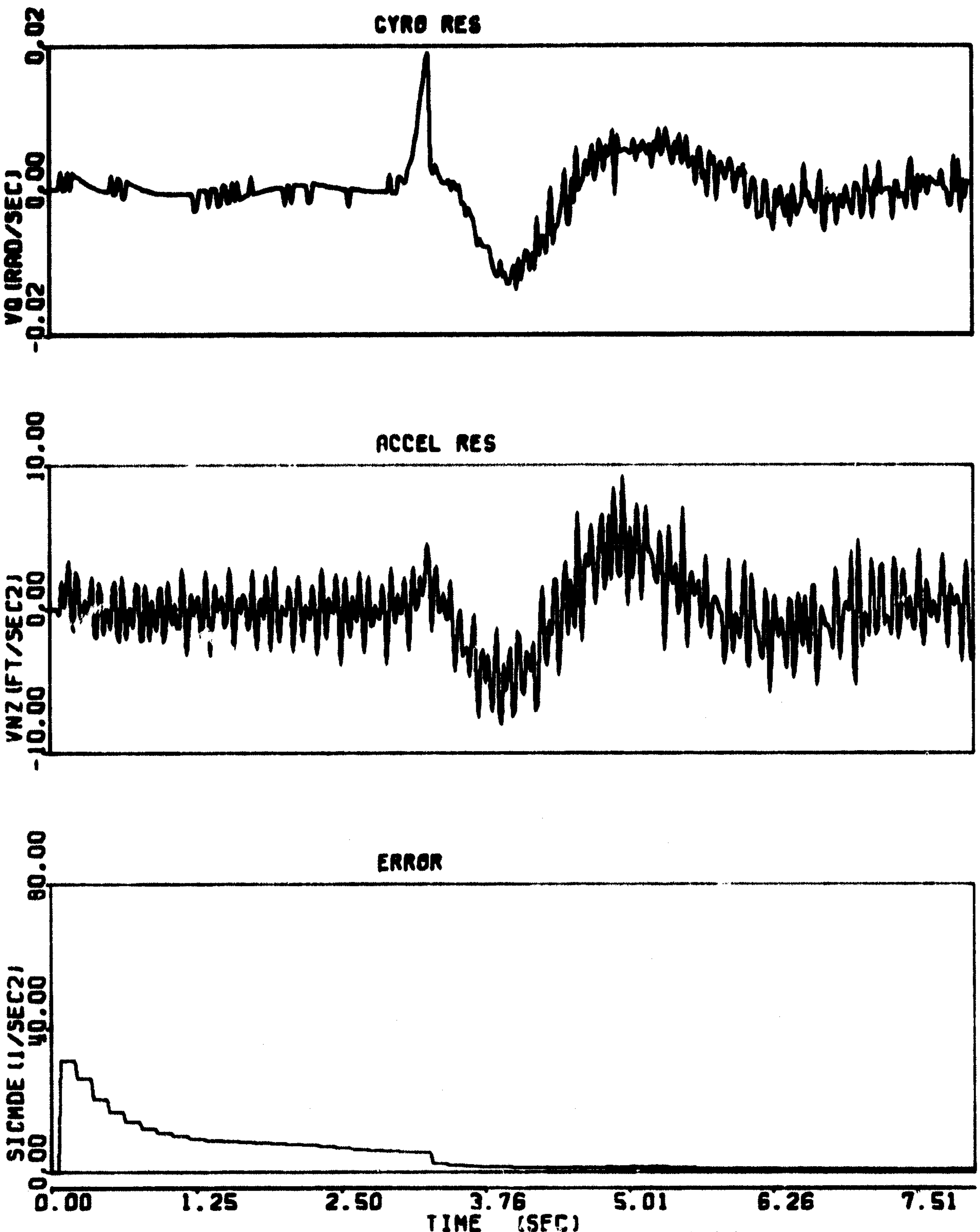

Figure B9. PCMLE Performance, Maneuver 3:3 (concluded)

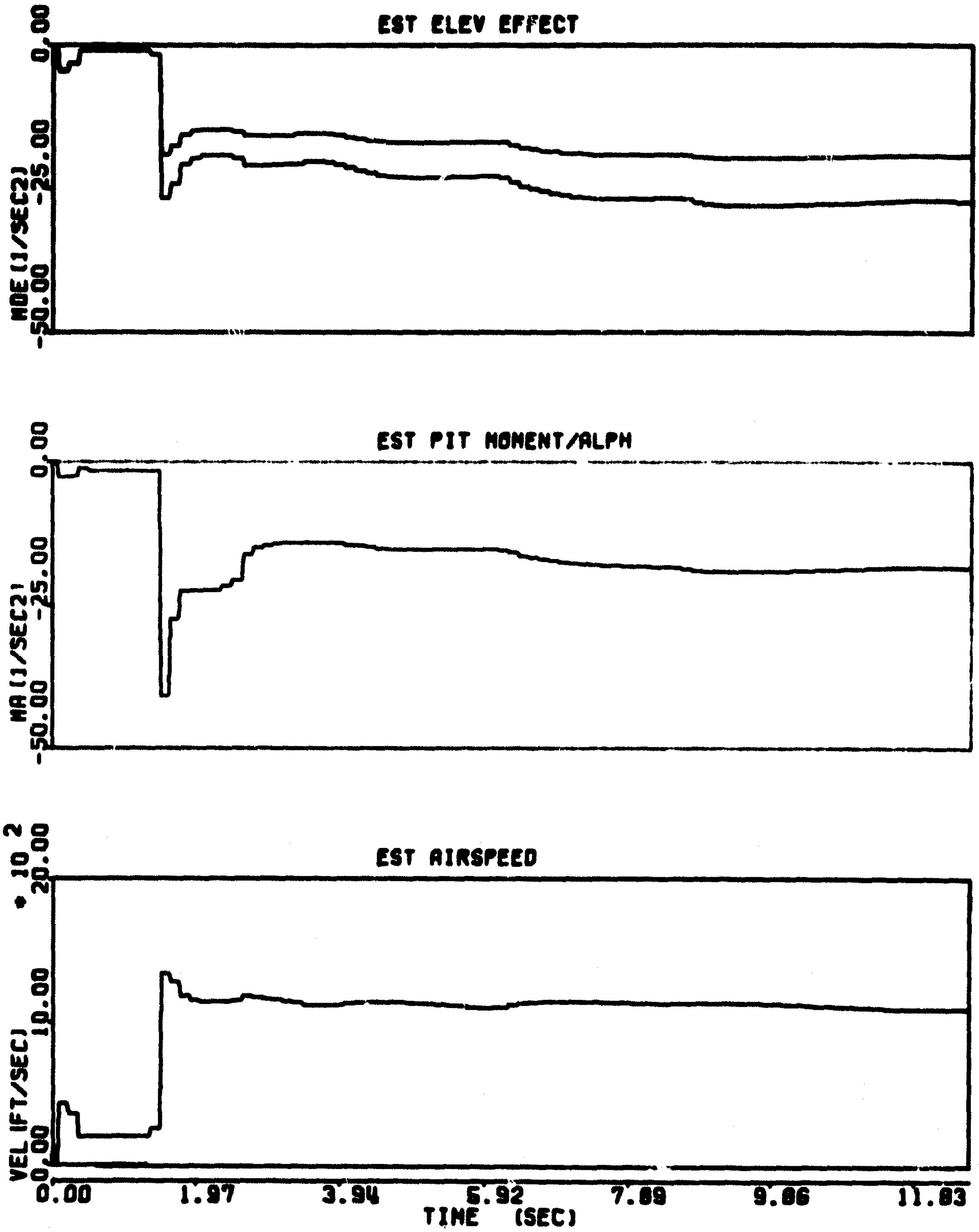

Figure B10. PCMLE Performance, Maneuver 3:4

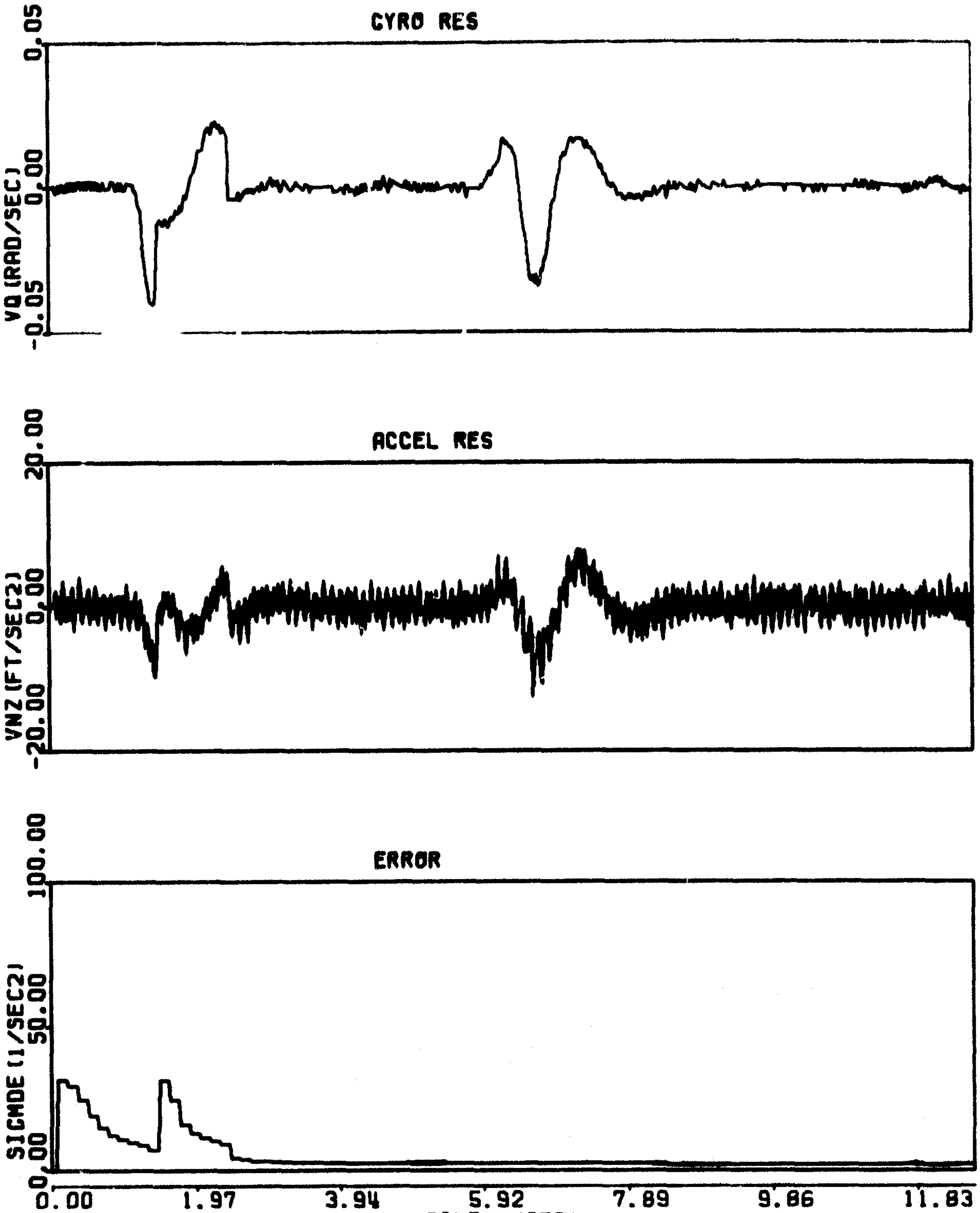

Figure B10. PCMLE Performance, Maneuver 3:4 (concluded)

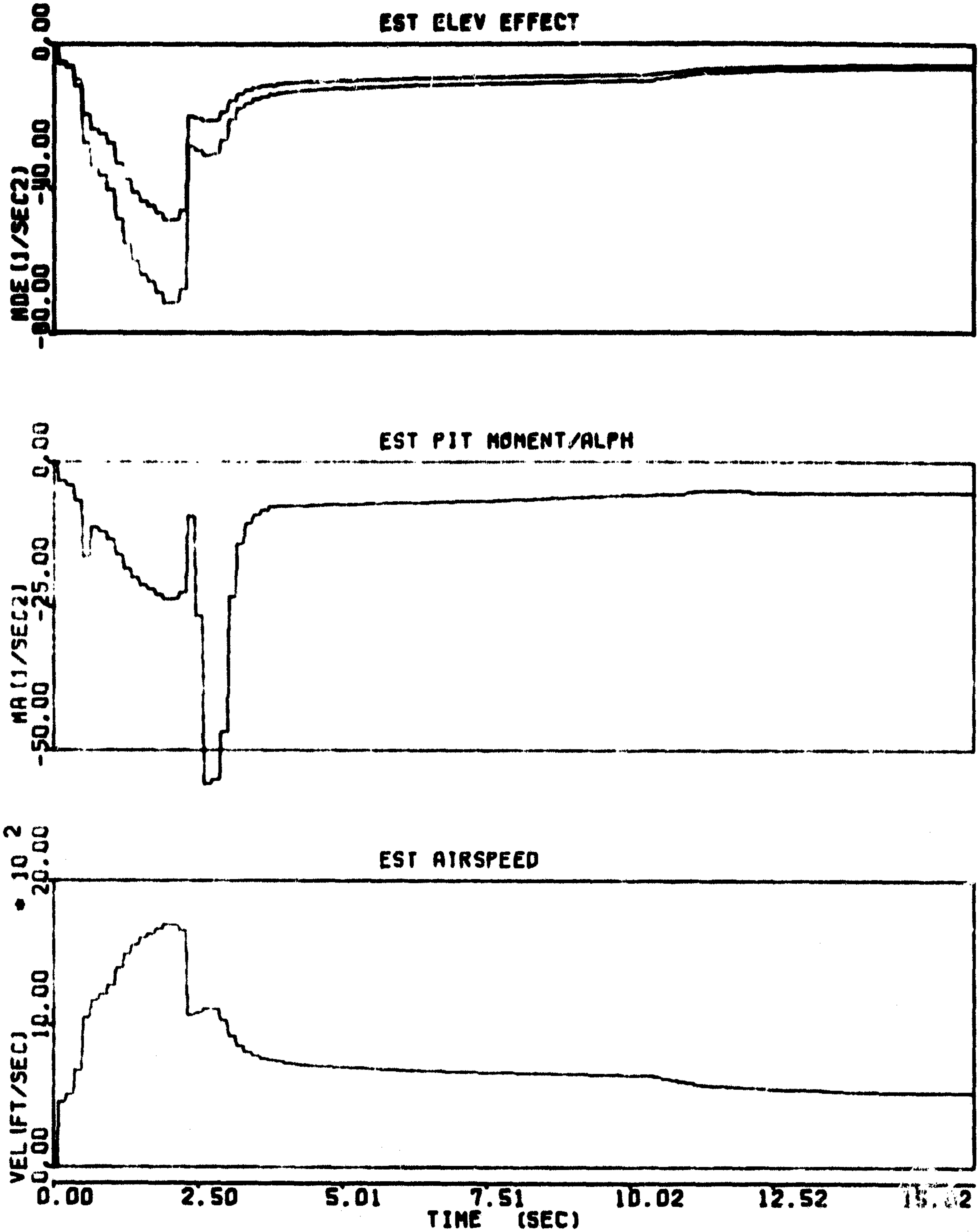

Figure B11. PCMLE Performance, Maneuver 3:5

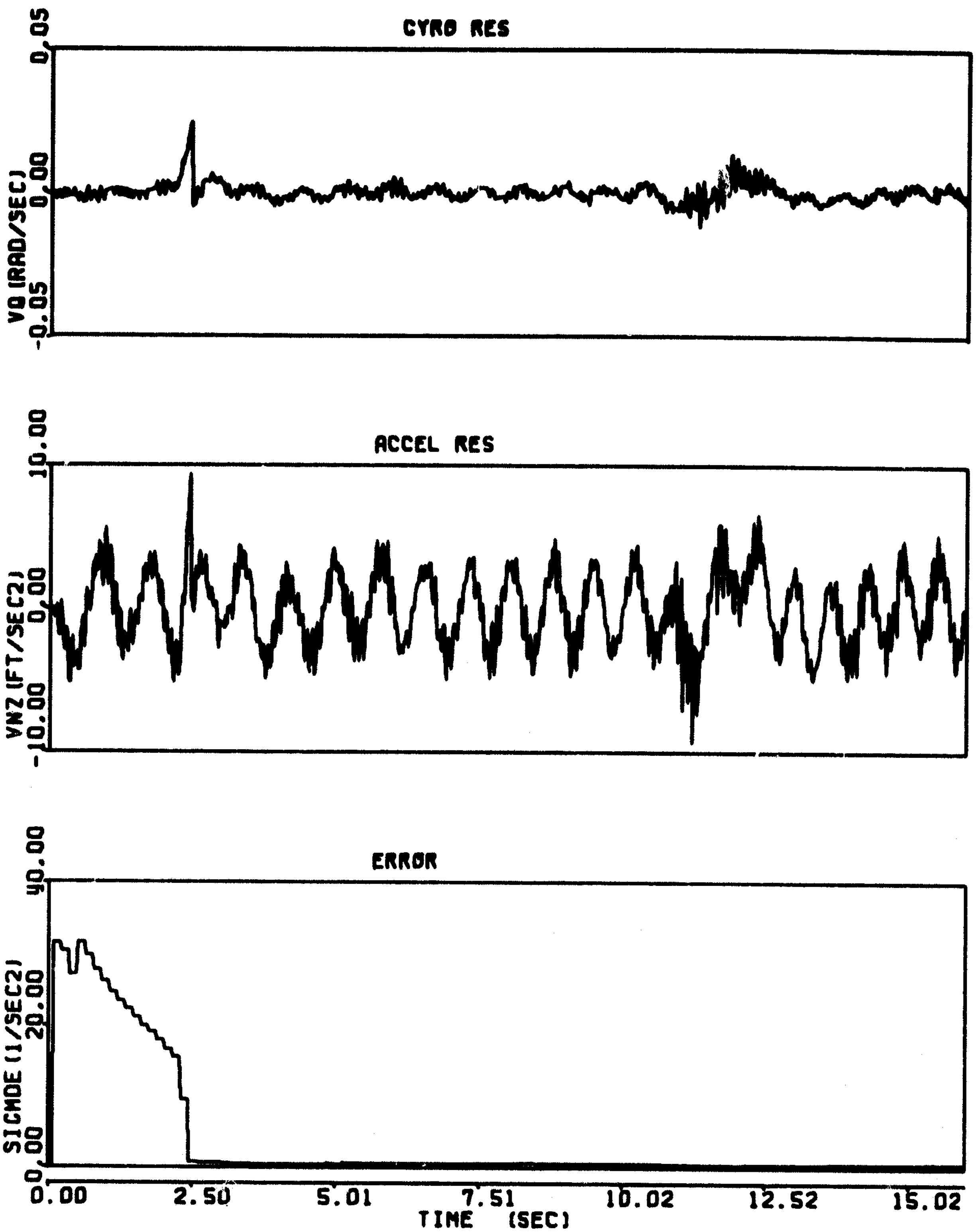

Figure B11. PCMLE Performance, Maneuver 3:5 (concluded)

APPENDIX C

PCMLE PERFORMANCE TIME HISTORIES: SECOND ITERATION

PRECEDING PAGE BLANK NOT FILMED

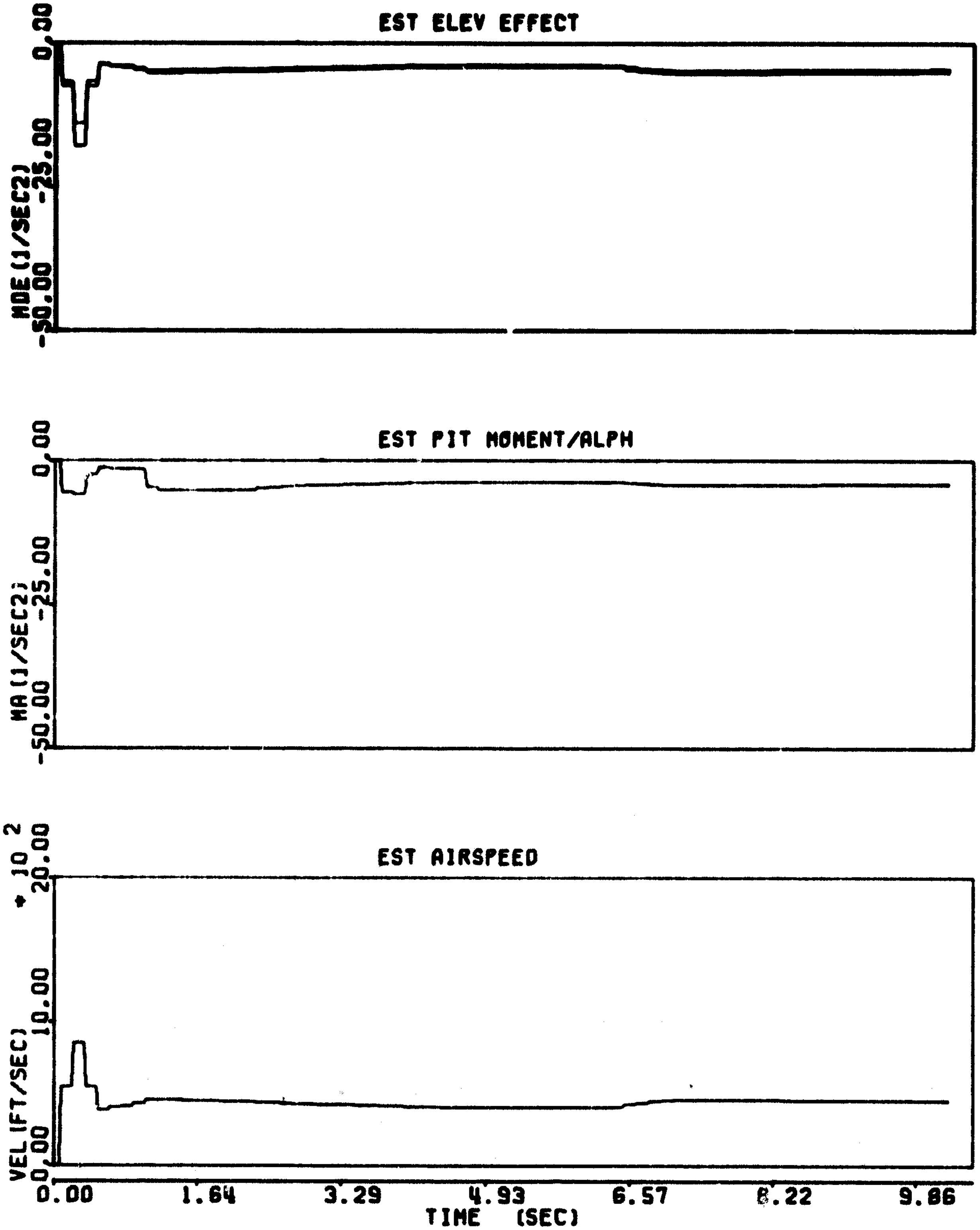

Figure C1. PCMLE Performance, Maneuver 2:1
(Second Iteration)

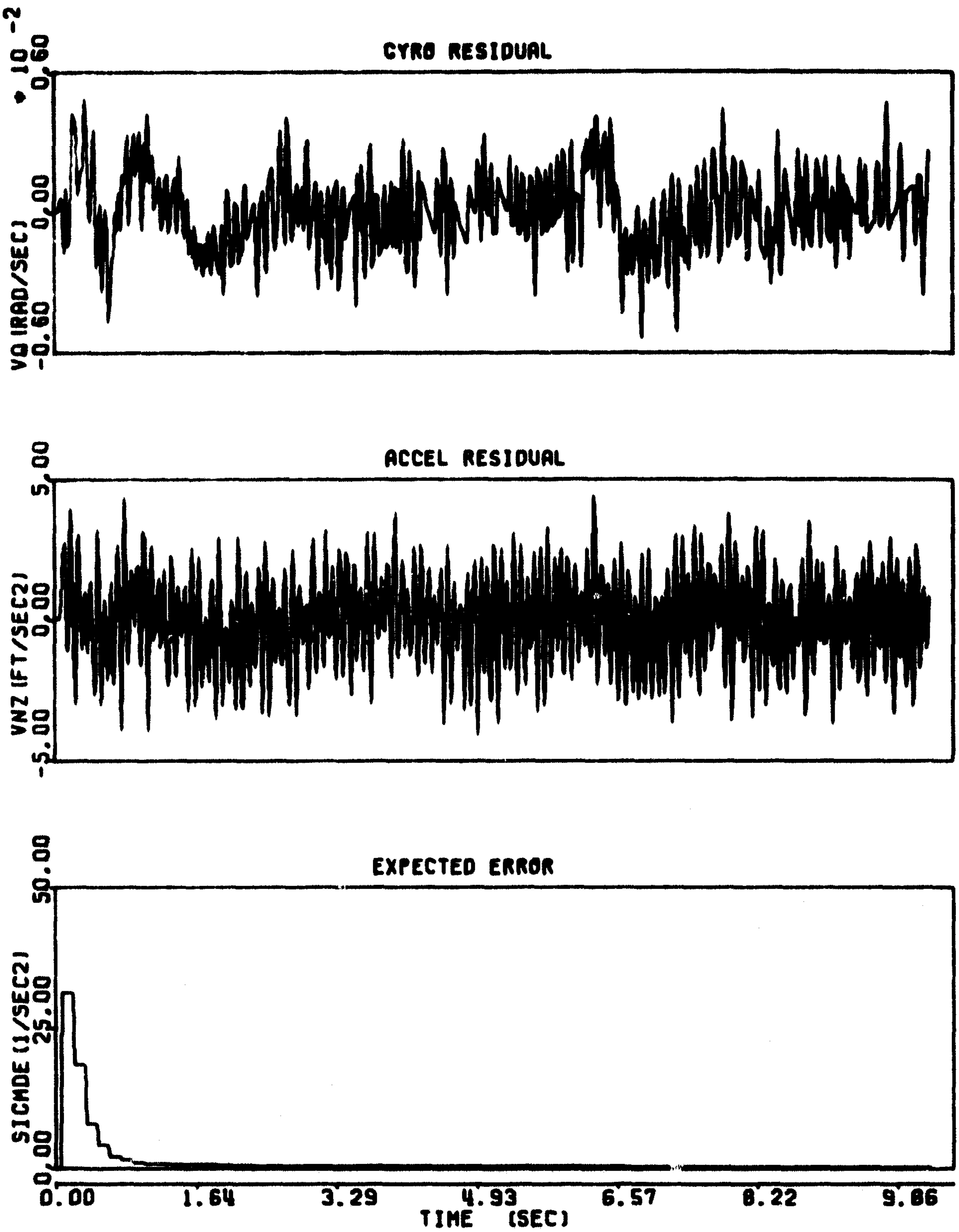

Figure C1. PCMLE Performance, Maneuver 2:1
(Second Iteration) (concluded)

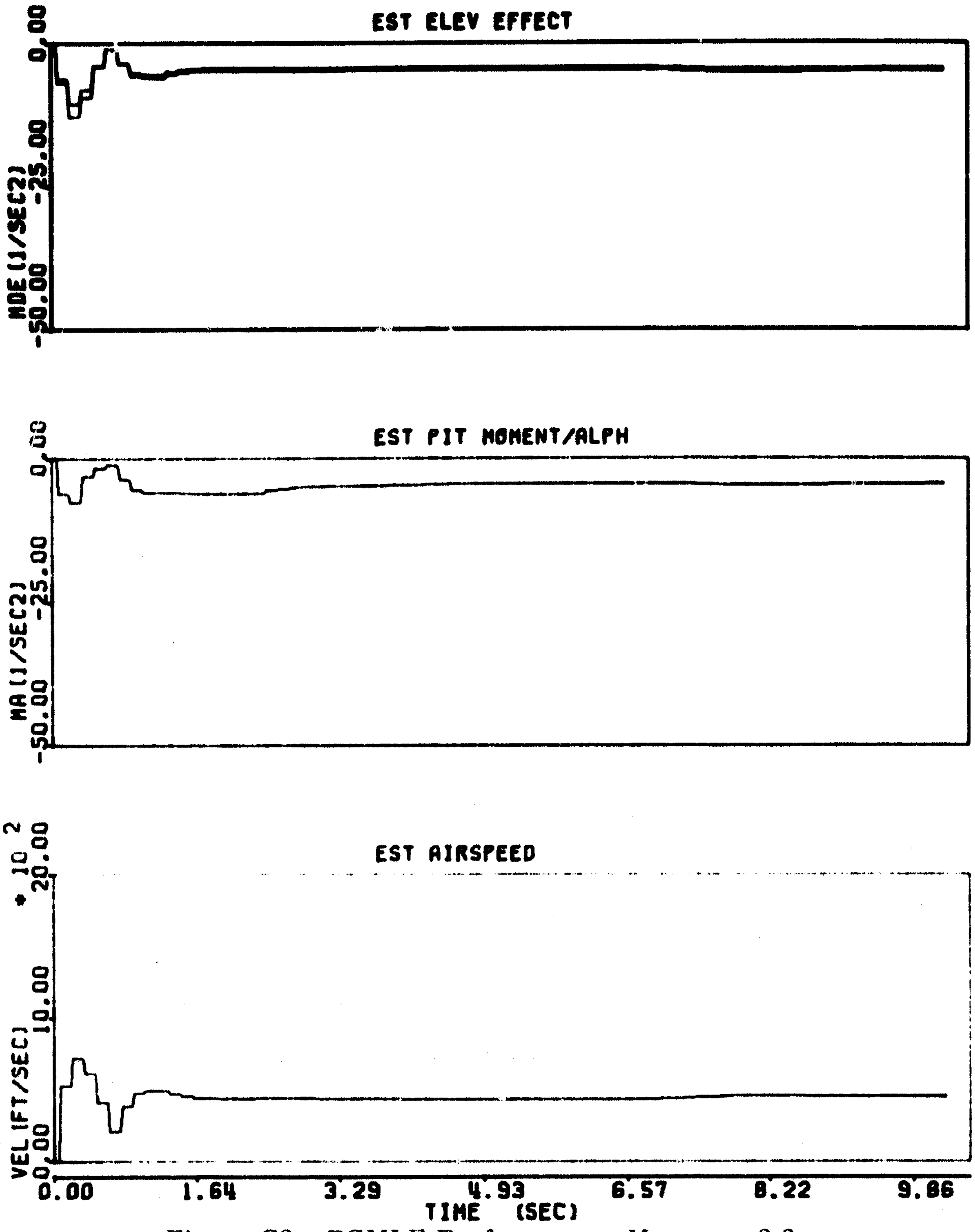

Figure C2. PCMLE Performance, Maneuver 2:2
(Second Iteration)

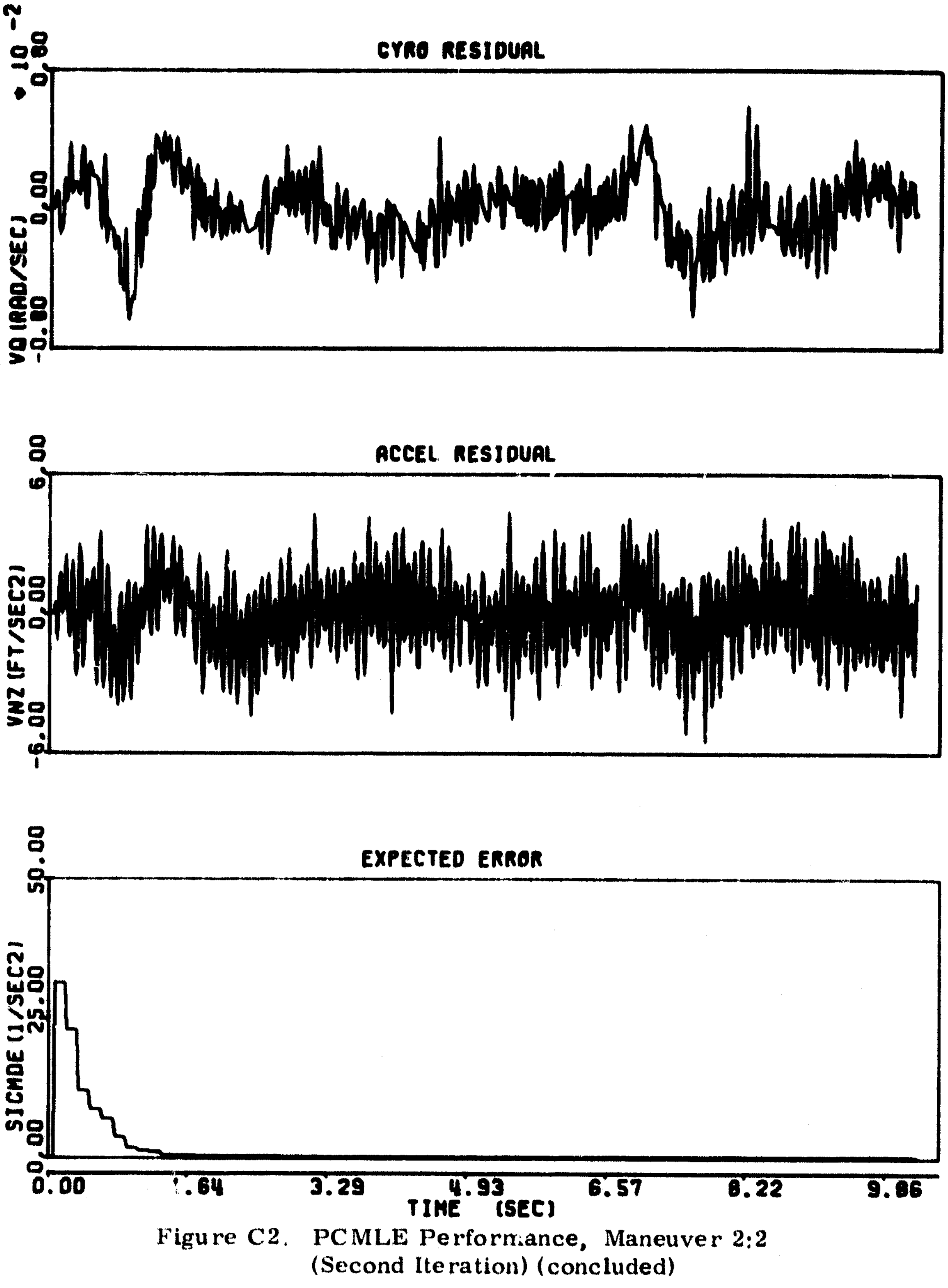

Figure C2. PCMLE Performance, Maneuver 2:2
(Second Iteration) (concluded)

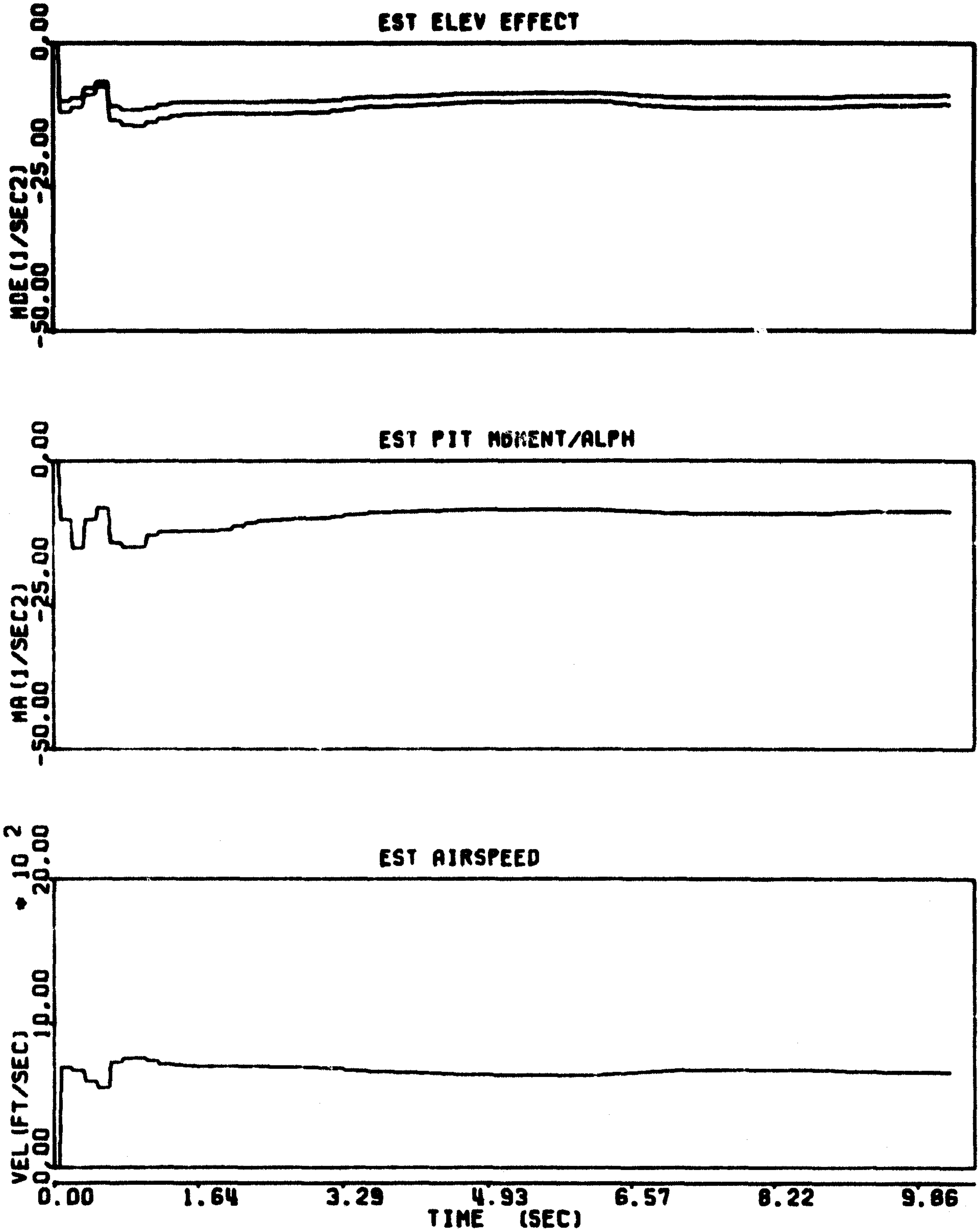

Figure C3. PCMLE Performance, Maneuver 2:3
(Second Iteration)

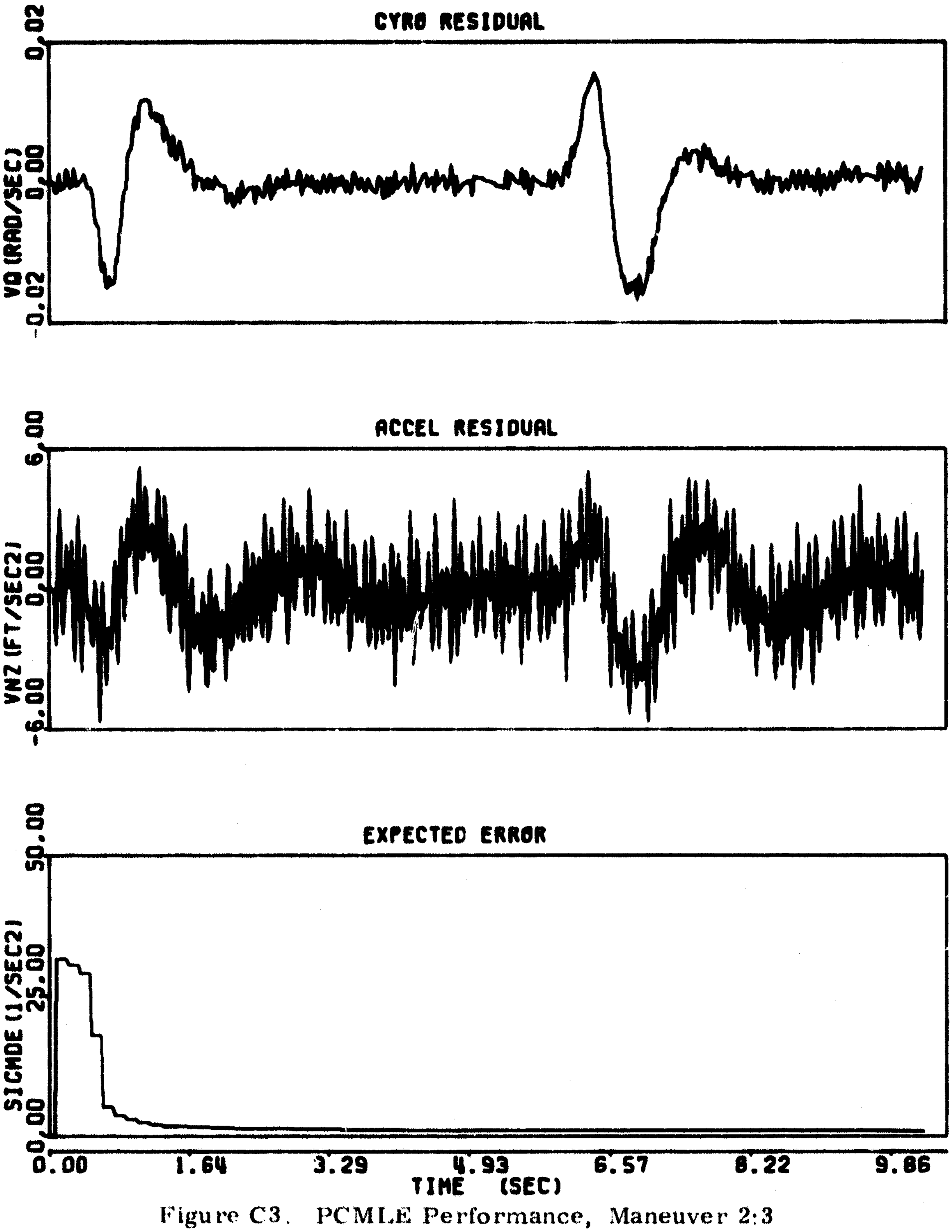

Figure C3. PCMLE Performance, Maneuver 2:3
(Second Iteration) (concluded)

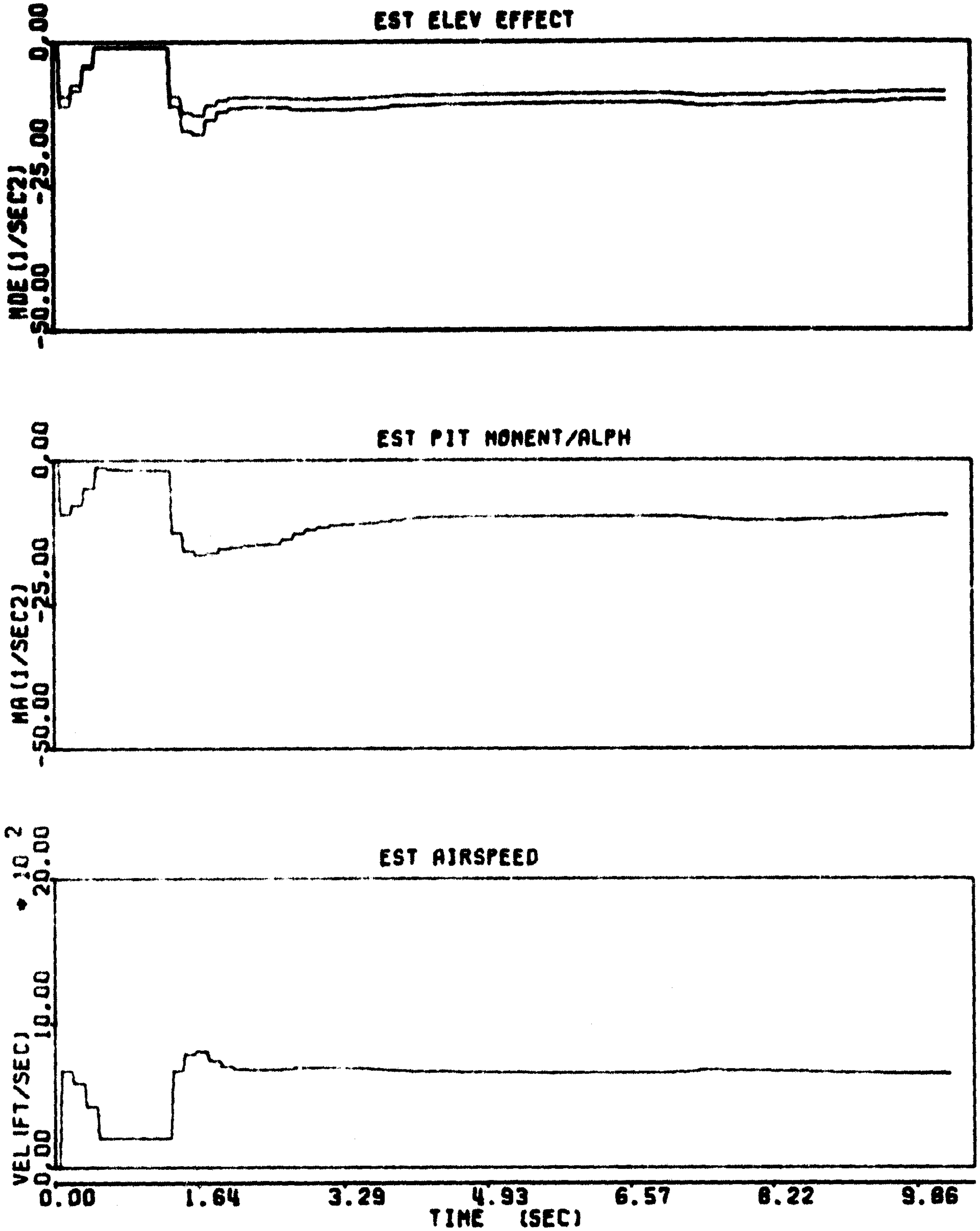

Figure C4. PCMLE Performance, Maneuver 2:4
(Second Iteration)

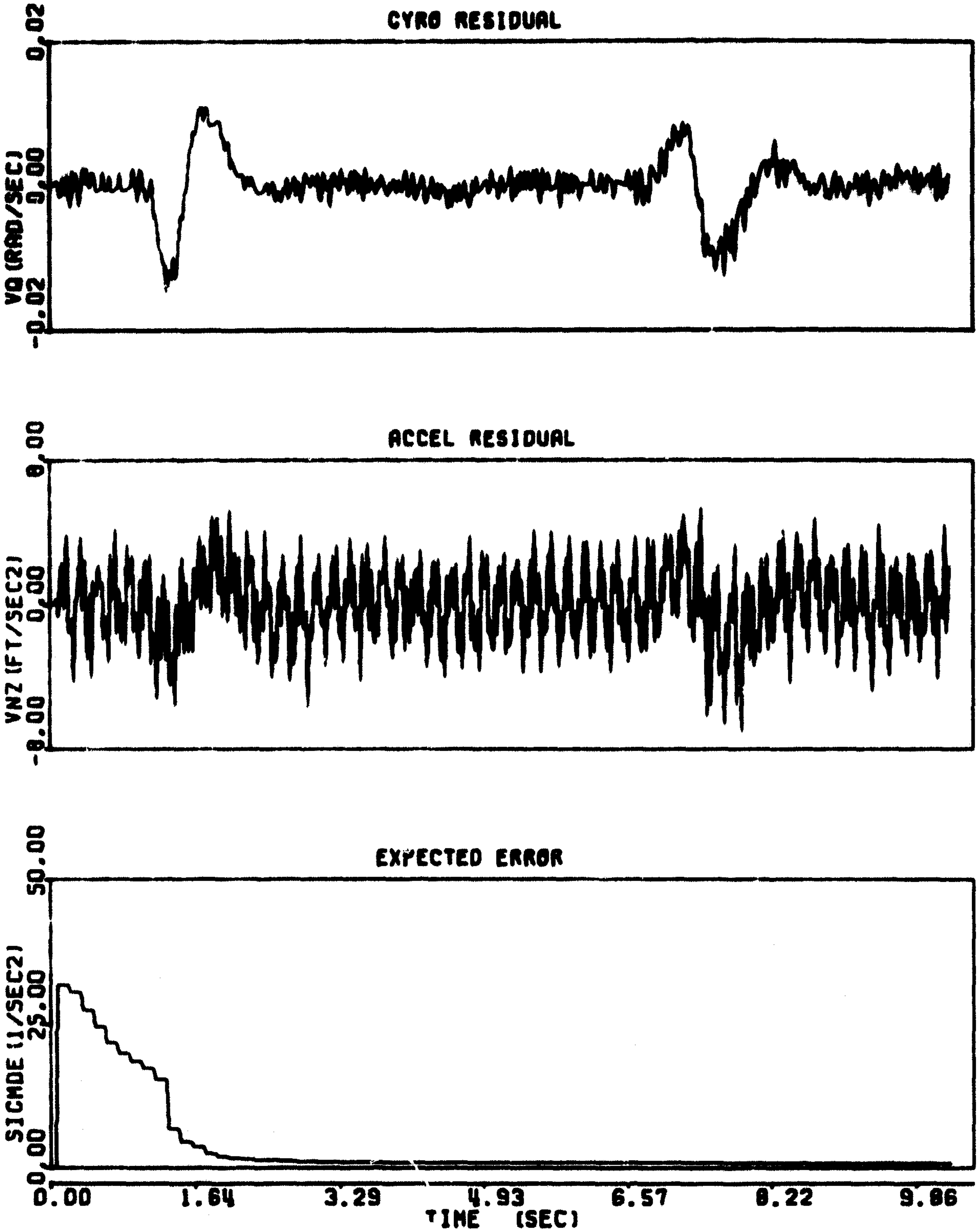

Figure C4. PCMLE Performance, Maneuver 2:4
(Second iteration) (concluded)

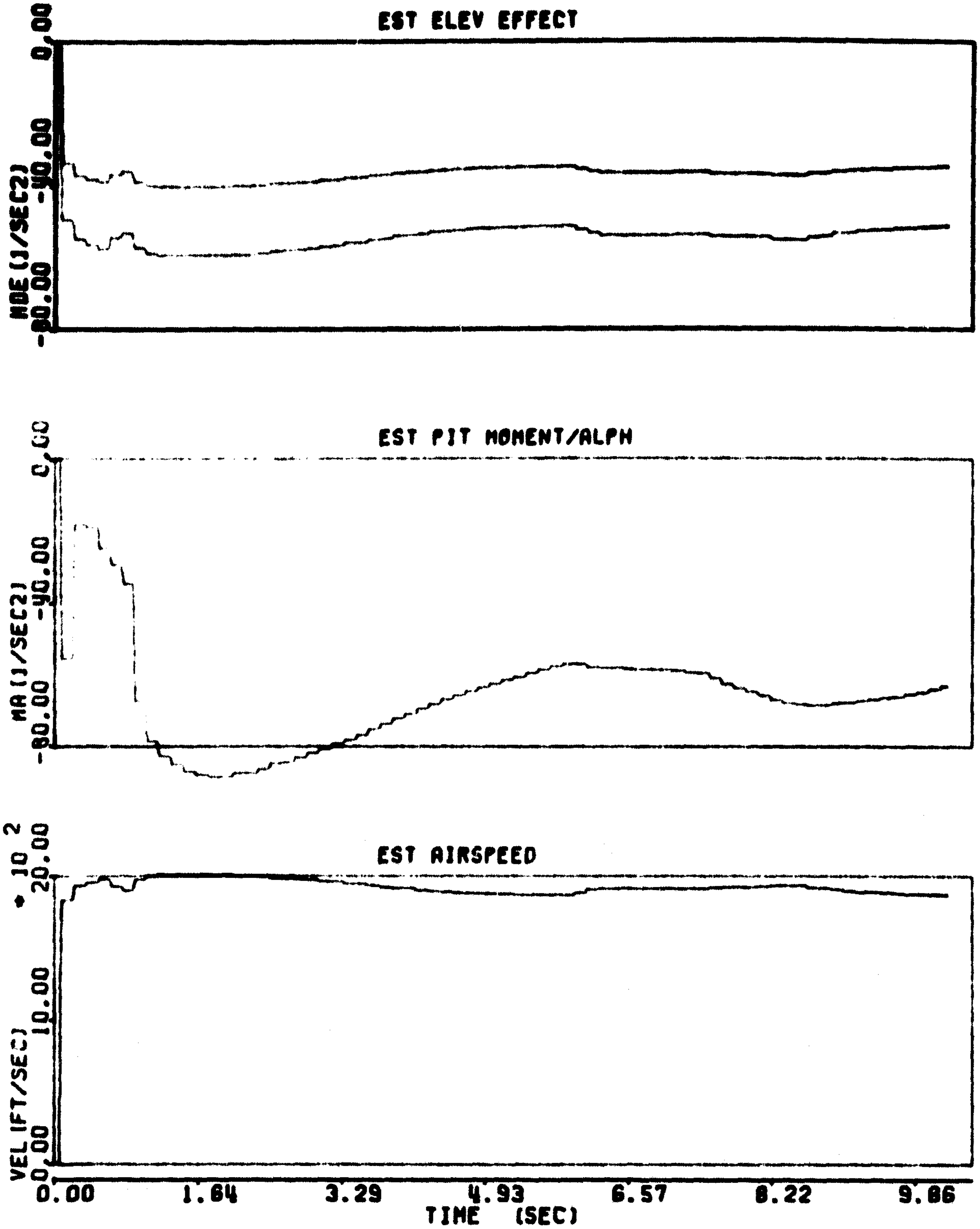

Figure C5. PCMLE Performance, Maneuver 2:5
(Second Iteration)

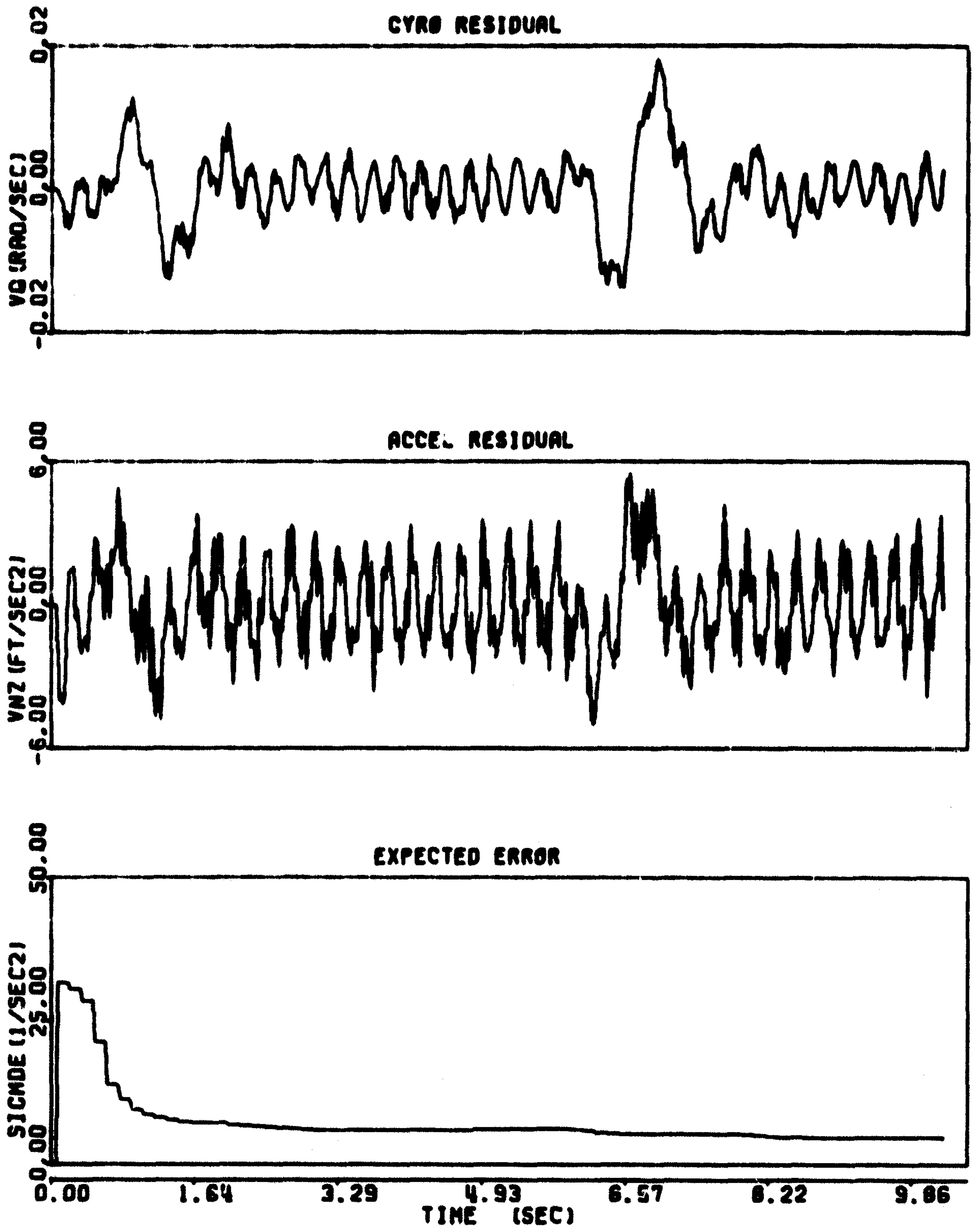

Figure C5. PCMLE Performance, Maneuver 2:5
(Second Iteration) (concluded)

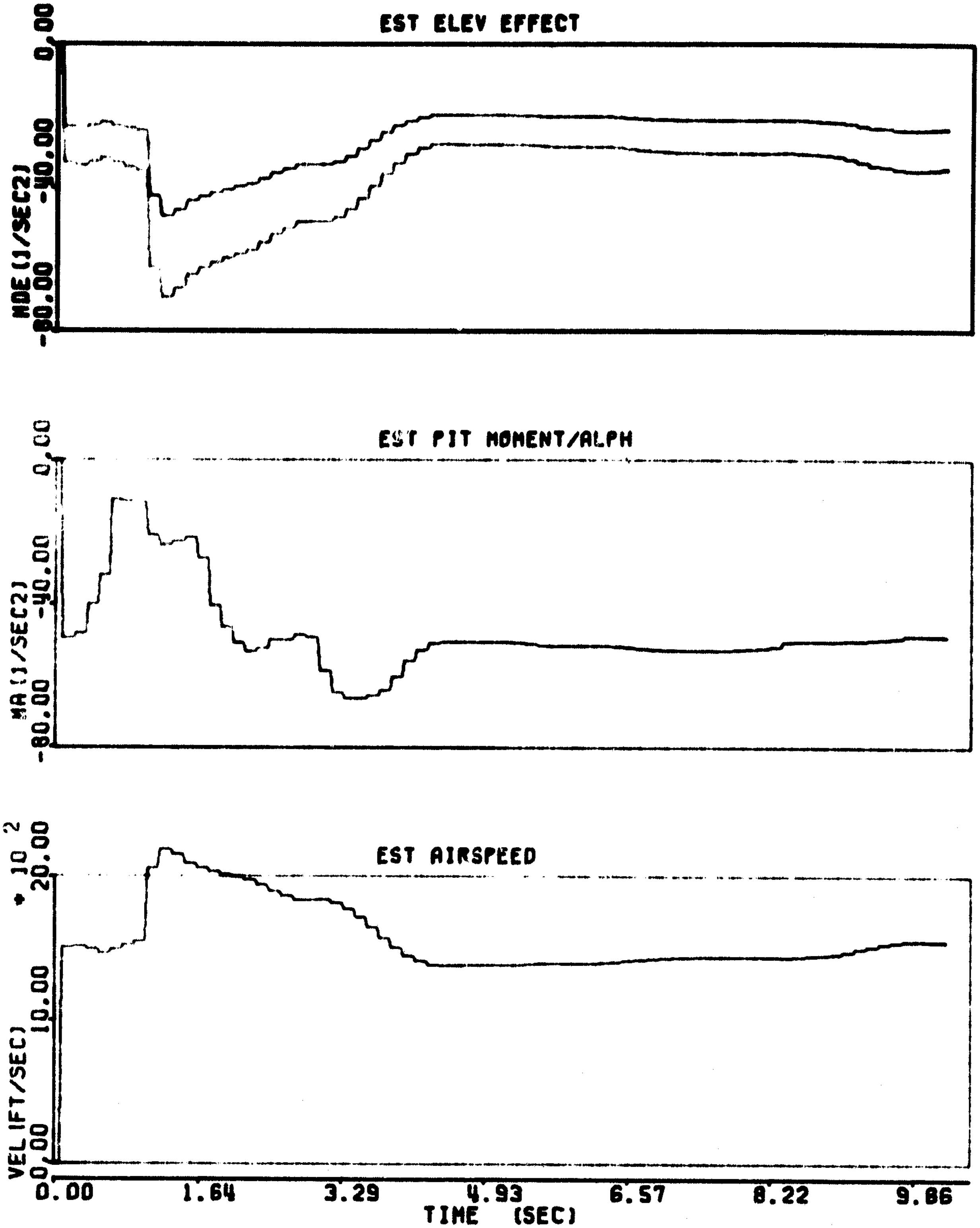

Figure C6. PCMLE Performance, Maneuver 2:6
(Second Iteration)

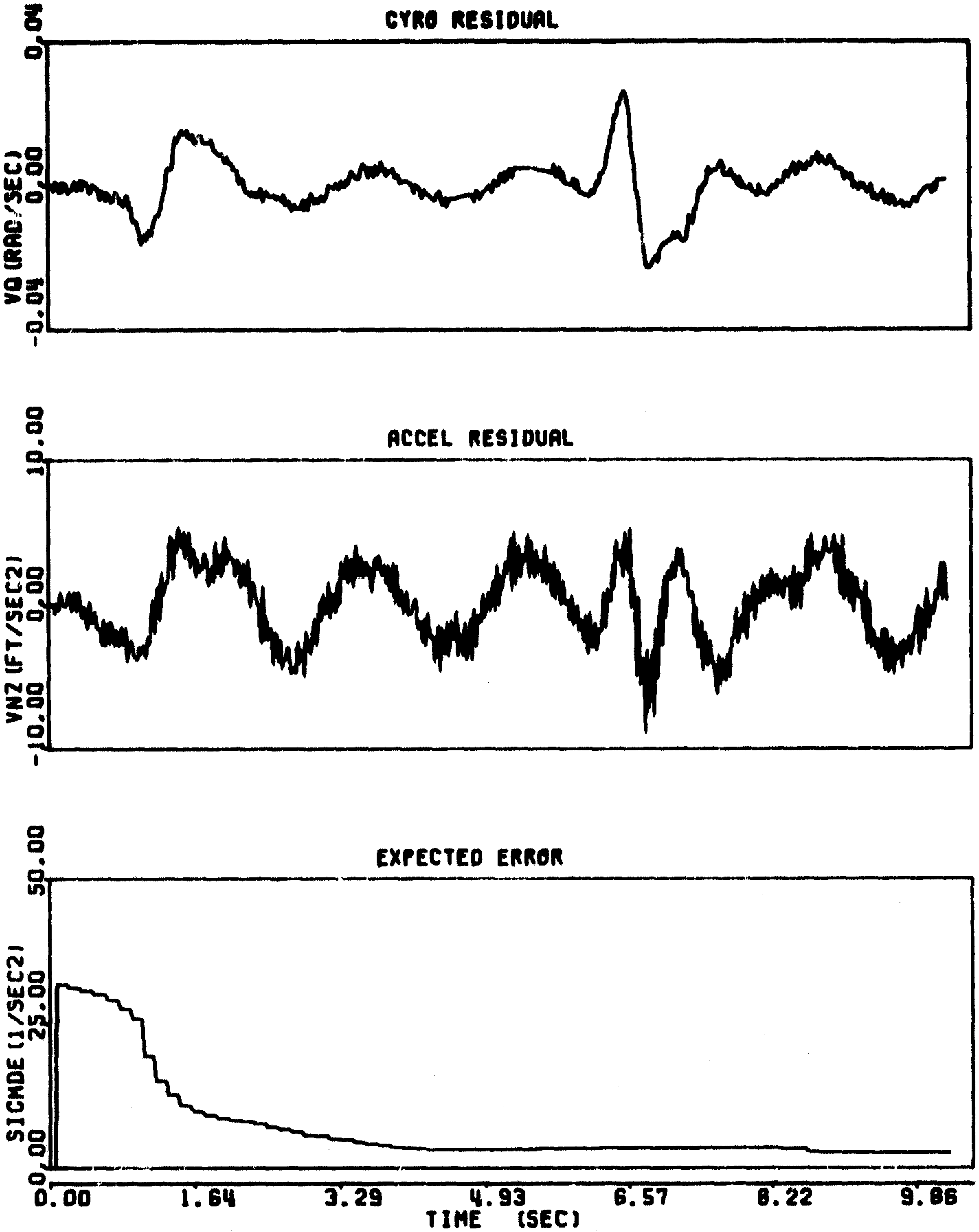

Figure C6. PCMLE Performance, Maneuver 2:6 (Second Iteration) (concluded)

REFERENCES

1. Hartmann, G. L., et al., "F-8C Adaptive Flight Control Laws," Final Report, NASA CR2880, June 1976.

2. Stein, G. and Hartmann, G. L., "F-8C Adaptive Control Extensions," Add-On Report, NASA CR2881, June 1976.

3. Edwards, J.W. and Deets, D.A., "Development of a Remote Digital Augmentation System and Application to a Remotely Piloted Research Vehicle," NASA TND-9941, Edwards, California, 1975.

4. Hartmann, G.L., "PCMLE Software Documentation," Honeywell Report F0459SD, NASA Contract NAS4-2344, October 1976.

5. Cunningham, T.B., et al., "Sensor Reduction with Analytical Redundancy," AFFDL-TR-77-25, Wright-Patterson AFB, Ohio, March 1977.

Conversion Factors to SI Units

To correct from-	To-	Multiply by-
ft	m	0.3048
ft/sec	m/sec	0.3048
ft/sec^2	m/sec^2	0.3048
psf	N/m^2	47.88

PRECEDING PAGE BLANK NOT FILMED